Modification and Application of Antibodies and Their Fragments for Immunostaining in Live Lymphatic Tissue Slices

Andrew Walter Lee Kinman

Greenwood, Indiana

B.A. Chemistry, Hanover College, 2012

A dissertation presented to the Graduate Faculty of the University of Virginia in Candidacy for the Degree of Doctor of Philosophy

Department of Chemistry

University of Virginia

August 2020

Abstract

The research presented in this thesis focuses on 3 major themes: 1.) the in-house modification of antibodies, 2.) the validation/testing of antibodies after modification, and 3.) the use of modified antibodies as an immunostaining reagent in live lymphatic tissue slices. For most research labs, the development of novel antibody-dependent methods or antibody-based research tools are often limited by the lack availability of commercial recombinant antibodies, which are best suited to efficiently generate fragments, bispecific, or otherwise modified antibodies. However, the in-house generation of recombinant antibodies is nontrivial. High costs, specialized equipment, and necessary expertise are barriers to in-house recombinant antibody production; thus, the average research lab will may choose to use monoclonal/polyclonal antibodies to make their desired modification by other, more cost effective, methods. **Chapter 2** discusses the use of enzymatic digestion of antibodies, as it is more cost effective and approachable than recombinant production for small-scale in-house generation of fragments. The benefits, challenges, validation, and suggested optimization workflow for enzymatic production of antibody fragments are presented in detail. **Chapter 3** discusses the application of microfluidics to address optimization and validation needs for another form of antibody modification – the labeling or conjugation of an antibody to another molecule or tag. When labeling, the number of labeled tags (labeling ratio) is often used to approximate the function/affinity of the antibody. Optimizations of these reactions can be time-consuming and costly; thus, there is a need for a rapid, cost-effective, and user-friendly (microfluidic) platform to test antibody labeling ratios. **Chapter 4** presents one such application of antibodies labeled with fluorophores for immunohistochemical staining of lymph node slices for spatial

determination of substructures and identification of cell surface markers in tissue samples. **Chapter 5** presents a novel method to observe the release of cytokine signals from immune cells in live lymph tissue using a conjugated bispecific antibody "dual affinity reagent." We discuss the production of the dual affinity reagent and propose several validation experiments for its use in observing spatially discrete cytokine release from lymph tissue in response to immune stimuli. We believe that studying live tissue spatial morphology changes and cytokine release in response to certain diseases may allow us in the future to obtain new unique insights into disease progression and may identify key pathways, events, or sub-structures to target for new therapies.

Acknowledgements

I would like to thank Dr. Pompano, for going above and beyond the responsibilities of an advisor. She was always available to participate in lengthy feedback meetings, provided constant encouragement, and her passion to perform great science was inspiring and infectious. I would also like to thank the entire Pompano lab, for friends I have made, for the parties, for the work lunches, and for always being there to share in both the highs and lows of graduate research. I also want to thank my parents for their constant support.

Lastly, I want to thank my wife Cassandra, without whom I would never have accomplished as much as I have. “I would rather spend one lifetime with you, than face all the ages of this world alone.”

Table of Contents

List of Figures

Chapter 1: Introduction

1.1 Importance and Applications of Antibodies

Antibodies are a critical tool for both therapeutic and research settings. After the advancement of producing antibodies via hybridoma cell lines in 1975, antibodies immediately became an invaluable tool for early development of therapeutics and biological assays.[1–3] As of late 2019, there are 79 antibodies approved for therapeutic use in the US/EU, with 3-4 new antibodies developed each year. This represents a $150 billion (USD) industry with the vast majority of antibodies developed for cancer treatments.[4] The size of the market reflects the approachability of antibodies as a therapeutic reagent, as antibodies often are highly specific and have far fewer side effects than many other drugs of similar purposes; hence development of therapeutics tend to initially focus on antibodies.[5] Furthermore, with the rise in interest of neurodegenerative diseases like Parkinson's, Alzheimer's, and Huntington's, antibodies have seen increased use by researchers to help further our understanding of these diseases. In comparison to therapeutics, antibodies for research is a $3.4 billion (USD) industry for which the majority use is for western blots and immunohistochemistry.[6] Outside of the clinical setting, antibodies are also incredibly important for use in a wider variety of everyday applications such as assays for pathogen detection in water and food, or more personal applications like pregnancy tests.

One primary and increasingly important application of antibodies is their use as an immunostaining agent for research purposes. The prevalence of this technique is largely due to its ease of use and versatility, as there is a wide selection of commercially available antibodies for most targets and antibodies conjugated with a number of labels such as

biotin/streptavidin, enzymatic labels, electrochemical labels, and fluorophores.[7,8] Fluorescent antibodies are often used to stain common surface markers/receptors which allow for the identification of cell phenotype or changes in cell morphology in response to activation, maturation, or other cell processes.[9] Techniques like flow cytometry take advantage of this specific staining for surface markers to provide single cell resolution; this requires dissociation of cells from tissue into a homogenous cell suspension.[10] When the tissue is left intact and studied as a whole, the observation of spatial morphology can be a critical tool for better understanding disease progression and immunological function that is otherwise not possible in-vitro. One example is diagnosis of cancer and tumor progression as cancerous markers are upregulated and can coincide with a change in local morphology.[11–13]

The application of antibody stains to study intact tissue is known as immunohistochemistry (IHC). Historically, much of IHC was performed on thin tissue slices that were cryogenically preserved or fixed; however, in the last few decades there has been a growing interest in using thick live tissue slices. While more difficult to handle, live tissue IHC preserves the tissue microenvironment (similar to in-vitro) and allows for the investigation of tissue function over time, including responses to both global[14] and local[15] stimulus which is prohibitively difficult to replicate in-vitro. This is incredibly beneficial for the study of disease progression by allowing us to observe tissue response in near real-time. In recent years there have been several publications on IHC labelling of live tissue, including live lung slices, prostate explants, and lymph node tissues.[14,16,17]

1.2 Antibodies function, production, and structure

Within our body's immune system, antibodies, also known as immunoglobulins (Ig) are produced in response to a foreign invader in the body, and help work to eliminate the invader. During an immune response, antigen presenting cells (APC's), such as macrophages and dendritic cells (DC), identify and internalize the foreign antigen. DCs will then migrate to the lymph node to deliver antigen to B cells and T cells. In the lymph node, B cells can bind to free or DC bound antigen, internalizing the antigen, and then presenting it on their surface via the major histocompatibility complex (MHC II). [18] T cells, activated by MHCII either by DC, B cells, or other APC's, will then secrete an array of cytokine signaling proteins which promote the B cells to mature into plasma cells and produce antibodies against the foreign antigen (Figure 1-1). The antibodies are secreted into the blood and lymphatic fluid, where they bind and coat (opsonize) any foreign body with a antibodies, thus marking it for lysis or phagocytosis.[19–21]

Antibodies for clinical and laboratory use are produced in a variety of ways. The early uses of antibodies relied on serum solutions produced from animal sources, which were affinity purified using target antigen.[22] Resulting serum solutions were polyclonal, containing several different antibody clones each targeting slightly different regions of the antigen for binding. While still useful for certain applications like immunoassays, its lack of specificity limited its use for more precise applications. For this reason, the technological ability to isolate monoclonal antibodies was an important advancement.[23] Monoclonal production starts with animal immunization, followed by isolation of B cells, which are hybridized with myeloma cells to produce long lasting cell lines. Antibody producing hybridoma cells can then be screened and cultured. While much more labor intensive to

produce, monoclonal has the advantage of specificity, as well as less batch to batch variation than polyclonal; and while more laborious, once a stable hybridoma cell line for the antibody is made, it is much quicker to reproduce antibodies.[24]

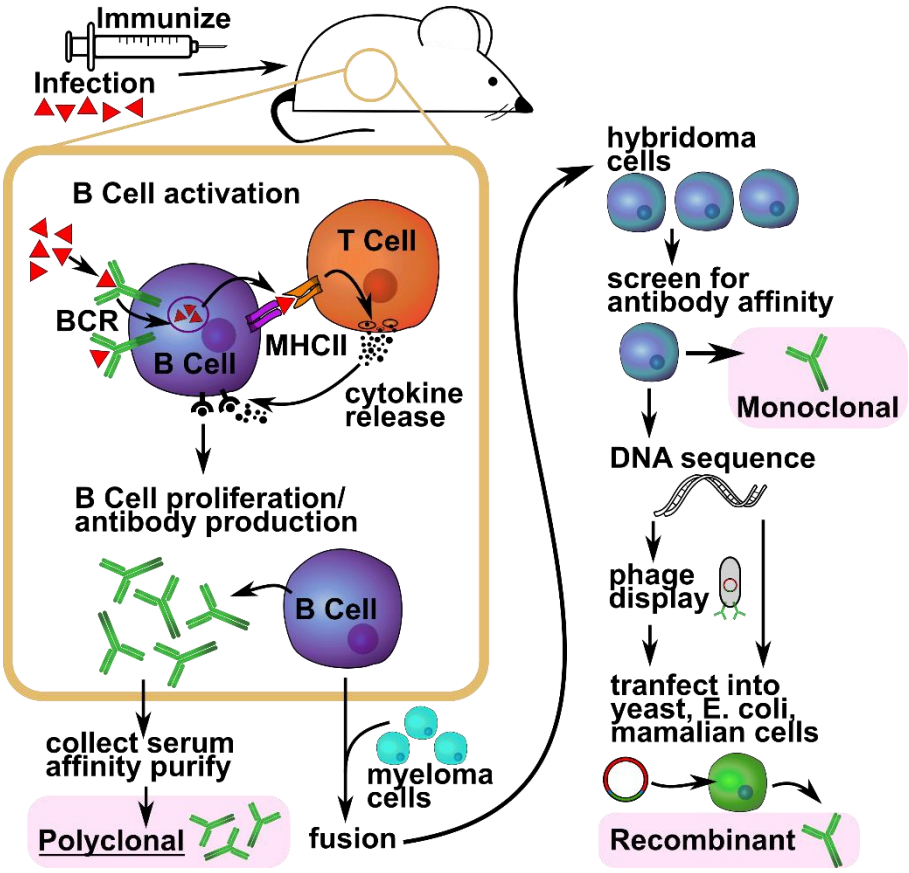

Figure 1-1: Production of antibodies in-vivo and in-vitro.Activated B cells produce antibodies. Each B cell produces a specific antibody clone, and together produce many (poly) clones, which can be purified from serum. Monoclonal antibodies can be produced by isolation and screening of B cell hybridomas. Polyclonal antibodies are produced by sequencing hybridoma DNA and transfecting sequence into host cell for culturing.

Similarly, recombinant antibody production can rapidly reproduce antibodies in much higher quantity than either polyclonal or monoclonal, and is rapidly becoming the next gold standard for antibody production. This higher throughput does, however, have a much higher initial cost than monoclonal production, as hybridoma cells then need to be

accurately sequenced before transfection into E. coli, yeast, or mammalian cells for large scale production. Because recombinant production is based on using a known sequence, it does have the advantage of being able to make modifications to the sequence to shorten the antibody into smaller fragments, make chimeric antibodies using mixed sequences (e.g. mouse and human), or tuning affinity/specificity by random mutations or screening of phage display libraries.[25,26] In the future, recombinant production is likely to become the preferred method of antibody production, however, its high upfront costs and specialized techniques limits its short-term commercial practicality.[26] Currently the vast majority of commercially available antibodies for a wide variety and often niche targets are produced from monoclonal hybridomas.

In biochemistry, the commonly referred to antibodies are the traditional Y-shaped Immunoglobulin G (IgG). As seen in Figure 1-2a, IgG is comprised of 2 heavy chains (HC; ~ 50 kDa each) and 2 light chains (LC; ~25 kDa each), held together by interchain cysteine disulfide bonds. For IgG, the number and placement of disulfide bonds is one of the primary differences between antibody isotypes (Fig 1-2b),[27] the most common of which are IgG1, 2a, 2b, and 3 and 4. However, there are other types, or classes, of antibodies (Figure 1-2c): IgA, IgD, IgE, IgG, and IgM; each with their own role in the immune system.[28,29] Yet, the vast majority of clinical and laboratory research is focused on using either IgM or IgG, with IgG being the more common of the two.

In general, when looking at the canonical structure of an IgG, there are several key components to recognize. Firstly, the HC and LC proteins are held together by disulfide bonds and form the arms of the classic antibody Y shape, also known as the fragment

antigen binding (Fab) region. This is the portion of the antibody that recognizes and binds an antigen.[30]

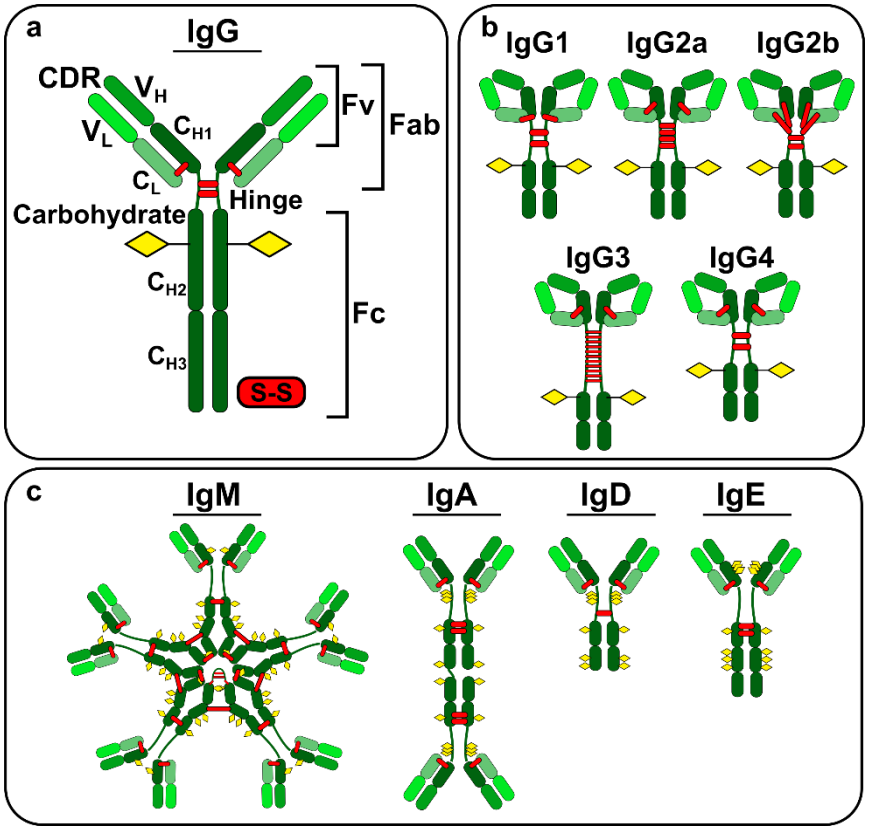

Figure 1-2: Structure of human antibody classes and isotypes. Adapted from Vidarsson G, Dekkers G, Rispens T. IgG subclasses and allotypes: from structure to effector functions. (2014) Front Immunol. 5:520.

The HC and LC that comprise the Fab region can further be divided into two subsections each. Near the N-terminal there is the variable region (V_L and V_H for light and heavy) and then the constant region (C_L and C_{H1}). As can be inferred from the nomenclature, the constant region is comprised of a sequence of amino acid (a.a.) residues that are conserved between all IgG's of the host (i.e. species that produces the antibody), although it will differ between hosts (mouse, goat, rat, etc). Conversely, the variable region

is specific to each antigen, and is what determines the clone of the antibody. For example, XMG1.2 and R4-6A2 are two rat IgG1 clones specific for murine IFNγ cytokine, however they differ in their variable regions, each targeting a different a.a. sequence of the cytokine target.[8] The targeted region of the antigen is known as the epitope, and the complementary region on the antibodies VL and HL is the paratope. Each paratope is comprised of 6 hypervariable complimentary-determining regions (CDR's), three from each VL and VH, whose specific sequence and shape conform and interact with the epitope a.a. residues through a mixture of non-covalent forces, i.e. hydrogen bonding, electrostatic, van der Waals, and hydrophobic forces.[31] As such, the antigen-antibody binding is reversable and can be disrupted by extreme pH's and high salt concentrations, weakening those forces or modifying the conformation of the antibody or antigen.

Because antigen binding is reversable, the binding can be modeled by Ab + Ag ⇌ C, where Ab is the antibody concentration, Ag the antigen concentration, and C the concentration of the bound complex. The affinity of the binding is often measured as the rate of dissociation over binding (dissociation constant Kd) where Kd = ([Ab] + [Ag])/ [C]. It is worth noting that the affinity of a whole antibody for its antigen is actually a measure of its avidity, as the affinity of the whole 2 Fab armed antibody will differ from an antibody fragment with only a single Fab arm.[30] The avidity is a measure of multiple affinities (for each arm of the antibody), and is in part affected by the orientation and positioning of the epitope and paratopes, as when the antigen dissociates from one Fab arm, it has a chance to diffuse to and bind the other Fab arm. Furthermore, as each Fab arm within a whole antibody is bound to one another by inter heavy chain disulfide bonds at the "hinge" region

(Figure 1-2), each Fab arm has some free range of motion that allows it to move closer in proximity to the bound antigen, increasing its avidity.[32]

Lastly, the crystallizable fragment (Fc) region (so named because upon its discovery, it was easily crystallizable[33]) is the bottom "tail" of the canonical Y shaped antibody. The Fc region is important for recognition by Fc receptors (FcR) on effector cells, such as macrophages.[34] Without the Fc region, effector cells would be unable to identify and eliminate an opsonized foreign antigen. Conversely, as the Fc region is recognized by Fc receptors within our own bodies as a non-foreign entity, if the antibody is from a different species, the glycosylations on the Fc region mark it as a foreign entity. It is for this reason that recombinant antibodies for therapeutics are often made from antibody fragments without the Fc region, transgenic humanized mammalian cells, or are chimeric combinations of a Fab (or just the V_H and V_L sequence) with a human Fc.[25,26]

1.3 Antibody modifications and effects on function

As mentioned previously, a wide variety of applications of antibodies require them to be labeled in some way, whether with a fluorophore or radio-label for IHC or with a drug for immunotherapies. There are a number of ways to provide stable covalent linkages between proteins and labels, however the most common strategies tend to focus on carboxylic, carbohydrate, amine, and sulfhydryl functional groups.[35–37] Perhaps the most common by far is using N-hydroxysuccinidmidyl esters (NHS-esters) for amine conjugation, as amine residues are found on most all proteins, as opposed to more rare and site specific cysteine sulfhydryls.[38] Amine residues are located all over the protein (depending on sequence) and they can often occur within the CDR region of the antibody.

Therefore high labeling ratios may sterically obstruct or chemically disrupt the binding region of the protein, while low ratios may offer insufficient activity (luminosity for fluorophores; efficacy for drugs).[39,40] Typical target ranges (using NHS esters) are ~2-5:1 for fluorophores and ~3-4:1 for drug conjugates (target varies by application and conjugate).[41,42] Furthermore, labelling reactions vary in efficacy depending on the prevalence of the targeted functional group and the specific label used, meaning that reaction optimization is often required because labeling ratios are difficult to predict.[43]

One type of modification that can be made to antibodies is the fragmentation of the antibody into smaller functional parts. The use of fragments is a growing trend in the development of antibodies for immunotherapies and IHC.[44] There are two main benefits of fragmenting antibodies: 1.) smaller fragments have increased diffusivity and can often penetrate deeper into tissue; and 2.) fragments often impart less immunogenicity or un-wanted cross reactivity into tissue.[45] For example, as mentioned previously, recombinant therapeutics often employ just a single Fab or even a single chain variable fragment (scFv) to prevent any capture (cross-reactivity) in tissue by Fc receptors, or identification as a foreign antigen. However, for all its benefits, production of antibody fragments is not without its share of challenges. For one, as previously mentioned, single Fab fragments have only a single binding paratope, decreasing avidity. Another one is that without an Fc region to stabilize the antibody, fragments are often cleared more quickly from the body.[45]

While recombinant antibodies are ideal for fragment expression, their production requires having a prior known sequence to modify and often necessitates the use of phage

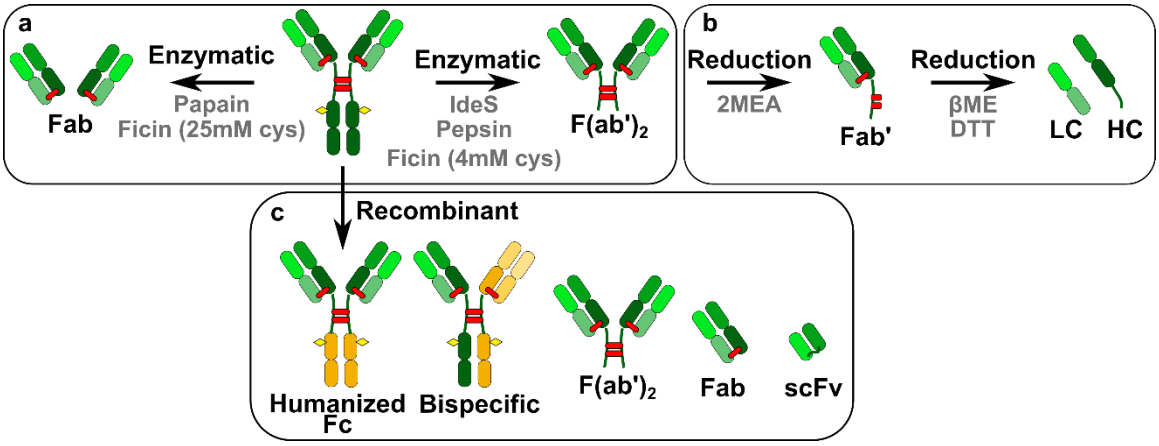

Figure 1-3: Generation of antibodies and fragments enzymatically or recombinantly. **a)** Papain can be used to make single Fab' fragments, whereas pepsin and IdeS can be used to make $F(ab')_2$ fragments, and Ficin can make both depending on amount of added cysteine. **b)** Single Fab' can be produced with hinge region reduction by 2MEA, and further disulfide reduction results in individual heavy and light chains. **c)** Recombinant production of antibodies can produce humanized (chimeric), bispecific, fragmented, or otherwise modified antibodies.

display libraries to screen for affinity (Figure 1-3c). This makes the production and use of recombinant fragments a labor intensive and costly venture.

An alternative to antibody fragments is the use of aptamers or peptides that can mimic antibody – antigen interaction. DNA (or RNA) based aptamers and peptide mimics are considerably smaller than antibodies, usually around 10-30kDa and 3-15 kDa respectively; meaning that they can often penetrate much deeper into tissue than antibody fragments can.[46,47] Several aptamers and peptides reported in literature have shown comparable sensitivity, affinity, and specificity to antibodies, and can be synthesized much easier than recombinant antibodies.[48] While aptamers and peptides are a promising and growing field of research, much like recombinant antibodies, there is an entry barrier for the average lab in the form of expertise, equipment and costs. There are few commercially available aptamers and peptides, necessitating that each lab synthesizes their own.

Furthermore, for much of the synthesis of these reagents there is no single standardized method leading to variability in sequence, specificity, and affinity between reagents synthesized between labs, and even within the same lab.[46–48]

In comparison, while being an older technique, enzymatic production of antibody fragments is a much more approachable methodology for many researchers. Enzymatic fragmentation of antibodies has been performed since the 1960's and 70's and has mostly focused on a handful of enzymes: pepsin, papain, ficin, trypsin (for IgM), and more recently IDeS (Figure 1-3a).[49–54] Each enzyme operates under different conditions, with different target regions, and with varying efficiencies. Pepsin primarily cleaves antibodies just below the hinge region separating the $F(ab')_2$ upper region of the antibody from the lower Fc portion, and requires acidic pH's (2-6).[49] Papain, on the other hand, requires a reducing agent and cleaves antibodies just above the hinge region resulting in single Fab fragments.[50] Interestingly the enzyme Ficin can cleave above or below the hinge region depending on the specific amount of reducing agent present during the reaction, shifting the reaction to favor single Fab or $F(ab')_2$ at high or low concentrations of cysteine respectively.[55] IdeS, like papain and ficin, is a thiol protease; yet, similarly to pepsin, it cleaves below the hinge region producing a $F(ab')_2$.[53] Lastly, trypsin is suitable for fragmentation of IgM pentamers. However, trypsin digestion of IgG results in a product with little to no functionally important fragments.[54,56] This kind of "over-digestion", while most prevalent with trypsin IgG, is also a concern with most of the enzymatic methods.

In general, while the enzymes tend to first target specific regions on the antibody due to sterics, once fragmented the enzymes can then continue to digest the antibody with

varying degrees of rapidity. Depending on the specific enzymatic rate for each type of fragment, it is possible to produce solutions with a mixture of unfragmented, desired fragments, and over fragmentation. Degree of fragmentation can also vary widely for antibodies from different species host and isotype. Notably the use of ficin is often limited to the IgG1 isotype, IdeS is limited to human IgG and a handful of other host isotypes, and pepsin is often cited as being resistant to IgG1.[57,58] Furthermore, as will be discussed further in chapter 2, fragmentation can differ between clones of the same host/isotype. Because of this, published reaction conditions are often only applicable to those specific clones. Even then, due to differences in expression source (recombinant, hybridoma, etc.), antibody structure and glycosylation's may differ, altering fragmentation. Once fragmented, the antibody can display different affinities or stability than the starting whole antibody. For example, the Fc region may impart mechanical stability to Fab arms of the antibody in addition to extending half-life (clearance from body). Without the Fc fragment, the hinge region connecting the individual arms of the $F(ab')_2$ become may become more flexible, potentially increasing avidity.[59] Conversely, single Fab's will have a reduction in avidity. Reaction conditions can also play a role in altered function, as reducing agents (papain, ficin) and low pH's (pepsin) may denature or mildly alter tertiary structure of CDR binding domains. Thus, antibody fragments need to be validated for any changes in affinity before use.

1.4 Antibody validation

It cannot be understated how important antibody validation is.[60] For some applications like pharmaceutical or preclinical trial antibody therapeutic drugs validation is absolutely critical, where deviations in efficacy can lead to increased mortality or

prevalence of unwanted side-effects.[60,61] Less critical (but no less important) lack of validation and batch to batch variability of research antibodies can lead to reproducibility problems, which may alter or invalidate research results, ultimately costing time and money.[62] In fact, this is a current issue within the biochemical and biomedical fields. There have been several minor comparison studies performed for specific categories of antibodies, such as specificity for G coupled protein receptors[63] and antibodies for epigenetic studies[64]. One study from the Human Protein Atlas determined that 50% of some 15,00 antibodies (both commercial and in-house) were not suitable for use in determination of protein distribution in tissue slices.[65] Results like these have led some researchers to anecdotally suggest that up to half of all commercial antibodies are unreliable or their data is not reproducible to some degree.[62] The specific causes can be many and vary depending on the type of research. Some simple explanations are batch to batch variability in the production process or differences from one producer to the other. For instance, producer A may produce a recombinant antibody in yeast cells, whereas producer B produces the same clone in mammalian cells. While the sequence may be the same, the host cells may affect factors like glycosylation and protein folding. Additionally, each producer may collect, purify, and store their antibodies under different conditions.[61] Production can also vary when operating at different scales, due to factors like lack of diffusion/poor mixing at larger scales. Other more difficult causes for the reproducibility crisis may involve biases from the researchers themselves, as technique and methodology may vary from researcher to researcher.[66] Reproducibility of antibodies for certain biological applications can also be confounded by the inherent variability of biological samples. For these reasons, it is

important for each lab to validate antibodies prior to use, even when bought freshly bought from a commercial vendor.

One reason to validate after purchase is often due to the lack of validation data provided by the vendor. There are few vendors that extensively validate each lot of antibody. For those that do, the price of the antibodies, which is already relatively expensive, increases. Often the antibodies have no validation data, or have been validated for one or two methods, such as western blot (WB) or enzyme linked immunosorbent assay (ELISA). Furthermore, depending on the vendor, the clone or isotype may not even be reported, let alone information on affinity or cross-reactivity. Additionally, unless the vendor's extensive validation also includes validation of each specific lot of antibody and show comparisons to previous lots, lot to lot variability may result in unforeseen complications with the buyers intended application.[60] Thus, it is critically important for each research lab to validate each antibody reagent prior to use.[67] Indeed, several major grant foundations, including the NIH, now require submission of reagent validation plans for antibodies.[68]

When validating an antibody, there are several factors to keep in mind. One factor is the choice of whether to validate the antibody against a native (in-situ), recombinant, or denatured antigen. The choice will largely depend on the target application for the antibody. For example, if the antibody is to be used for western blots, it should be validated against a denatured antigen, as the denatured antigen epitope will likely differ from the native form and have different affinity for the antibody. Conversely, if the antibody is to be used for immunohistochemistry or flow cytometry (FC), the antibody should be

validated against the native antigen produced in-situ, as even recombinant antigen may contain different glycosylation's or undergone different protein folding.[69] Another challenge is identifying or controlling for cross reactivity (off target binding). Good standard positive/negative controls to use for IHC/FC cross reactivity are cell-depleted primary cell cultures (isolation of target cell/antigen) or knock-out genetic samples.[67] Once again, the intended application is important, as cross-reactivity against a different antigen may not disqualify use of the antibody if that antigen is not present in the experimental system. This is one of the primary reasons why antibodies or the methodology for staining with antibodies needs to be re-validated for IHC use in different tissues. Lastly, antibodies should be validated periodically over time, especially if they have undergone any freeze/thaw cycles. Furthermore, as mentioned previously, in-house labeling or modifications of antibodies can be unpredictable and often lack precision in reproducibility, e.g. due to changes in the reagents over time (hydrolysis, aggregation, denaturing, etc.), thus necessitating validation before use.

1.5 Microfluidics for antibody testing

Microfluidics is a promising platform for antibody testing and validation.[70–72] While microfluidics has an incredibly wide variety and rich history of other applications, there has recently been a growing interest to perform reagent validation on chip.[73] This is especially true for antibodies, as the "reproducibility crisis" is precipitating the need for each lab to perform in house validation.[60] In house validation can often be time consuming and expensive, as biological reagents like antibodies or their targets are often costly. Additionally, for those labs unfamiliar with these types of biological validations, many of these assays may require extensive training. Hence, there is a need for assays that are quick,

cost-effective, and user-friendly. Microfluidics are well suited to addressing these needs, as they allow for the use of µL – nL reagent volumes, can be multiplexed to perform multiple assays at the same time, and can perform multiple assays steps sequentially on the same device, earning them the moniker of "lab on a chip".[74] Background information on microfluidics is provided in the next section.

In the past decade there has been a growing interest and number of publications interested in antibody validation/testing using microfluidics. There are assays for a variety of antibody applications and types of validation. For instance, droplet microfluidics has been used to rapidly screen antibody production from single B-cells/hybridomas.[75,76] On chip droplet assays can often involve antibody binding to target antigen[77] or even lysis of cells for DNA analysis for a specific antibody sequence.[73,78] Other microfluidic assays on chip allow for the direct measurement of antibody affinity[71,79], binding kinetics[80], analysis of glycosylation's[81], or even size-based rheometric measurements of antibody aggregate formation in therapeutic formulations.[82]

1.6 Brief history and physics of microfluidics

Microfluidics, as the name implies, allows for the manipulation of nL-µL volumes of fluid via the application of patterned fluidic channels (mm – nm). The field of microfluidics first evolved from micro electromechanical systems (MEMS) in the engineering field.[83] It was recognized that the same microchip fabrication process could be used to make enclosed channels on the silicon substrate. After the development of some early micro-devices, such as those made to perform gas chromatography on chip[84], a 1990 paper by Manz et al. predicted the potential of these devices to perform many different

processes on a single chip.[85] These predicted devices would be capable of sampling, sample pre-treatment, assay, and detection; for which he coined the phrase "total analysis system" (TAS). As interest grew, the devices moved from silicon wafers to glass as a cost-saving method. This also allowed for the use of visual detection methods. However, the biggest breakthrough advancement of the field was in 1999 by Whitesides with the fabrication of microfluidic devices in poly(dimethylsiloxane) a.k.a. PDMS.[86] PDMS is an attractive material, as it allows the retention of fine details when producing a molded copy of devices fabricated onto a silica master. The molding process allows for the duplication of many devices from 1 master, preventing wear and tear and need for multiple fabrications of the master. PDMS is inexpensive, optically clear, and can easily be treated to bond with itself, allowing for the production of sealed/enclosed channels. The stiffness of PDMS can also be tuned to be more elastic or more rigid depending on the desired application. This has allowed for the production of microfluidic valving, where a thin layer of PDMS over a channel can be pressurized to deform into and block the fluidic channel underneath. Additionally, PDMS is non-toxic and oxygen/gas permeable, making it an attractive platform to culture live cells and tissues on. Since the addition of PDMS fabrication there has been continuing advancement and experimentation with devices fabricated in (or in combination with) other materials such as: paper devices for lateral flow immunoassays[87], polylactic acid (PLA) plastics for centrifugal assay devices[88], and more recently, a variety of plastics and polymers for both fused deposition modeling (FDM)[89] and stereolithography (SLA) 3D printing.[90]

Because microfluidics operates on such a small scale, the hydrodynamics and physical principles can be markedly different from that of benchtop/large volume solution handling. The forces of a liquid at the smaller scales can be modeled by the equation for Reynolds number, a unitless number which describes the inertial and viscous forces of a fluid.

$$Re = \frac{\rho v L}{\mu} \tag{1-1}$$

Where Re is the Reynolds number, ρ is the density (kg/m^3), ν is the velocity (m/s), L is the length dimension (diameter) (m), and μ is the dynamic viscosity of the fluid (kg/m s). Notably for microfluidics, as the size decreases the fluid flow becomes increasingly affected by the viscosity of the solution. At Reynolds numbers < 2100 fluid flow transitions from turbulent flow (Re > 4000) to laminar flow. At this regime, fluid mixing is dominated by diffusion. This is one major benefit of microfluidics, as diffusion time is directly related to square of the distance (Equation 3), meaning that as the size decreases the time for diffusion rapidly decreases.

$$t(s) = \frac{x^2}{2D} \tag{1-2}$$

Without turbulent mixing, this allows for reactions to occur much faster in microfluidic devices as compared to traditional benchtop assays, such as immuno-assays in a well plate. The smaller volumes also allow for the use of fewer reagents. The small features of a microfluidic device also take up minimal space on the chip, allowing for multiple reactions to fit onto a single chip (multiplexing). The major limitations for microfluidics are the signal to noise (S/N) that can be achieved by the detection method, as well as the ability to reliably fabricate smaller and smaller features.

1.7 Description of research goals and concluding remarks

The research presented in this thesis focuses on 3 major themes: 1.) the in-house modification of antibodies, 2.) the validation/testing of antibodies after modification, and 3.) the use of modified antibodies in novel research. For most research labs, the development of novel antibody-dependent methods or antibody-based research tools is often limited to what is commercially available. While there is a there are a wide variety of whole polyclonal and monoclonal antibodies available, there is a significant deficiency in available antibody fragments. This is likely due to the increased costs associated with recombinant production of antibodies and a previous lack of demand for fragments. However, research projects utilizing live tissue explants or the development of novel immunotherapies increases can benefit from the use antibody fragments. **Chapter 2** discusses the use of enzymatic digestion of antibodies, as it is more cost effective and approachable for small-scale in-house generation of fragments. The benefits, challenges, validation, and suggested optimization workflow for enzymatic production of antibody fragments are presented in detail.

Chapter 3 discusses the application of microfluidics to address another form of antibody modification validation– the labeling or conjugation of an antibody to another molecule or tag. When labeling, the attached tag can often block or occlude the antibody binding domains, reducing the affinity of the antibodies. The number of labeled tags (labeling ratio) is often used to approximate the function/affinity of the antibody. Optimizations of these reactions can be time-consuming and costly; thus, there is a need for rapid, cost-effective, and user-friendly (microfluidic) platform to test antibody labeling ratios prior to reagent validation.

Chapter 4 presents an application of antibodies labeled with fluorophores for use in live lymph node tissue slices. Fluorescent antibodies are often used for immunohistochemical staining of tissues for spatial determination of substructures and identification of cell surface markers in tissue samples. However, these antibody reagents need to be validated with use for each new type of tissue methodology. This chapter covers the use of antibodies in in live lymph node tissue slices, including the challenges and caveats to immunostaining live tissue.

Lastly, **Chapter 5** presents a further application of both enzymatically fragmented and labeled antibodies for use in a novel method to perform a cytokine immunoassay within live tissue. Spatially resolved information of live tissue can be greatly beneficial to better understand certain disease progressions. However, this resolution in tissue is currently limited to cell surface markers. The assay presented in this chapter, which is still a work-in-progress, would allow for the direct capture and visualization of secreted signaling molecules on the cells from which they were released within discrete regions of the tissue.

In summary, antibodies are an important tool for a number of number of applications. However, the use of antibodies for novel research are often limited by commercial availability. For such applications antibodies need to be modified or generated in-house. This work discusses the modification of antibodies, their validation, and their use in novel research. **Chapter 6** discusses the impacts as well and the future prospects for this type of research.

Chapter 2: Optimization of Enzymatic Antibody Fragmentation for Yield, Efficiency, and Binding Affinity

Adapted from:

Kinman AWL and Pompano RR. Bioconjugate Chemistry 2019, 30, 3, 800-807

2.1 Abstract

Enzymatic antibody fragmentation has been well studied for various hosts and isotypes, but fragmentation patterns also vary unpredictably by clone, and optimizing Fab or F(ab')2 production by trial and error consumes large quantities of antibodies. Here, we report a systematic strategy for optimizing functional F(ab')2 production via pepsin digestion from small quantities of IgG. We tested three key parameters that affect fragmentation: pH, enzyme concentration (% pepsin w/w), and reaction time, and found that pH had the greatest impact on fragmentation yield and efficiency. We then developed a systematic approach to obtaining acceptable yields, digestion efficiency, and binding affinity. Three case studies are described to illustrate the approach. We anticipate that this work will provide a quick and cost-effective method for researchers to produce antibody fragments from whole IgG, avoiding haphazard trial and error.

2.2 Introduction

Antibody fragments have enjoyed widespread use in a variety of disciplines ranging from bioanalytical immunoassays to pharmacological research. As discussed in **Chapter 1**, their small size and lack of an Fc-mediated binding region allow for better penetration into tissue and specificity for numerous applications.[45,91–93] This is especially important in applications like live tissue immunostaining (Figure 2-1). For example, **Chapter 4** discusses that because antibodies have an Fc region, when staining live lymph node tissue, an additional antibody reagent needs to be added to block Fc receptors on macrophages and B cells. The concerns for Fc blocking are twofold, as 1) the blocking antibody might not block 100% of FcR, resulting in FcR capture of the primary antibody and loss of spatial resolution, and 2) binding the Fc receptors may initiate an immune response; both of which would have to be accounted for with the proper controls.

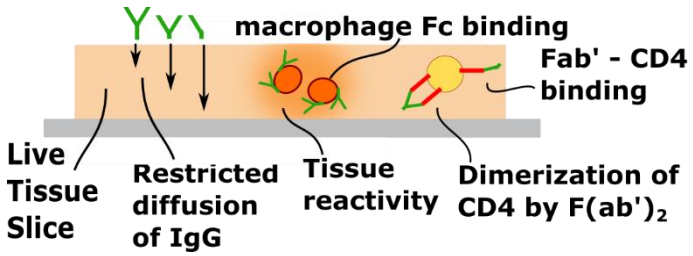

Figure 2-1: Antibody fragments are more beneficial to use in live tissue than whole antibodies.

Another issue, as mentioned, is that the penetration (diffusion) of whole antibodies into tissue is slower compared to small fragments. This is especially important in the development of antibody-drug therapies. For example, tumors often lack sufficient vascularization, meaning that drugs must rely more on diffusion to penetrate into them.[44,94] Additionally, diffusion of antibody reagent into cancerous tissue is often hindered, as cancerous tissues can have more densely packed collagen fibers in the extracellular matrix

(ECM).[44] Diffusivity and its effect on drug efficacy is one of the main reasons why there has been so much interest in developing therapeutic recombinant antibody fragments.[45]

Whole antibodies can also generate some other difficulties for use in live tissue or even long-term cell culture analysis. One example is that for some surface bound cell receptors, such as CD4 on T cells, can be dimerized when bound by a whole antibody. This dimerization can occur because antibodies are bivalent (i.e. they have two binding "arm" domains; see Figure 1-2). When the CD4 surface protein of T cells is dimerized, it alters function and down-regulate expression and internalize the CD4 surface marker.[95–97] In instances like these, it is often beneficial to use an antibody fragment which lacks the Fc region and is either monovalent or bivalent. For example, this was a primary driving factor for using a Fab' fragment for analysis of T cell cytokine production in live tissue (**Chapter 5)**.

Antibody fragments, while extremely useful, do have some notable drawbacks. For one, it is believed that the Fc region of the antibody can impart some biological stability, as fragments without Fc are often cleared from tissue much faster.[45] This may not be an issue for ex-vivo immunostaining or cell culture staining, however it is a consideration for in-vivo use. It may also be the case that the Fc region imparts some rigidity to the hinge region of the antibody.[59] This can affect the degree to which the binding "arms" can move to bind their target, and thus affects the avidity/affinity of the antibody. The avidity can also be affected by the valency of the antibody fragment. Monovalent fragments have only one binding "arm" and are less able to re-bind their target after release, whereas bivalent fragments with 2 binding arms have a better chance to re-bind the released target, bind, or

stay bound to another nearby target (like during CD4 dimerization).[32] There has also been some publications that suggest that antibody fragments are more prone to aggregation, likely due to increased hydrophobic interactions caused by lack of glycosylation from Fc region, and loss of structural rigidity from disulfide bonds (for Fab' and scFv) resulting in partial unfolding.[98] Lastly, another challenge to using fragments is their lack of commercial availability and difficulty to produce.

There are two primary ways to produce such fragments: digestion with an enzyme,[99] or expression of a recombinant antibody fragment. Recombinant production of whole antibodies requires knowledge of the sequence of the antibody and a lengthy process of production as described in **Chapter 1** (Figure 1-1),[100] hence, commercial whole recombinant antibodies are expensive and often unavailable in wide diversity of host, isotype, and targets. This is doubly true for recombinant antibody fragments. Thus, for specific and novel purposes, recombinant fragments would need to be generated in-house, requiring time, money, and expertise that the average research lab may not have. It is worth briefly noting here that there are alternatives to use of antibody fragments, namely the use of small peptides or DNA aptamers that can mimic the binding of an antibody. This topic will be discussed further in **Chapter 5,** however in summary, these mimics and aptamers share some of the same advantages such as size but can suffer from specificity (cross-reactivity) and can be similarly difficult to produce. The alternative and more approachable method for antibody fragments is by enzymatic digestion.

As discussed in **Chapter 1**, IgG antibodies can be enzymatically fragmented by a number of enzymes. The most common enzymes are pepsin, papain, IdeS, and ficin.

Briefly, these enzymes operate under different conditions, target different sequences and regions of the antibody, and has different efficiencies for different types of antibodies. The work presented here in this chapter focuses specifically on pepsin digestion, as 1) it produces bivalent $F(ab')_2$ fragments, which were the type of fragments desired by our lab, and knowing that we could further reduce to Fab' if needed; and 2) pepsin is one of the only enzymes that works reasonably well for Rat IgG antibodies, which is one of the most common host type antibodies that we use in our lab.

Pepsin is a 35 kDa member of the aspartic protease family and can be found in the stomach lining of most organisms, although the most common form of pepsin used in scientific research is derived from pigs (porcine).[101] Pepsinogen, a non-enzymatically active precursor of pepsin, is produced by chief cells in the stomach. During transportation to the acidic conditions of the stomach, pepsinogen undergoes autolytic cleavage of a 44 amino acid residues to produce pepsin.[102] Porcine pepsin is most enzymatically active at a pH of 2, and shows a 90% reduction of activity at pH < 1.5 and only 75% active at pH 4.5. At a pH of 6.5 pepsin is inactive and at pH's above 7 pepsin is irreversibly denatured.[103] Pepsins stability at acidic pH's is due to the fact that it consists largely acidic residues, approx. 42, that act to stabilize the active conformational state in the acidic environment of the stomach.[104] Loss of enzymatic activity occurs at higher pH's is caused by changes in conformational state from the loss of the hydrogen bonds and ion based interactions from acidic residues.[105] The active site of pepsin consists of two aspartic acid residues, Asp32 and Asp215, which hydrolyze the C-N peptide bonds.[106] The active site of pepsin also contains a flexible loop, or "flap", that forms over the active site after the conformational

rearrangement from pepsinogen to pepsin[107]. This flap contains several residues, like Thr77 which forms hydrogen bonds with substrate, which helps to properly orient the substrate into the active site.[108]

The specificity of pepsin is for bulky aromatic amino acids like phenylalanine, tyrosine, and tryptophan. Pepsin has shown to cleave at both the P1 and P1' positions of these residues, especially if they are next to Ala, Glu, Asp, Leu, Gly.[109] In IgG antibodies, pepsin will preferentially cleave the aromatic residues located near the hinge region first, with varying specificity based on antibody isotype and clone. Typically antibodies are digested by pepsin at pH's around 4.4 to prevent denaturation and loss of antibody function, however certain isotypes like rat IgG1 have shown significant resistance to pepsin digestion unless performed at more acidic pH's, where denaturation of the antibody allows for better access to pepsin active site.[52] Because of issues like this, pepsin digestion of an antibody must be optimized by adjusting pH, digestion time, and concentrations to alter the rate of pepsin digestion and specificity for cleavage site to produce desired fragments.

Enzymatic digestion with pepsin to produce antibody fragments is by far more approachable than recombinant production; however, even though enzymatic antibody fragmentation with pepsin has been studied since the 1960's and 70's, due to the inherent variability of antibodies, most laboratories still must optimize the fragmentation of each particular antibody by trial and error. The specific sequence, number and location of disulfide bonds, glycosylation's, and tertiary structure can vary from antibody host, isotype, and clone. This inherent variability of antibodies can also result in lower production yields than recombinant, which is one reason why enzymatically produced

fragments are rarely commercially available (although there are several commercial services willing to optimize and produce fragments for a hefty fee). More commonly, there are instead commercial kits for fragmentation which are widely available and allow each lab to perform the necessary optimizations themselves. These kits often list suggested digestion conditions based on reported trends for isotype and host species.[49,51,52,110–112] In general, the trend for efficiency of digestion by pepsin is human IgG > rabbit IgG > mouse IgG > goat IgG; and IgG2b > IgG3 > IgG2a > IgG1. However, reports of fragmentation as a function of clonal differences are anecdotal.[55] Most publications that report fragmentation efficiency often only look at a single clone, or list general isotype trends based on a small handful (1-2) clones. Thus, in-house fragmentation of an un-reported antibody can necessitate optimization by the user. Furthermore, the success criteria for fragmentation may vary based on the intended use of the fragments. Yield, purity, or efficiency of the reaction are frequent criteria. Another is the retention of binding affinity; depending on the reaction conditions, enzymatic digestion can impair function through aggregation or denaturation.[112] There is no one optimal procedure for fragmentation reactions because each antibody and reaction presents unique challenges and goals.

A systematic approach to antibody fragmentation is needed to accelerate progress in laboratories working to generate their own antibody fragments. Such a procedure may prevent optimization from devolving into a series of trial and error experiments, which can quickly become cost prohibitive due to high price of antibodies. In this paper we report the development of such an approach for fragmentation by pepsin, designed to identify a set of conditions that meets the acceptance criteria for yield, digestion efficiency, and function

as quickly as possible. We focused on digestion by pepsin to generate $F(ab')_2$ fragments, which offer a higher avidity than single Fab fragments. We systematically determined the importance of pH, amount of enzyme, and digestion time in producing functional fragments from small (50 – 1000 ug) quantities of commercially available antibodies. Three case studies were used to illustrate the method and to identify key factors to be aware of when optimizing.

2.2 Experimental Procedures

2.2.1 Filter Preparation procedure

The following procedures used Amicon Ultra 0.5-mL 50-kDa molecular weight cut off (MWCO) centrifuge filters (Fisher Scientific, Waltham, MA) for concentration and buffer exchanges of antibody samples. In preliminary work, we found that PEO-coating was critical to prevent loss of protein to the filter when working with small quantities of antibody; we estimated that up to 10 μg of antibody was lost to an unblocked filter. Therefore, the Amicon filters were coated with 100 kDa polyethylene oxide (PEO) (Fisher Scientific) before use.[113] PEO solution (50 mg/mL) was centrifuged in the filter at 14,000 x g for 3 min, then manually rinsed out with DI water. The filters were then centrifuged with DI water for 14,000 G for 3 min, then inverted and centrifuged at 1,000 G for 1 min before use.

2.2.2 Antibody fragmentation procedure

The antibody clones used were HRPN, R4-6A2, XMG1.2, GK1.5 (Bio X Cell, West Lebanon, NH), and RA3-6B2 (BioLegend, San Diego, CA). Antibodies were buffer exchanged to the desired pH by using a PEO-treated 50-kDa MWCO centrifuge filter to

put them into 100 mM formic acid buffer (pH 2.8 – 3.5) or 20 mM sodium acetate buffer (pH 4.0 – 5.0). These buffers were made in house with formic acid or sodium acetate in DI water and adjusting the pH with HCl or NaOH. All reagents were from Fisher Scientific unless otherwise noted.

Antibodies were fragmented using immobilized pepsin on 6 % agarose resin (pepsin resin, Fisher Scientific). This pepsin product was reported to have 1-1.5 mg/mL enzyme in a mix containing glycerol storage buffer. The same batch of pepsin was used for all samples (LOT: SB246536, activity 10,012 Units/mL). To prepare the pepsin resin for use, it was removed from storage buffer, pipetted into a 0.5 mL Peirce spin column (Fisher Scientific), centrifuged for 30 s at 100 G, and resuspended in the desired pH buffer (i.e. formic acid buffer or acetate buffer). Next, the immobilized pepsin and the buffer-exchanged antibody solution were mixed together so that the final concentration of antibody was 1 mg/mL. The sample was placed in an incubator at 37 °C on a shaker, shaking gently for the duration of the reaction. After the reaction, fragmented antibody sample was separated from immobilized pepsin using a 0.5-mL Peirce spin column, which allows the antibody solution to pass through while retaining the resin-bound enzyme above the column. The immobilized pepsin resin was rinsed several times with phosphate buffered saline (PBS, no calcium or magnesium). The sample (eluent from the first and subsequent rinses) was collected, then buffer exchanged into PBS and concentrated using a PEO-coated 50-kDa MWCO centrifuge filter. $F(ab')_2$ fragments were confirmed (Figure 2-2) via reduction of cysteine disulfide bonds by beta mercaptoethylamine (2-MEA, Fisher

Scientific) or affinity purification using anti-Fcγ antibody (Jackson ImmunoResearch, West Grove, PA). Antibody samples were stored at 4°C in PBS until analysis.

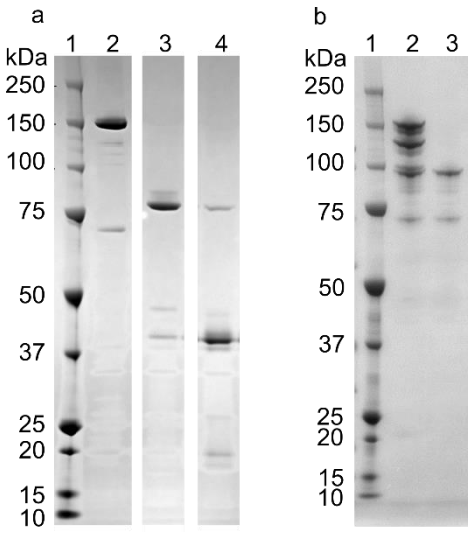

Figure 2-2: Identities of F(ab')2 fragments.were confirmed by disulfide reduction or Fc-removal **(a)** Cysteine disulfide reduction by 2-MEA shows F(ab')2 at 80 kDa to single Fab' fragments at 40 kDa. Lane 1: MW ladder; Lane 2: clone GK1.5 whole antibody; Lane 3: Pepsin digest of GK1.5 (pH 3.5, 10% pepsin, 3 hr); Lane 4: 25mM 2-MEA for 45 min. **(b)** Antibody purification using Goat anti-rat IgG Fcγ immobilized on 6% agarose resin. Purification is expected to remove any fragments with intact Fc regions, including undigested antibody. 1: MW ladder; Lane 2: Pepsin digest of clone HRPN (pH 4.4, 100% pepsin, 2 hr); Lane 3: purified HRPN digest sample after overnight incubation with anti-rat IgG Fcγ resin.

2.2.3 SDS PAGE and analysis of data

Antibody fragmentation samples were analyzed using 4-12 % Bis Tris NuPAGE SDS PAGE (Fisher Scientific) with MOPS buffer (Fisher Scientific). To preserve the structure of antibodies and $F(ab')_2$ during analysis, the samples were not reduced (no beta-mercapto ethanol) and were not heat-treated, unlike standard treatment prior to SDS PAGE. In addition to the fragmentation samples and controls, a standard curve (1 mg/mL – 0.1 mg/mL) of corresponding whole antibody was also run on the gel. A Precision Plus molecular weight ladder (BioRad, Hercules, CA) was included in lane 1. Samples were prepared according to vendor specifications using Lithium dodecyl sulfate (LDS) sample buffer 4X (Fisher Scientific) and DI water. Sample loading was calculated to never exceed 1.5 µg/lane. SDS PAGE was run at 175 V constant for 52 min, which was long enough for

the solvent front to reach the end of the gel. Gels were stained with Commassie R-250 (Fisher Scientific) as per vendor instructions.

Images of gel were collected on a ChemiDoc XRS+ (BioRad), and images were analyzed using Image Lab v5.2.1 (BioRad). Using Image Lab, the integrated stain intensity (area under the curve, AUC) was found for each protein band, and background subtraction and peak selection were performed uniformly across all samples within the same gel (Figure 2-3). Using the standard curve and molecular weight ladder, mass and molar concentrations of each band were calculated, as well as % yield (Eq 1). Digestion efficiency (Eq 2) and purity (Eq 3) of $F(ab')_2$ were calculated using peak areas. When samples were

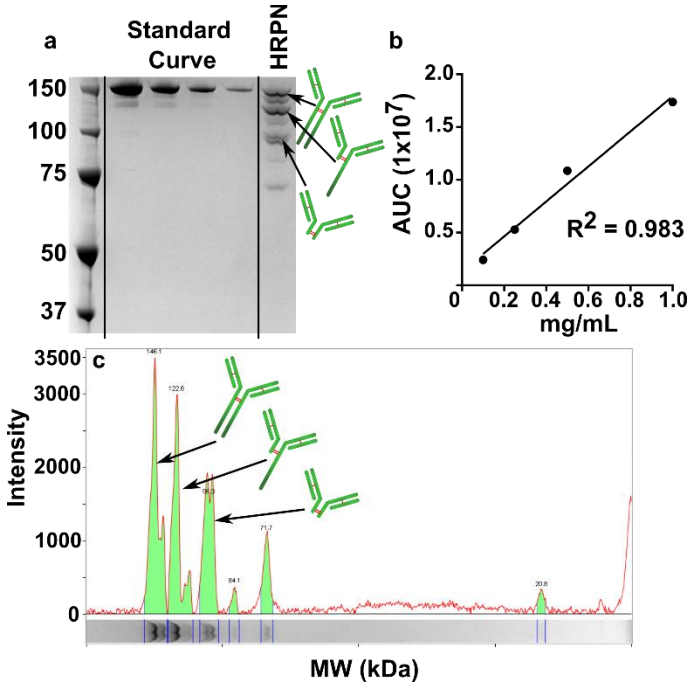

Figure 2-3: Calibration curve in SDS PAGE **(a)** Calibration curve and example antibody fragmentation on SDS PAGE. **(b)** The area under the curve for integrated intensity values of each standard is linear with respect to concentration. **(c)** An example of obtaining integrated (AUC) values from each band observed on gel for HRPN sample.

run in duplicate on the gel, the average AUC was used for analysis. LOD for Comassie stained images is approximately 0.1 – 0.05 mg/mL.

2.2.4 *Preliminary ELISA for affinity experiment*

A preliminary experiment was performed to confirmed that antibodies in solution did not excessively bind antigen on plate; i.e. binding of antibody to antigen on plate will not significantly alter the concentration of antibody in solution, and thus will not significantly affect the equilibrium kinetics of antigen antibody binding in solution. Binding of antibody onto plate antigen acts as indirect measure of how much free (unbound) antibody is in solution. The target antigen was coated onto 2 high-binding plate in PBS overnight at 4°C. Wells were blocked for 1 hour with block solution. A range of antibody concentrations were added to the first plate and incubated for 2 hours. The antibody solutions were then pipetted out and added to the wells of the second plate. HRP-conjugated goat anti-rat $F(ab')_2$ secondary antibody was added to the plates at 0.5 µg/mL in block solution. All washing steps were performed with 0.05% Tween-20 in PBS. Plates were developed using TMB substrate and absorbance values were read at 450 nm on a plate reader. Concentrations of antibody and plated antigen were chosen which resulted in < 20% difference in loss of antibody in solution from plate 1 to plate 2.

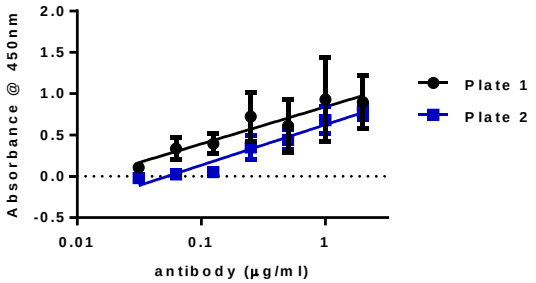

Figure 2-4: Example of preliminary affinity data. This data uses clone: R46A2.

2.2.5 *ELISA for affinity*

An ELISA was performed to measure the affinity of antibody fragments for their target protein antigen, as compared to the affinity of whole antibody precursors, by following the procedure outlined in published protocols.[114,115] In this assay, a fixed concentration of antibody was equilibrated with antigen in solution, with the antigen at concentrations ranging from below to above the IC50 of binding, and then the mixture was added to a plate coated with the antigen. Antibody that bound to the plate was detected using a labelled secondary antibody. This assay design produces a negatively-sloped sigmoidal curve whose midpoint reports the IC50 of the antibody-antigen interaction. IC50 is expected to be similar to the K_D for the low coating concentrations of antigen used here (SI methods). The detailed procedure was as follows:

$F(ab')_2$ samples from fragmentation were visually confirmed to be > 98% free of products that contained an Fc region by non-reducing SDS-PAGE before affinity analysis (i.e., > 98 % efficiency). The antigens used were recombinant mouse interferon gamma (IFN-γ, Peprotech, Rocky Hill, NJ) and soluble mouse CD4 protein–his tag (Sino Biological, Wayne, PA). The general procedure was as follows: Serial dilutions of antigen (0 – 256.4 nM, in 2-fold or 5-fold dilutions) were prepared in 1 % BSA and 0.05 % Tween-20 (Fisher Scientific) in PBS (block solution), and then mixed 1:1 v/v with a constant concentration (6.67 nM final concentration) of antibody in block solution (mixed sample). Mixed samples were stored overnight at 4 °C. Separately, the antigen was coated onto a high-binding plate (Corning Costar 96 well ½ area, #3690; Fisher Scientific) in PBS overnight at 4°C (IFN-γ at 1-3 µg/mL, CD4 0.2 µg/mL), after which the wells were blocked

for 1 hour with block solution. The mixed samples were added to the plate and incubated for 2 hours, then washed. Horseradish peroxidase enzyme (HRP) -conjugated goat anti-rat $F(ab')_2$ secondary antibody (Jackson ImmunoResearch) was added to the plate at 0.5 µg/mL in block solution. All washing steps were performed with 0.05% Tween-20 in PBS. Plates were developed using TMB substrate (Fisher Scientific) and absorbance values were read at 450 nm on a plate reader (CLARIOstar; BMG LabTech, Cary, NC). Sample curves were fit in GraphPad Prism 6 with a sigmoidal 4 parameter curve (Eq 4), where X is log of antigen concentration, Y is absorbance, min and max are the plateaus of the sigmoidal curve on the Y axis, and HillSlope describes the steepness of the slope.

$$Y = min + \frac{max - min}{1 + 10^{(Log(IC50 - X) * HillSlope)}} \quad (2\text{-}1)$$

2.3 Results and Discussion

2.3.1 Fragmentation yield and efficiency varies by clone under identical conditions

Here we focused on fragmentation of rat IgG antibodies because of their widespread use to detect antigens in murine tissues. Like other species of antibodies, rat IgGs differ in their sensitivity to pepsin depending on isotype (IgG 2c > 2b > 2a > 1), with less sensitive isotypes requiring longer digestion times, more enzyme, or lower pHs.[52] However, these isotypic trends may not always translate to individual clones or preparations of antibody. Clonal factors such as primary sequence can determine how the antibody unfolds under acidic conditions, which may impact the efficiency of pepsin cleavage.[116] In addition, the degree of glycosylation can vary based on host, isotype, and

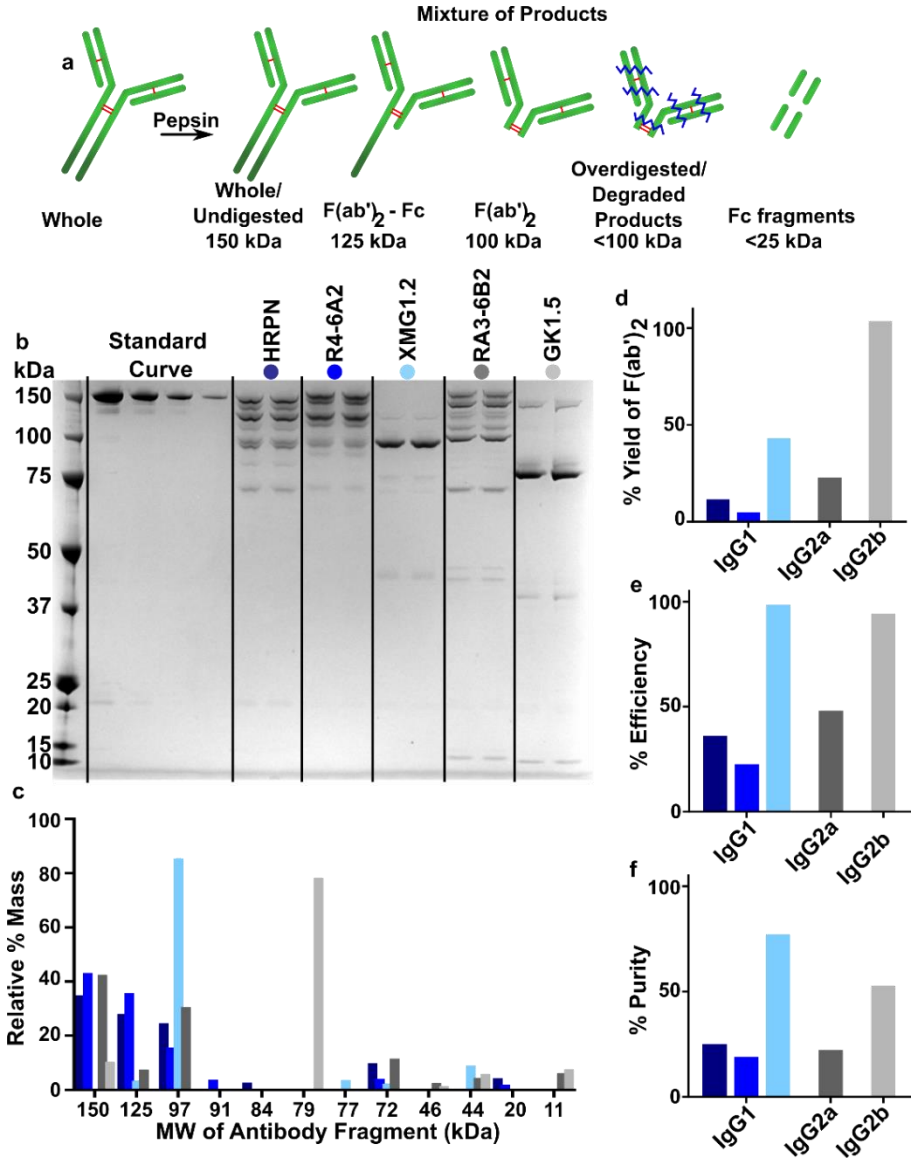

Figure 2-5: Antibodies of different clones, regardless of isotype, can fragment differentlyunder the same conditions. **(a)** Reaction scheme for pepsin digestion. The pictured fragments are the most likely products for the bands observed at those molecular weights, for a canonical 150 kDa antibody. **(b)** Non-reducing SDS PAGE of antibodies digested at pH 4.4 with 125% Pepsin (%w/w) for 2h at 37°C. N=1 per condition and were ran in duplicate on gel (two lanes per condition). Lane contents are listed above each lane. Molecular weights (MW, kDa) of the ladder in Lane 1 are listed at the left. Note that for GK1.5, $F(ab')_2$ appears at a non-canonical weight of 80 kDa. **(c)** To quantify the fragmentation pattern, the relative mass % of all sample bands were quantified using a gel imager. **(d)** % yield, **(e)** digestion efficiency, and **(f)** the purity of $F(ab')_2$ produced the tested conditions. efficiency, and **(f)** the purity of $F(ab')_2$ produced the tested conditions.

recombinant culture conditions, and the sterics of the glycans can alter the interaction between an antibody and the active site of pepsin.[117]

To illustrate this variation, we digested multiple rat IgGs with pepsin under identical conditions. Four clones used commonly for immunological experiments, spanning three isotypes, were selected for study: three clones of rat IgG1 (HRPN: isotype control, R4-6A2: anti-mouse IFN-γ, and XMG1.2: anti-mouse IFN-γ), a rat IgG2a (RA3-6B2: anti-mouse/human CD45R/B220), and a rat IgG2b (GK1.5: anti-mouse CD4). We tested a fragmentation condition that is typically recommended by commercial vendors: 1 mg/mL antibody at pH 4.4, using 125 % w/w pepsin for 2 hours.

Fragmentation followed patterns typical for most antibodies (Figure 2-4a). Residual unfragmented IgG appeared in the SDS-PAGE at ~ 140-160 kDa. Most of the antibodies ran as a doublet of peaks (except clone GK1.5), possibly due to multiple conformational states of the proteins (Figure 2-4b). This may be a result of only partially denaturing the samples with SDS and not performing a heat treatment and disulfide reduction of samples before gel analysis. Doublets were observed in undigested samples as well (data not shown). For most clones, the $F(ab')_2$ fragment appeared close to the canonical molecular weight of 90 - 100 kDa, with a partially digested product (likely loss of a single Fc heavy chain) at ~ 125 kDa. Even this could vary, however, as seen with clone GK1.5, whose $F(ab')_2$ appeared at ~ 80 kDa. The identity of the $F(ab')_2$ bands were confirmed in one of two ways: 1) treatment of the sample with 2-MEA reducing agent, which eliminated the $F(ab')_2$ band by reducing cysteine disulfides connecting the two Fab' regions, resulting in a 40-50 kDa band indicative of single Fab' fragments, or 2) passing the sample through an

anti-Fc-γ affinity column, which removed incompletely digested products and retained the $F(ab')_2$ band (Figure. 2-1).

The SDS-PAGE data was used to quantify the yield (Eq. 1, Figure. 2-4d) of $F(ab')_2$, digestion efficiency (Eq. 2), and purity (Eq. 3) of the reaction:

$$\%\ yield\ of\ F(ab')_2 = \frac{mol\ of\ F(ab')_2\ produced}{mol\ of\ starting\ IgG}\ x\ 100 \tag{2-2}$$

$$\%\ F(ab')_2\ Efficiency\ = \frac{F(ab')_2}{\begin{matrix}Undigested\ (150\ kDa) \\ +Partially\ Undigested\ (125\ kDa) \\ +F(ab')_2\ (100\ kDa)\end{matrix}}\ x\ 100 \tag{2-3}$$

$$\%\ F(ab')_2\ Purity\ = \frac{F(ab')_2}{all\ products}\ x\ 100 \tag{2-4}$$

Efficiency is distinct from purity as a readout, as efficiency reports on the conversion of the intact IgG to $F(ab')_2$, whereas purity is concerned with the ratio of $F(ab')_2$ to all fragments produced. Efficiency was defined as the percent of $F(ab')_2$ product out of undigested and partially undigested products and purity was defined as the percent of $F(ab')_2$ out of the total products, including all of the smaller fragments (Fc fragments and other small over-digested/degraded fragments). Thus, conditions that have a high digestion efficiency could potentially have a significantly lower purity due to the inclusion of smaller fragments (Figure 2-4e-f). Whether purity or efficiency is the more relevant metric will depend on the intended use of the product. Here, we used efficiency because our goal was primarily to remove the Fc region from the antibody, and smaller fragments would not affect our downstream applications.

Under these conditions, both the yield and efficiency of digestion varied more than 10-fold between clones and isotypes of rat IgG. Even amongst the three IgG1s, $F(ab')_2$ yield ranged from 4.0 to 42 %, and efficiency between 9.2 and 99 %. These data clearly demonstrate the need for tailored reaction conditions for each antibody clone if high yield, efficiency, or purity is desired.

2.3.2 *Fragmentation efficiency and yield are most sensitive to pH*

There are multiple variables that affect the efficiency and yield of an enzymatic fragmentation reaction, including reaction time, temperature, pH, concentrations of antibody and enzyme, and mixing during reaction. For these experiments, we focused on three variables that had a significant impact in prior studies: pH, ratio of enzyme to antibody (% w/w), and reaction time.[112] The reaction time and the ratio of enzyme (pepsin) concentration to substrate (antibody) concentration drive the reaction based on enzyme kinetics, whereas pH has a more indirect effect by impacting enzymatic activity and protein unfolding. Pepsin is most active at a pH of 2, and gradually loses activity as pH is increased until being irreversibly denatured at a pH of 6.[103] In addition, it is thought that as pH decreases, some antibodies may slightly unfold or denature, increasing the accessibility of the antibody to the pepsin's active site.

Because the three selected variables are not independent, small trial-and-error-based changes in reaction conditions can easily result in under or over-shooting the desired efficiency, with a trade-off in yield. For example, the optimal enzyme concentration likely increases at higher pH as the enzyme loses activity, so changing only the concentration or only pH is not ideal. In this situation, a systematic Design of Experiments approach, (or

alternatively the use of artificial neural networks or machine learning) proves especially useful to quickly identify the most critical parameters.[118] Rather than vary one variable at a time, multiple variables are tested simultaneously to identify critical variables and co-dependencies.

Here, we used this systematic approach to determine which variable had the greatest effect on the % yield of the $F(ab')_2$ fragment and efficiency of the reaction. We fragmented a rat IgG1 isotype control (HRPN), an inexpensive and readily available antibody, and simultaneously tested all three variables with two levels each (2^3 = 8 combinations of conditions). The array of conditions tested was representative of oft-suggested conditions for antibody fragmentation: pH at 2.8 or 4.4, pepsin concentration at 1 or 20 %, and reaction time at 2 or 6 hr. The antibody concentration was kept constant at 1 mg/mL, and all reactions were conducted at 37 °C with continuous gentle agitation.

Over this range of conditions, a change in pH had the greatest impact, followed by change in concentration of pepsin (Figure 2-5). Digestion at a low pH of 2.8 produced the highest yields and efficiency of HRPN $F(ab')_2$, reaching 99 % yield and 100 % efficiency at the optimal condition (Table 1). While it is possible that varying the pepsin concentration or time over a greater range (e.g. 1 %– 200% pepsin or 1 h – 24 h) may increase the impact of those variables, higher concentrations and times can lead to over-fragmentation and/or degradation of the antibody.[119]

2.3.3 *Identification of acceptance criteria*

Practically speaking, for most experiments, optimizing for the highest possible yield and efficiency is unrealistic and unnecessarily laborious. It is more useful to define

in advance the "acceptance criteria" – the minimum values of yield and efficiency (and function) that are considered sufficient. The values of acceptance criteria will depend on the application. The requirement for % yield is likely driven by cost considerations and the quantity of the fragment that is required for downstream use. The required purity and efficiency of the reaction depends on both the intended use and how easily the products can be purified by subsequent processing. Finally, the requirement for functionality (i.e. binding affinity) depends on whether the fragment will be used for antigen binding, versus simply being sequenced.

Whether reaction efficiency is a priority likely depends largely on the available options for downstream purification. When working with small quantities of antibody (50 µg per reaction), isolation of functional $F(ab')_2$ fragments from other fragments may be

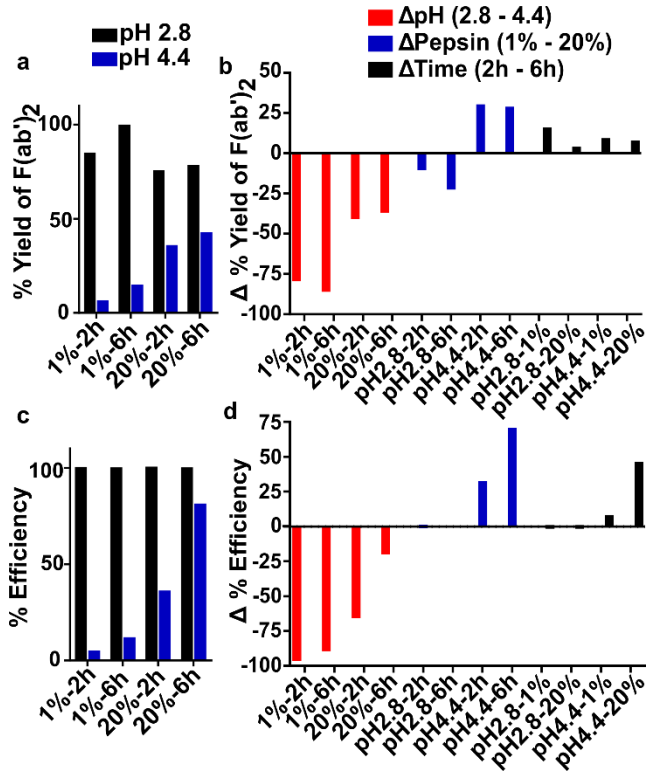

Figure 2-6: A change in pH had the greatest effect on yieldand efficiency of $F(ab)_2$ production by pepsin. Rat IgG1 clone HRPN was fragmented under $2^3 = 8$ conditions of pH, % pepsin (% w/w), and time. (a) % molar yield of $F(ab')_2$ produced in each condition. (b) The change in yield as a result of increasing pH, % pepsin, or time. (c) % efficiency of reaction in each condition. (b) The change in efficiency as a result of increase pH, % Pepsin, or time. N=1 for each reaction condition. Conditions were measured twice on SDS PAGE.

challenging. Microscale size exclusion chromatography is the best option, but requires specialized equipment.[120] For many antibodies, affinity-based techniques such as proteins A and G, which bind to antibody Fc regions, may prove a suitable means to remove residual unfragmented or partially fragmented products from the mixture.[121] For others, however, this approach is not viable. For example, protein A has little to no affinity for rat IgG. Protein G does have some affinity for rat IgGs, especially rat IgG2a, but it binds both the Fc and Fab regions of the antibody, compromising its use for purification.[121–123] Thus, for easily purified antibodies, especially those available at large scale, a mediocre efficiency (~50-80%) may be acceptable, but for others a much higher efficiency is needed.

2.3.4 Case Studies: *On reaching acceptable yield, efficiency, and function in real life*

As a series of case studies, this approach to optimizing fragmentation was applied to three rat IgG's (Table 1). We intended to use the F(ab')$_2$ fragments as detection reagents in applications such as flow cytometry, ELISA, and immunofluorescent staining of tissue.[92] Acceptance criteria were determined based on this set of applications as follows. Given that the selected clones were available in bulk from commercial vendors, we determined that a yield of > 50 % was sufficiently cost effective to accept. However, for some of the intended applications, residual Fc regions would be detrimental. Because of the difficulty of further purifying rat F(ab')$_2$ fragments, we prioritized reaction efficiency over yield, and initially required a efficiency of > 90%. Finally, because we intended to use the fragments for antigen binding, it was also critical that the binding affinity remain high, ideally within 2-fold of the IC50 of the original antibody as measured by an affinity ELISA. In each case,

we first screened conditions for yield and efficiency, then confirmed the binding affinity of the product.

Table 2-1: Optimized digestion conditions and results

Clone	Isotype	Antigen	Apparent $F(ab')_2$ MW	pH	Time (h)	% Pepsin (w/w)	Yield	Efficiency	IC50 (nM) of $F(ab')_2$
HRPN	IgG1	α-HRP	100	2.8	6	1	99.2	99.4	-
GK1.5	IgG2b	α-mouse CD4	80	3.5	2	10	100	91.8	14.5
R4-6A2	IgG1	α-mouse IFN-γ	100	5.0	24	100	14.7	99.8	7.4
XMG1.2	IgG1	α-mouse IFN-γ	100	5.0	4.5	50	67.8	97.9	0.41

- Indicates that sample was not tested/measured

Case Study 1: First, we sought to produce $F(ab')_2$ fragments from anti-mouse CD4 (clone GK1.5), which is a rat IgG2a antibody. CD4 is a canonical phenotypic marker for helper T cells in flow cytometry and immunofluorescence. Based on the results shown above, in which pH had the most significant impact on the fragmentation, the pH was varied in three levels from 2.8, the optimal value for HRPN, and the traditional pH 4.4, which is recommended in many commercial kits. The % pepsin was varied simultaneously in two levels from 1 to 10%. Reaction time was held constant at a convenient value (2 hr).

Once again, we observed that pH had a substantial impact on yield and efficiency (Figure 2-6a-b), especially at lower pepsin concentration. Pepsin concentration also had a substantial impact, especially at higher pH, where it was presumably less active. Fortunately, one of the tested conditions (pH 3.5, 10% pepsin, 2 hours) surpassed the

acceptance criteria for yield and efficiency (Table 1), and thus further optimization was not required. The $F(ab')_2$ product from that condition was subsequently tested for affinity, and was found to have comparable affinity to its whole antibody precursor (~15 nM IC50 for both; Figure 2-6c). Thus, this condition was accepted for further use. This case study demonstrates the usefulness of screening multiple pHs over a limited range of pepsin

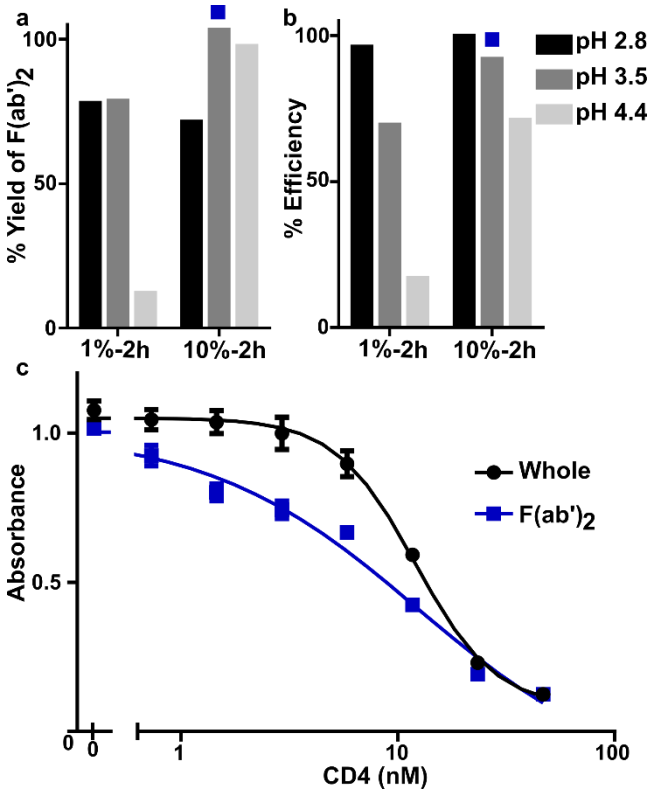

Figure 2-7: Case Study 1:pH had the greatest effect on F(ab')2 yield for anti-CD4 clone GK1.5 **(a)** % molar yield and **(b)** efficiency of $F(ab')_2$ produced during fragmentation. N=1 per condition. The condition marked with blue square was tested by **(c)** indirect ELISA to measure affinity of $F(ab')_2$ fragment as compared to whole antibody. IC50: $F(ab')_2$ – 14.5 nM; Whole – 15.6 nM. N=3 per condition. Data was fit with 4 parameter curve in GraphPad Prism.

percentage and reaction time, which can quickly identify a near optimal condition that can be further refined if needed.

Case Study 2: We found that for some antibodies, despite modulating pH, time, and % pepsin, it was difficult to obtain high yield and efficiency simultaneously. For example, this phenomenon occurred with fragmentation of anti-mouse IFN-γ (clone R4-6A2), a rat

IgG1 antibody. IFN-γ is a cytokine, i.e. a protein involved in extracellular signaling between immune cells, that is critical for adaptive immunity. In attempting to optimize this antibody, we tested pHs of 3.5, 4.0, and 5.0 with a wide range of pepsin concentrations and reaction times, in an extensive series of optimization experiments. We observed that a pH of 5.0 produced the greatest yields, and at lower pH such as pH 2.8 the antibody denatured and aggregated (data not shown). At pH 5.0, yields were never above 50 %, and increasing the efficiency by increasing the pepsin concentration or time often came with a further tradeoff in yield due to over-fragmentation (Figure 2-7a,b). Given our acceptance criteria and priorities outlined above, the most suitable condition was pH 5.0 with 100 % pepsin w/w for 24 hours, which had the highest efficiency but the lowest yield (Table 1). When the $F(ab')_2$ fragment from that condition was tested for affinity, its IC50 was comparable to the affinity of whole (unfragmented) antibody (Figure 2-7c), so this condition was

accepted for further use. This case study demonstrates the need to compromise between acceptance criteria for some antibodies.

Case Study 3: As a final case, we generated F(ab')$_2$ fragments from anti-mouse IFN-γ (clone XMG1.2), a rat IgG1 antibody. This antibody forms an ELISA pair with R4-6A2 for detection of IFN-γ. Based on the results above, we initially screened several conditions at pH 2.8 and 4.4 (Figure 2-8a,b). Digestion at pH 2.8 resulted in denaturation and aggregation of antibody and thus was unable to be quantified. A pH of 4.4 produced high efficiency with 50% pepsin, but yield was lower than desired. Therefore, in an effort to increase yield, we kept the 50% pepsin concentration, raised the pH to 5.0, and screened reaction time as a third variable (Figure 2-8d,e). This increased the yield with minimal loss of efficiency. Interestingly, in both scenarios, the apparent affinity of the F(ab')$_2$ fragment was ~50-fold higher than that of the intact antibody (Figure 2-8c,f). One potential

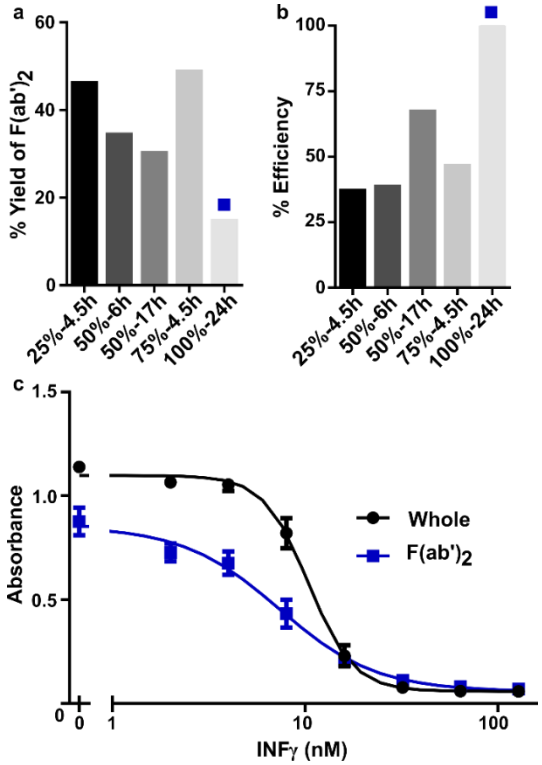

Figure 2-8: Case study 2:For one antibody, the yield of F(ab')$_2$ was inverse with respect to efficiency. (a) % molar yield and (b) efficiency of F(ab')$_2$ fragment production for anti-IFN-γ clone R4-6A2 at pH 5.0. N = 1 per condition. The condition marked with a blue square was tested by (c) indirect ELISA to measure the affinity of the F(ab')$_2$. IC50 for F(ab')$_2$ – 7.4 nM; Whole – 10.4 nM. N=3 per condition, data was fit with 4 parameter curve in GraphPad Prism.

explanation may be that the removal of the Fc region increases the flexibility of the hinge between the Fab arms, reducing steric strain and improving bivalent binding.[32] In summary, this case study indicates that even small modulations in pH can increase yield, especially for antibodies that aggregate at low pH, and that $F(ab')_2$ fragments can sometimes have improved affinity over their parent IgG.

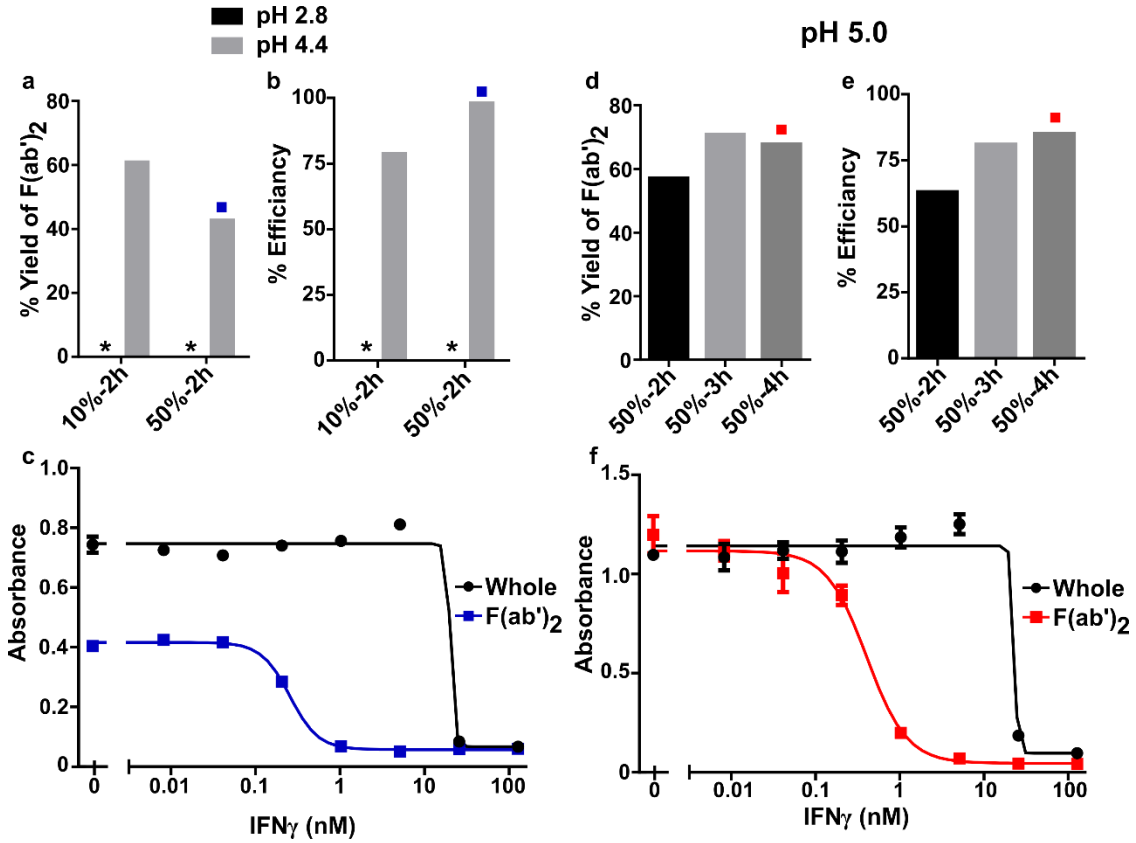

Figure 2-9: Case study 3:Yield and efficiency can vary with pH. Digestion of anti-IFN-γ clone: XMG1.2 at pH 2.8 and pH 4.4 has **(a)** % molar yield and **(b)** efficiency of $_{F(}$ab')$_2$ produced (* aggregation/ unable to be quantified). **(c)** affinity ELISA of best condition (marked with blue square). IC50: F(ab')$_2$ – 0.25 nM; Whole – 20.4 nM. Digestion at pH 5.0 shows increased **(d)** yield and (e) efficiency of F(ab')$_2$ produced, and has maintained affinity as measured by **(f)** affinity ELISA (tested condition marked with red square). IC50: F(ab')$_2$ – 0.41 nM; Whole – 23.0 nM. N=1 per fragmentation condition and ran in duplicate on SDS PAGE. N=3 per indirect ELISA condition, data was fit with 4 parameter curve in GraphPad Prism.

***2.3.5** Summary: Suggested optimization procedure*

Given the wide range of possible conditions for fragmentation, it is reasonable to ask where one should start when working with a new antibody. If resources are abundant, then a thorough initial screen could be performed over a wide range of conditions (Figure 2-9), using Design of Experiments to reduce the number of conditions tested. However, often both time and reagents are precious. If a simple first experiment is desired, based on

our experience with the antibodies above, we suggest the following four conditions: pH (2.8 and 4.4) x pepsin (10 % and 50 %), with a reaction time of 2 hours. Afterwards further optimization can be performed if the acceptance criteria are not met, using the results of the first screen to point to the next set of conditions. After screening, once a condition with suitable yield, efficiency, and affinity is found, further minor changes to the condition can be made to "dial in" on the exact specifications desired. For example, one could increase digestion time by 10-30 minutes to boost digestion efficiency by 5-10 % depending on exact conditions used.

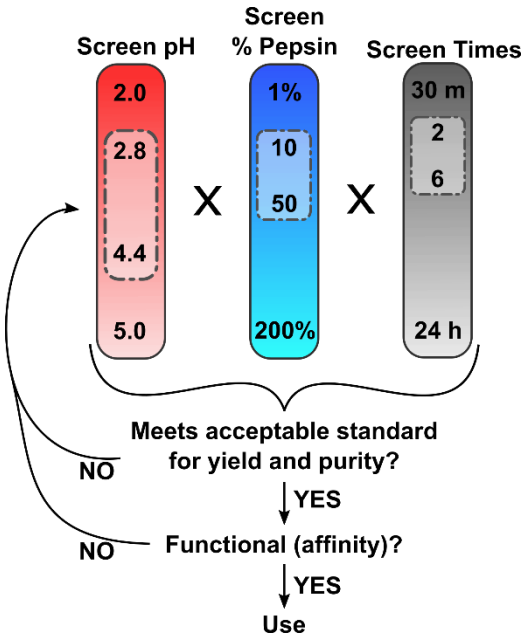

Figure 2-10: Suggested approach to optimization of fragmentation by pepsin. Each column represents one variable for optimization. Ideally, at least pH and % pepsin should be optimized simultaneously. The values displayed on each column represent its normal range for fragmentation. Highlighted in gray dashed boxes are conditions suggested for a simple first experiment: pH (2.8 and 4.4), Pepsin (10% and 50%), and a time of 2 or 6 hours. Afterwards further testing can be performed if needed to meet acceptance criteria.

2.4 Conclusions

In this work we have outlined a simple yet systematic strategy to reach desired levels of yield, efficiency, and function of $F(ab')_2$ fragments from small quantities of IgG, including analysis of affinity after enzymatic digestion. We determined that optimization over a range of pHs has the largest impact, likely because it directly impacts the activity of

pepsin and the steric constraints of interaction with the active site of the enzyme. pH screening may be followed by or conducted in parallel with optimizing the ratio of pepsin to the antibody. Reaction time had only a small impact and did not always require optimization. This process can be re-iterated until desired yield, efficiency, and function of $F(ab')_2$ fragments is achieved. This general outline for fragmentation has been performed successfully for several antibodies used routinely in our lab. We envision that this work will provide a quick and cost-effective guide for researchers to produce in-house generated antibody fragments, without the need for recombinant expression or haphazard trial and error approaches.

Chapter 3: Small scale, parallel optimization of protein conjugation reactions on a user-friendly microchip

3.1 Abstract

Labeling of antibodies with fluorophores is a common precursor to immunostaining, immunoblotting, and other detection techniques. The resulting mole ratio of label-to-protein, or labeling ratio, significantly impacts the function of the conjugate and should ideally be optimized carefully prior to reagent validation. However, current optimization is performed empirically in conventional microcentrifuge tubes, which require a minimum of 30-50 μg protein per reaction due to surface adsorption and minimal volume and concentration requirements. For precious proteins such as antibodies, optimization at this scale is cost prohibitive or even unfeasible. A simple, rapid analysis of protein labeling is needed to conserve time and reagents, and optimized reagent ratios should be directly scalable for lab use. Slip Chips offer a unique solution to these issues by providing a hand-operated platform that requires no specialized equipment or training to operate. To perform and analyze multiple labeling reactions in parallel, we have developed a Slip Chip microfluidic device that uses 10-fold less reagent and performs multiplexed label ratio reaction for optimization, excess reagent removal, and UV-Vis detection on chip. This device is designed to user-friendly, requiring no specialized equipment other than pipet and plate reader.

3.2 Introduction

Labeling of antibodies with fluorophores is a common precursor to immunostaining, immunoblotting, flow cytometry, and other bioanalytical studies. While there are a wide variety of commercial fluorescent antibody reagents available, there can often be a lack of available reagents for niche or developing areas of study. Or as is often the case, the antibody is available commercially, but only with fluorophores that do not work with the user's specific microscope filters or with experimental setup/fluorophore panel chosen. Thus, antibodies will have to be conjugated in-house.

There is decades old chemistry showing how to provide stabile covalent linkages between proteins and labels such as fluorophores, chromophores, nucleic acids, and drugs.[36] Labeling reactions often use functional groups such as amines and sulfylhydryls to bond to, using chemistries such as N-hydroxysuccinidmidyl esters (NHS-esters) and maleimides, respectively.[35–37] NHS-ester amine conjugation chemistry is often used as it relies upon amine residues that can be commonly found on most all proteins, as opposed to more rare and site specific cysteine sulfhydryls. However, as amine residues are highly abundant and located all over the protein, the degree of derivatization must be precisely controlled as it can impact both the proteins functionality and the labels activity. High labeling ratios may sterically obstruct or chemically disrupt the binding region (CDR) of the antibody, while low ratios may offer insufficient activity. It may also be that within a normal Poisson distribution of label ratios, antibodies with higher ratios do not bind to their targets, thus decreasing the concentration of functional antibody in solution.[39,40] This can be further exacerbated in antibody fragments, as there is less non-CDR regions that could

be labeled. In addition to affinity, many fluorophores lose emission intensity at high labeling ratios due to self-quenching.[39,124,125]

Typical target ranges (using NHS esters) are ~2-5:1 for fluorophores and ~3-4:1 for

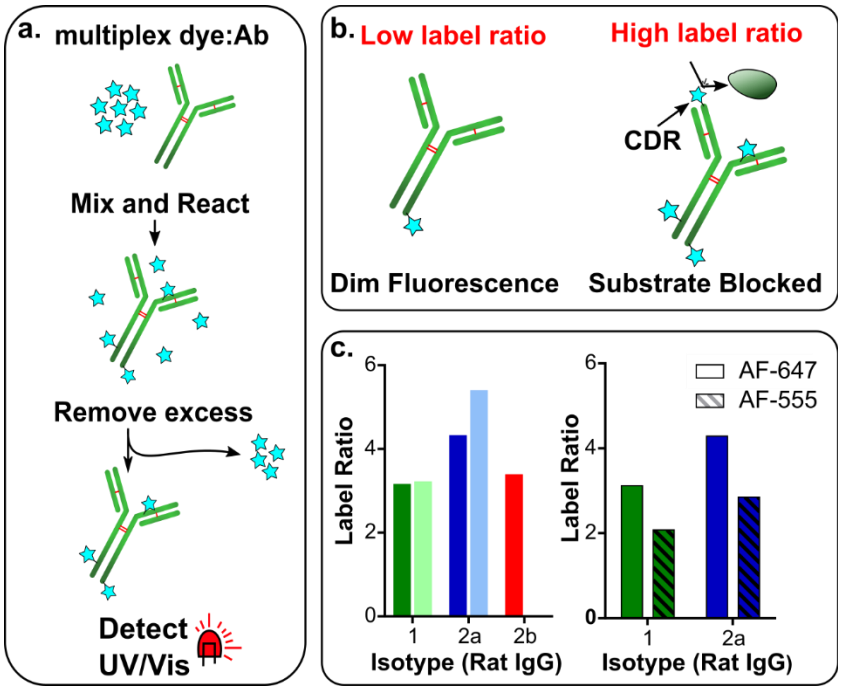

Figure 3-1: Antibody labeling **a)** Schematic for optimization by testing multiple dye:Ab ratios. **b)** If label ratio is too low then fluorescent intensity is low, and if label ratio is high then fluorophores may block binding region (CDR) and lower affinity. **c)** Example label ratios results of different clones and isotypes of Rat IgG's labeled with both succinimidyl ester Alexafluor-647 and Alexafluor-555.

drug conjugates, however the target ratio may vary by application, specific antibody, and conjugate label.[41,42] Reaction optimization is often required because labeling ratios are difficult to predict (Figure 3-1).[43] These reactions vary in efficacy depending on the prevalence of the targeted functional group and the specific dye used; in addition most of the reagents are strongly susceptible to hydrolysis, causing variation over time and between lots.[126–128] Because of the variability of the conjugation reaction and its potential effect on both antibody and label function, it is clear that labeling should be optimized for any new conjugate, prior to or as a part of reagent validation.

Optimization is often accomplished through a series of experiments performed with varied mole ratios of linker to protein (e.g. 10 – 20-fold excess). Using traditional benchtop methods, such as pipetting into sample tubes and using centrifugal filters, consumes a substantial amount of reagent (30-50 ug per reaction). The minimum reaction amount is due to practical concerns, such as surface adsorption (~10 μg) of protein onto sample tubes and filters.[113,129] Losses like this can be difficult to prevent, as blocking the surface with non-specific proteins like BSA, a common practice for immunoassay plates, cannot be done without interfering with certain cross-linking chemistries (e.g. succinimidyl esters). Other reagents such as Tween or polyethylene glycol (PEG) can be used to block non-specific adhesion, but they cannot prevent all loss.[113] In addition to surface adsorption, some loss due to dead volume and surface wetting can occur during separation of excess un-reacted label from protein. Often size exclusion separation filters require minimal volumes (~10-20 μL) to overcome these limitations. Furthermore, labeling reactions often recommend to use protein concentrations ≥ 1 mg/mL for reasonable reaction timescales (< 24 hr).

During labeling there are often 2 competing reactions: the conjugation of the linker to the target protein, and hydrolysis of the linking reagent. When reagents are at lower concentrations, the reaction slows, allowing more time for linking reagents (e.g. NHS esters) to hydrolyze.[130] For proteins that are expensive or difficult to produce, systematic optimization at this scale is cost prohibitive. This may cause researches to use a series of guess and check experiments, rather than starting with a systematic approach. A simple,

rapid analysis of protein labeling is needed to conserve time and reagents, and optimized reagent ratios should be directly scalable for lab use.

As discussed in **Chapter 1,** there are have been several publications aimed at testing/validating antibodies with traditional PDMS based microfluidics, and of those, several investigate on-chip labeling and purification of antibodies and fluorophores; often with capillary gel electrophoresis (CGE) and laser induced fluorescence (LIF). However, many of these are not specifically aimed at optimizing labeling reactions for scale-up; rather they are either aimed as a reagent prep method for a total analysis system (TAS) or as a direct method to generate labeled antibodies for use.[131–133] Those that do investigate labeling optimization are not multiplexed, and may calculate labeling ratio of sample off chip by more traditional methods such as UV/VIS spectrophotometry.[134] Slip Chips offer a unique solution to these issues by providing a hand-operated platform that requires no specialized equipment or training to operate. Slip Chips, first developed by the Ismagilov lab, are a unique subset of microfluidics that benefit from the traditional conventions of microfluidics such as using small volumes of sample/reagent nL to µL and ability to be multiplexed. Slip Chips also offer the additional advantage of being reconfigurable and allowing for the breaking/connecting of fluidic pathways or reservoirs.[135] A Slip Chip is made of two rigid surfaces, often glass, that a pressed together with a thin layer of immiscible oil in between, allowing for the surfaces to slide past one another. Features etched into the surfaces contain aqueous fluidic droplets that can then be connected or isolated with a simple slipping motion. This makes it ideal for performing tasks such as

dilution or mixing of samples on chip, without the need for pump-controlled flow or complicated valving systems (i.e. chip is hand operated).

Slip Chips have been used to perform chemical assays, PCR, and culture of both bacterial and mammalian cells.[136–139] However, combining multistep chemical reactions with molecular separation is an innovative use of the Slip Chip design. In addition, while electrophoresis on a Slip Chip has been demonstrated,[140,141] that technology requires integration of electrodes to the chip and an external power supply. Simple, power-free size-based molecular separation has not been demonstrated in a reconfigurable device. In this paper we cover a Slip Chip device which is designed to perform all steps of a conjugation reaction optimization on chip: dilution series of dye on chip with multiplexed labeling reaction, removal of excess fluorophore, and UV-VIS analysis. This chapter contains on-going research, and as such will contain information regarding the philosophy of the design to meet specific goals, initial and on-going test results, detailed information regarding troubleshooting major challenges, as well as discussing proposed future experimentations.

3.3 Methods

3.3.1 Fabrication

Glass etching – Chip designs were etched in 2.5 x 2.5 inch photomask blanks (Telic Company) of fused silica quartz glass with 1 µm low reflective chrome and 1 µm AZ1500. Designs were patterned with EVG620 mask aligner (EVG), AZ developer (AZ Chem), chrome etch 20% w/v $(NH_4)_2Ce(NO_3)_6$ with 0.6M $HClO_4$ (Fisher Scientific), and wet etched in HF + HNO3 (30: 4.5: 10 v/v HF:HNO3:H20).

The sample feature dimensions of the chip were designed for compatibility with analysis on plate reader; 300 µm depth and 2 mm diameter. Volume of sample features were calculated (Equation 1), where V is volume, r is radius of circular mask feature, and h is etched height. Dimensions of dilution features were calculated by same method to precisely dilute samples from 1x to 0.8x, 0.6x, 0.4x, 0.2x (100 um depth). Corrections for exact dilutions were made by calculating volumes based on observed etch dimensions of features. Etched dimensions were observed by widefield microscopy (Zeiss Zoom). Holes in chip glass were drilled @ 1500 rpm with Dremel 4000 rotary tool (Dremel) in a Dremel Drill Press (Dremel 220-01 workstation, Dremel) and 1/32" DLC coated carbide end mill; ball end, 4 flute; and a 1/8" Carbide ball end mill, DLC coated drill bits (McMaster Carr)

$$V = \pi r^2 + 0.5\pi^2 h^2 r + {}^2/_3\,\pi h^3 \tag{3-1}$$

***3.3.2** Silanization*

The glass chips were salinized with Trichloro(1H,1H,2H,2H-perfluorooctyl)silane fluorosilane (Sigma Aldrich) after 10min plasma cleaning via vapor deposition for 90 minutes. To prevent atmospheric humidity affecting vapor deposition of silane, the desiccator was purged with N_2 gas (Praxair). Afterwards the chip was placed in a 120 °C oven for 30-60 minutes, and then rinsed with ethanol (Fisher Scientific) and deionized water.

Methacrylate silane: A 0.01" thick PDMS (Stockwell Elastomerics) mask was cut using Cricut Maker (Cricut, South Jordan, UT). The PDMS mask was placed on the chip and covered all surface features except for the features to contain the gel. The chip was

placed into a vacuum chamber for 10 minutes, then removed and checked for any air pockets, loss of contact between mask and chip. The chip was placed back into the vacuum chamber for 10 minutes and then plasma cleaned for 1 min to remove fluorosilane from un-masked (gel) features. The PDMS mask was removed and 3-(Trimethoxysilyl)propyl methacrylate (methacrylate silane; Sigma Aldrich) 1:20 in Ethanol was then deposited onto the chip by immersion into silane solution for 90 minutes.

3.3.3 *Prep of gel*

The top layer of the chip containing gel features was assembled against thin PDMS backed with a thick glass coverslip. A solution of 30% polyacrylamide gel @ (29:1 acrylamide : bisacrylamide) (Fisher Scientific) with 4 mg/mL Lithium phenyl-2,4,6-trimethylbenzoylphosphinate (LAP) photo-initiator (Fisher Scientific) was pipetted into the chip. The gel was exposed to 8 mJ/cm2 of 405 nm light for 1 minute. The thin PDMS and glass coverslip was removed, and the Slip Chip layer with gel was stored in DI water until use.

3.3.4 *Chip assembly (and reagent pipetting)*

Both layers of the chip were dried and any dust removed by blowing with N2. The chip was assembled with Fc40 oil with 0.5% triethyleneglycol mono[1H,1H-perfluorooctyl]ether surfactant (RfOEG, made in house). Reagents of protein sample in PBS buffer, fluorophore dye in DMSO, and DMSO or PBS buffer were pipetted into the chip.

3.3.5 *Surface tension measurements*

Contact angle measurements of DI water and PBS droplets on fluorosilinazed chip surfaces were taken on a ram-hart goniometer in Fc40 oil. Images were analyzed by Image J.

3.3.6 *Characterization of selective salinization*

To test selective surface modification of the chip with fluorosilane and methacrylate silane, 20% polyacrylamide gel (Fisher scientific) in water with 1mg/mL LAP photoinitiator was pipetted over the surface features of the chip and crosslinked with 405nm light. The gel was then scraped away to observe any regions that adhered (due to surface crosslinking of gel to methacrylate silane) or wetted to the surface of the chip (lack of fluorosilane).

3.3.7 *Dilution of dye*

Dilutions of dye were validated by testing multiple dilution ranges on chip with a model dye iron (III) thiocyanate ($FeSCN^{2+}$). Concentrations of $FeSCN^{2+}$ were made using 1M solutions of FeNO3 and KSCN (Fisher Scientific). $FeSCN^{2+}$ solutions were loaded onto the chip along with deionized water. Dilutions were performed by slipping dye wells ($FeSNC^{2+}$) over buffer wells (DI water) and letting sit for 10 minutes. The wells were then slipped apart and imaged by brightfield widefield microscopy (Zeiss Zoom). Using Fiji (Image J) the average pixel intensity of each dye sample and background was taken and transformed into an absorbance using the equation $A = -\log(\frac{Pix\ Int\ dye}{Pix\ Int\ bkg})$. On chip dye dilutions were compared to off-chip benchtop dilutions using pipets. Off chip dilutions

were loaded onto chip for image analysis to control for differences in pathlength and background noise.

3.3.8 *Diffusion of sample*

Time for complete mixing/diffusion of sample was tested by filling dye wells with 0.1 mM fluorescein solution in DI water, and slipping over sample well filled with DI water. Diffusion of dye was imaged by widefield microscopy (Zeiss Zoom). Images were taken at 1, 5, 10, 15, and 30 minutes.

3.3.9 *Extraction of dye using an on-chip size exclusion gel*

A sample well containing 1 mM free fluorescein and 0.25 mg/mL AlexaFluor 594 (AF-594) labeled antibody was slipped over a series of three wells containing 20% polyacrylamide (Fisher Scientific). A line-scan was obtained to measure fluorescent intensity over time. Image analysis was performed with Image J. We should note that we are not measuring the pore size of the gel, but rather using concentrations of gel that are reported to be withing the desired pore size range.

3.4 Results:

3.4.1 *Design considerations and fabrication*

This device goal of this device is to provide a low-cost, easy to use, analytical tool to perform multiple antibody – succinimidyl ester conjugations on chip with readout. In order to facilitate these goals, we chose the Slip Chip format, which as mentioned above, allows for the connecting and breaking of fluidic pathways by slipping each layer of the chip relative to one-another (Figure 3-2a). This prevents the need for complex valving systems and need for expensive pumps. Additionally, the reagents can be added simply by

pipet and the device can be hand operated. This makes the device approachable for non-microfluidic savvy users. To further enable easy-to-use compatibility, we chose to UV/VIS as the readout method and design the chip to be placed into a common plate reader for analysis.

The device is designed to perform 6 conjugation reactions, including a control, and uses <10 uL total of antibody (at 1mg/mL), or other large protein of interest, and < 5uL total of a succinimidyl ester - fluorescent dye, or other small MW UV/Vis quantifiable analyte (Figure 3-2 b,c). The features of this device are designed with circular or curved geometry to prevent a need for high pressure filling, as rectangular geometry often requires higher pressures to overcome surface tension of aqueous droplets to completely fill in the corners. In addition, so as to prevent unwanted mixing of different loaded reagents, the features on the device have been appropriately spaced.

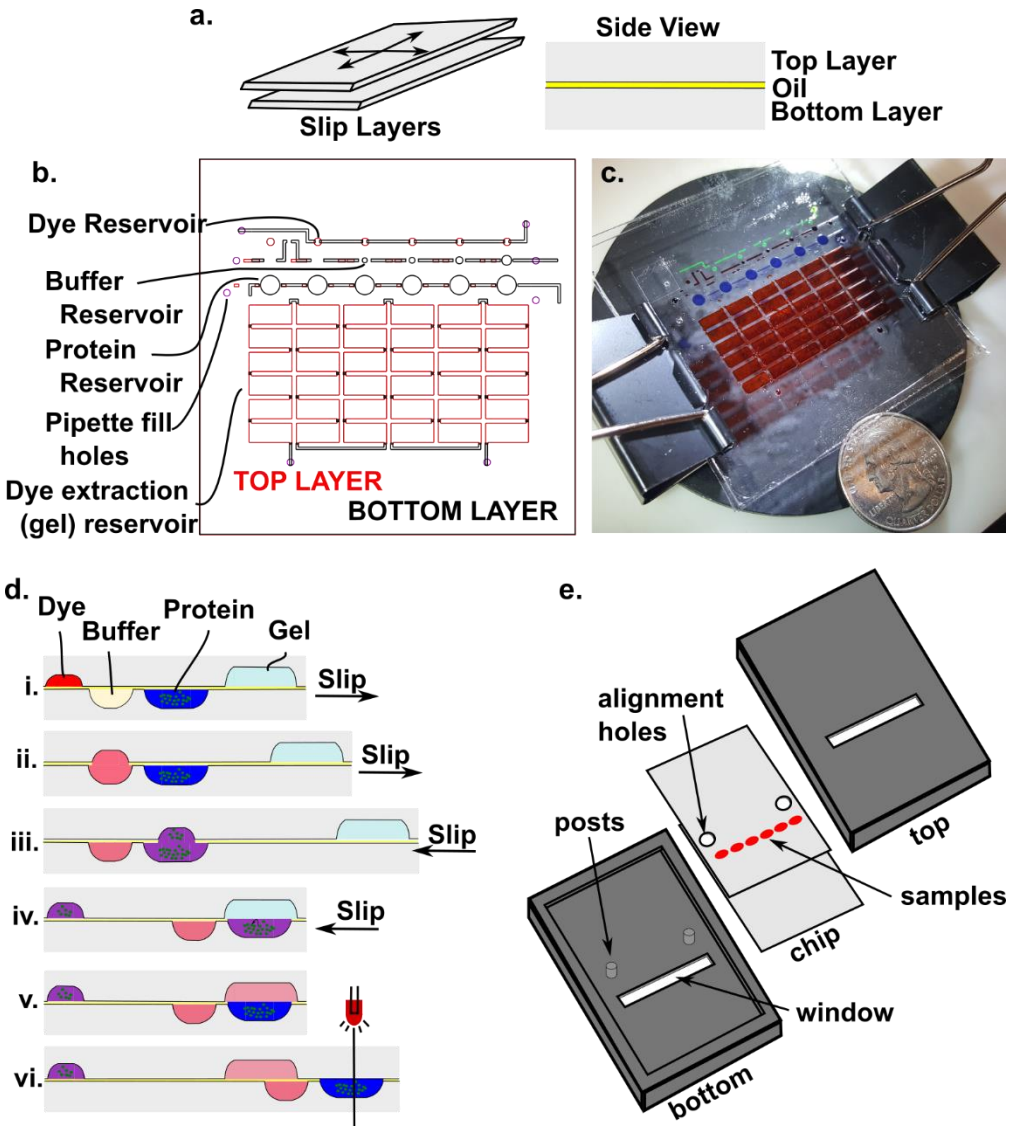

Figure 3-2: Fabrication and design of Slip Chip. A Slip Chip is comprised of **a)** 2 layers separated by a thin layer of oil that can slip by one another. **b)** Preliminary design of Slip Chip and **c)** example of Slip Chip filled with dyes. Green for fluorescent dye, brown for buffer, blue for protein sample, and red for gel. **d)** Procedure schematic for operation of Slip Chip. **e)** Slip Chip can be fitted into a 3D printed holder that can then be placed in a plate reader for analysis.

The device itself consists of 3 functional sub-units: dilution, labeling reaction, and removal of excess dye. Then followed by UV/Vis analysis on a plate reader. On-chip

dilution of the dye is set to specific pre-determined ratios, as set by the etched dimensions (Fig 3-2d ii). However, the specific range of the dilution can be altered by loading in different starting concentrations of dye (Supplemental excel sheet). For the labeling reaction, the volume of the dye reservoir is kept at 5% of the volume of the protein sample so as to prevent (mitigate?) denaturing of the sample, for dyes in non-aqueous solvents like DMSO (Fig 3-2d iii). Removal of excess dye has been initially designed to be performed by a series of on chip dialysis steps wherein reservoirs are filled with a dense gel and a photoinitiator. Once crosslinked, the gel acts as a molecular weight cut off (MWCO) filter, where large MW protein sample cannot diffuse into the gel but small MW dye can (Figure 3-3). This passive size-based diffusion separation method was chosen for several reasons.

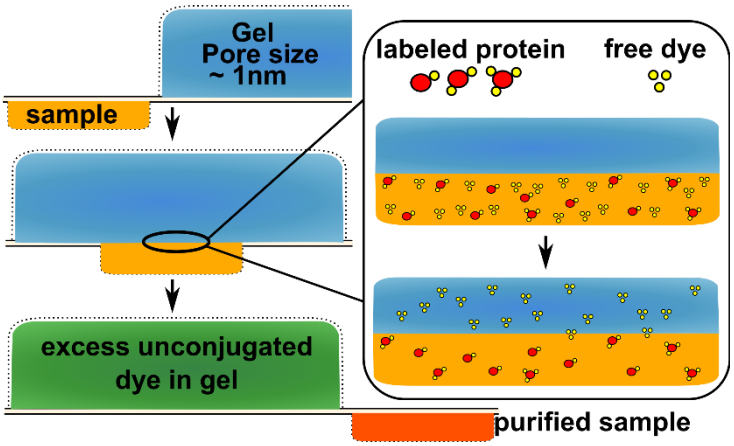

Figure 3-3: Schematic for excess un-reacted dye removal via passive diffusion into gel matrix. Gel with nanopores excludes large MW protein sample, keeping the protein sample concentrated within sample well, while allowing small MW dye to diffuse into gel matrix. The sample is purified of excess dye by slipping over a series of gel reservoirs.

Firstly, the most common separation methods for traditional microfluidics is often pressure based or electrophoretic chromatography. Because a SlipChip relies on oil to seal the gap between layers, any excessive pressure applied to the liquid sample (like those needed for column chromatography) will cause the sample to burst out of its features and leak into the

gap/oil layer. While electrophoretic separation has been shown on a SlipChip, it requires the use of an external power supply and addition of carefully inserted electrodes to function. Our goal with this chip was to provide a simple user-friendly detection, for which we believed UV/Vis detection via a plate reader would be the most user-friendly as most labs and research institutions have access to a plate reader which is quick and easy to use. Similarly we considered other detection methods such as fluorescence polarization and surface plasmon resonance, but determined that, at least initially, it would be complicated to incorporate into our chip and require specialized equipment.

The device is fabricated in quartz glass, so that absorbance measurements of proteins at 280nm can be performed (Fig 2c vi). Furthermore, for UV/Vis detection via a plate reader the sample reservoirs were sized to approximately 2mm diameter to match similar well sizes found in 1536 well plates. Additionally, to increase S/N, the sample reservoirs were etched 300um deep providing a longer optical pathlength; however due to wet etching being isotropic, the etch depth could only be so deep without increasing the lateral footprint of the features beyond a desired size. The faces of the device were fluorosilanized to provide a non-wetting surface for aqueous samples and fluorophores in organic solvent. Fluorosilane also allowed for the wetting of the fluorinated (FC40) oil used to provide lubrication for slipping. RfOEG surfactant was used to help prevent adhesion/fouling of glass surface from protein, and did not significantly change interfacial tension of solution droplets as measured by contact angle (data not shown).

A 3D printed adapter was fabricated to hold the chip for placement into a plate reader for UV/Vis analysis of labeling ratio (Fig 3-2e). The adapter is designed with similar

dimensions to that of a well plate and holds the chip in an easy snap fit. Additionally, the adapter was designed with posts that fits with drilled holes in the chip, which accurately and reproducibly aligns the sample reservoirs over a viewing window. The samples, now positioned in a specific x,y coordinate can be analyzed on a plate reader using the "custom plate" template available in the software. Alternatively, if no custom plate option is available, the chip can be designed so that the sample wells are aligned with an existing well plate format.

3.4.2 *Validation of modules and preliminary data*

To perform on chip dilution, the chip was designed to dilute dye by preset volumes of 0x, 0.2x, 0.4x, 0.6x, 0.8x, and 1x the initial concentration of dye added. The specific range of excess dye to antibody can be controlled by varying the initial dye or antibody concentrations. For example, if a 150kDa antibody at 1 mg/mL was loaded onto the chip along with 2.8 mM dye it would result in 0 to 20x M excess dilution range, whereas loading 1.4 mM dye results in 0 to 10x M excess range. Testing multiple fluorophore: protein ratios (f/p's) on chip requires the accurate dilution of dye to the right concentration and volume to then react with a constant amount protein. The dilution accuracy was tested by comparing dilutions of a $FeSCN^{2+}$ solution, which produces a deep red color measurable by visible absorbance (Figure 3-4 a,c). 100mM $FeSCN^{2+}$ and water was loaded onto the chip and slipped to dilute the $FeSCN^{2+}$ with water. At the size range of these features, the Reynolds number (Equation 1-1) is quite low, indicating that any mixing occurs via diffusion. The on-chip dilution was complete within 10 minutes, which agrees with the calculated diffusion rate. Off chip measurement performed in 500uL tubes, then samples

were loaded onto chip to compare. To measure absorbance a 16-bit black and white image was taken and the pixel intensity (I) of each sample and background (I_0) was measured. The calibration curve was found to be linear with a R^2 of 0.99. Dilution of Alexafluore-647 fluorophore was also performed and showed a linear trend with R^2 of 0.98 (Figure 3-4b).

After dye dilution, the next step is to mix and react dye (e.g. an AlexaFluor-NHS ester) with the protein sample. In preliminary work, we tested the rate of mixing by diffusion. The dye well was filled with fluorescein and the sample well with buffer, and then slipped to overlap. As expected for a small molecule diffusing these distances (800 µm from edge to edge of the aligned reservoirs), mixing was complete in 30 minutes (Figure 3-5).

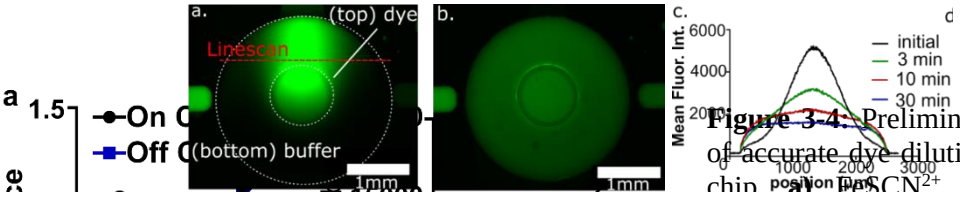

Figure 3-4: Preliminary validation of accurate dye dilution on and off chip. $FeSCN^{2+}$ solution was

Figure 3-5: On-chip mixing of dye and sample goes to completion in minutes. Here, the dye well was filled with fluorescein (green) and the protein well with buffer. **a)** Image collected at 30 sec, and **b)** at 30 min after slipping to overlap. **c)** Line-scan data showed that mixing was complete after 30 min, and was 84% complete after 10 min.

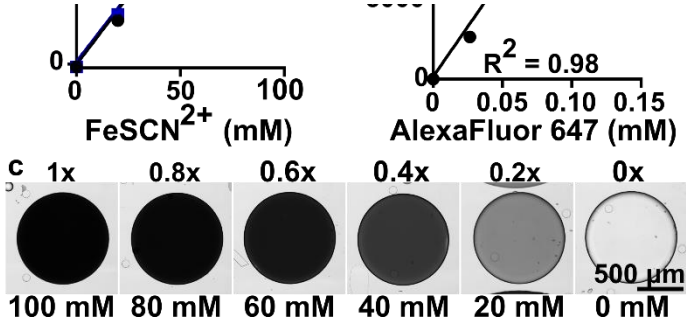

After conjugation, unreacted dye must be removed from the product solution prior to optical measurement. While most microfluidic protein separations are performed using electrophoresis, we have patterned a size-exclusion monolith (gel) to achieve simple, power-free separation of proteins from unreacted dyes. We should note that we are not measuring the pore size of the gel, but rather using concentrations of gel that are reported to be withing the desired pore size range. A 20% polyacrylamide gel precursor solution with Irgacure photo-initiator was pipetted into the chip and then polymerized into place with UV light. In preliminary results, we found that this gel efficiently separated a mixture of AlexaFluor-594-labelled antibody from fluorescein dye (Figure 3-6). However, the soft gel distorted upon slipping, causing solution to flow around it and decreasing the yield of protein after the separation.

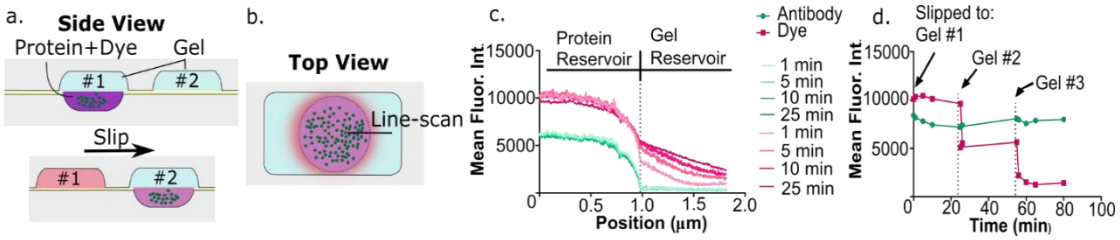

Figure 3-6: Extraction of dye using an on-chip size exclusion gel.**a)** A sample well containing fluorescein and AlexaFluor 594 (AF-594) labeled antibody was slipped over a series of three wells containing 20% polyacrylamide. **b)** Top view: sample well (circle) aligned beneath the larger gel well. A linescan was obtained to measure **c)** fluorescent intensity over time for the AF-594-antibody (green) and fluorescein (red). The concentration of dye in the gel increased over time, whereas the concentration of antibody remained constant. **d)** Mean fluorescent intensity of the AF-594-antibody and dye over three dye removal steps. After 80 min, the AF-594-antibody retained 95% of its original intensity, whereas fluorescein retained 14%.

3.4.3 *Troubleshooting incorporation of gel matrix into a Slip Chip*

Incorporation of a gel matrix into a Slip Chip device differs greatly compared to standard PDMS chips or capillary gel electrophoresis, with a number of unique challenges requiring a whole host of new techniques to solve. The primary difference between the Slip Chip and other chips is that Slip Chips have open faced channels and features that are not

sealed or enclosed by bonding to another layer. This facilitates the slipping motion of the chip, wherein open-faced channels or features on each layer/face of the chip can be slipped atop one another to connect those features, or slipped apart to break those connections. The chip uses fluorinated surface chemistry, as well as fluorinated oil, to both provide lubrication for slipping, and to effectively entrap the aqueous sample (much like droplet microfluidics) preventing the aqueous sample from leaking into the gap between the Slip Chip layers. This tends to function well, as the surface tension (interfacial tension) of the aqueous droplet keeps it contained within the fluorinated channel/feature and the fluorinated oil "capsule". However, if the interfacial tension is lowered (e.g. by a surfactant) or if the capillary pressure applied to the aqueous droplet is too high (e.g. high inlet pressure, or slipping into a constrained geometry feature) the aqueous droplet will expand and leak into the gap.

During the incorporation of a typical gel matrix into an enclosed PDMS chip or capillary, the surface of the channels is often treated with a polymerizable silane. This is done so that, as the gel begins to contract during polymerization, it polymerizes to the channel walls, thus preventing it from pulling away and creating void spaces. This is exactly what was observed in a Slip Chip device without polymerizable silane. Additionally, because the Slip Chip slips, the gel will shift during slipping, pealing back from one side wall and bunching up at the other end, causing shear stress and eventually tearing of the gel. Addition of a polymerizable silane presented a unique challenge for Slip Chips. The treatment with a polymerizable silane requires the removal of the fluorinated silane surface of the chip, where removal needs to be specific only to the desired channels

that are, once again, in an open-faced device. Because the fluorinated silane surface chemistry along with the oil keeps the aqueous sample from leaking, this makes it exceedingly difficult to remove the surface silane by flowing in a silane stripping solution, such as concentrated NaOH. To solve this issue, we protected the other surfaces and features of the chip by covering them with a layer of PDMS. While not bonded, a sufficiently smooth and planar PDMS layer can be pressed into conformal contact with the chip, and effectively "sealed" by application of moderate pressure. Using this method, we have designed two techniques to strip fluorinated silane. The first is used only for large features. Using a circuit cutter, a maker tool similar to a printer that can precisely cut designs with a small blade, we pattered and cut a thin PDMS cover for the chip. This PDMS mask exposes only the features to be filled with gel. The chip and PDMS cover can then be plasma cleaned to selectively strip away the fluorinated silane. The second method is for features too small for the circuit cutter to pattern. This method also requires that the stripped features be a continuous channel with inlets and outlets. This method uses a PDMS cover backed by rigid glass, and is sealed by application of pressure. A stripping agent can then be flowed through the channel and then rinsed away. The chip can then be bathed in

a solution of polymerizable silane, where the presence of fluorinated silane prevents the polymerized silane form adhering to the un-stripped features.

Once silanized, we observed that gel does indeed adhere to the side walls of the chip, however if the gel is added to an assembled device using fluorinated oil, the oil in some cases can often block and prevent polymerization to the wall of the device (Figure 3-7). Additionally, if the device is slipped at anytime before polymerization, the gel will leak into the gap by a very small amount. During normal function of the chip this is not a

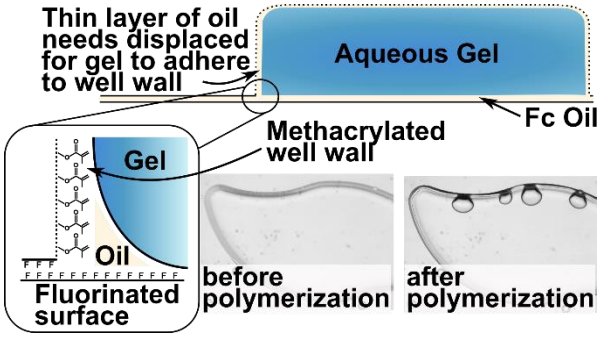

Figure 3-7: Polymerization of polyacrylamide gel in assembled chip with oil. The gel does not always displace the oil coating the walls of the chip, and thus may not adhere to methacrylate walls of chip.

problem for liquid samples, as this leaking is very miniscule. However, as the gel polymerizes and hardens, the leaked gel will then begin to shear and tear away from the bulk body of the gel. This causes small pieces of gel to become trapped and collect in the gap layer, eventually forcing the chip layers apart, increasing the gap, and causing leaking of aqueous sample. To solve this issue, we designed the chip to only have gel filled features on a single layer of the chip, requiring a non-broken continuous channel of gel with a dedicated inlet and outlet. We also used the PDMS sealing method, as described above, to remove the need for fluorinated oil sealing. But this method comes with new challenges. As the PDMS is not hydrophilic, the aqueous gel does not wet to it. This prevents the gel

from conforming into the corners of the channel where the feature side walls meet the PDMS surface, leaving a small trapped air layer (Figure 3-8). Because the PDMS is not bonded and channels are only enclosed due to applied pressure, attempts to make the PDMS surface hydrophilic resulted in the aqueous gel wetting so well to it that the gel leaked outside of the channels.

Another challenge we have observed is the wetting of sample to the gel (Figure 3-9). Because there is a gap between layers of the chip, as the samples slip across the gel, the sample wets to the gel leaving a thin layer of sample behind. Over the course of several slipping steps this can result in significant loss of sample. This issue is further compounded by the contraction and swelling of the gel. This problem is specifically an issue with

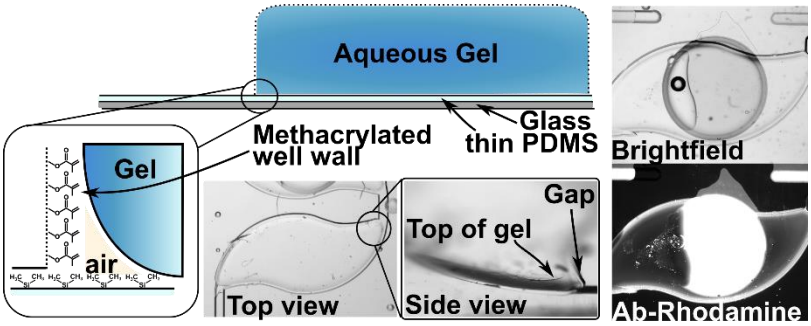

Figure 3-8: Polymerization of polyacrylamide gel in assembled chip without oil. Due to a non-hydrophilic PDMS surface chemistry, the gel does not wet into the top corners of the well, leaving a gap which aqueous sample can be trapped.

hydrogels such as polyacrylamide, which was initially chosen due to its ability to be polymerized with nanopores. Although the gel is adhered to the channel walls, it will contract away from the face of the chip, a process which is exacerbated as the gel dries out loosing moisture content. Conversely, once the gel comes into contact with aqueous sample, the gel begins to absorb the sample and swell (Figure 3-10). This eventually forces

the two layers of the chip apart, creating air gaps and facilitating leaks. To solve this issue, we are currently investigating the use of rigid polymers (non-hydrogels) that will not swell, and which will maintain their shape after polymerization.

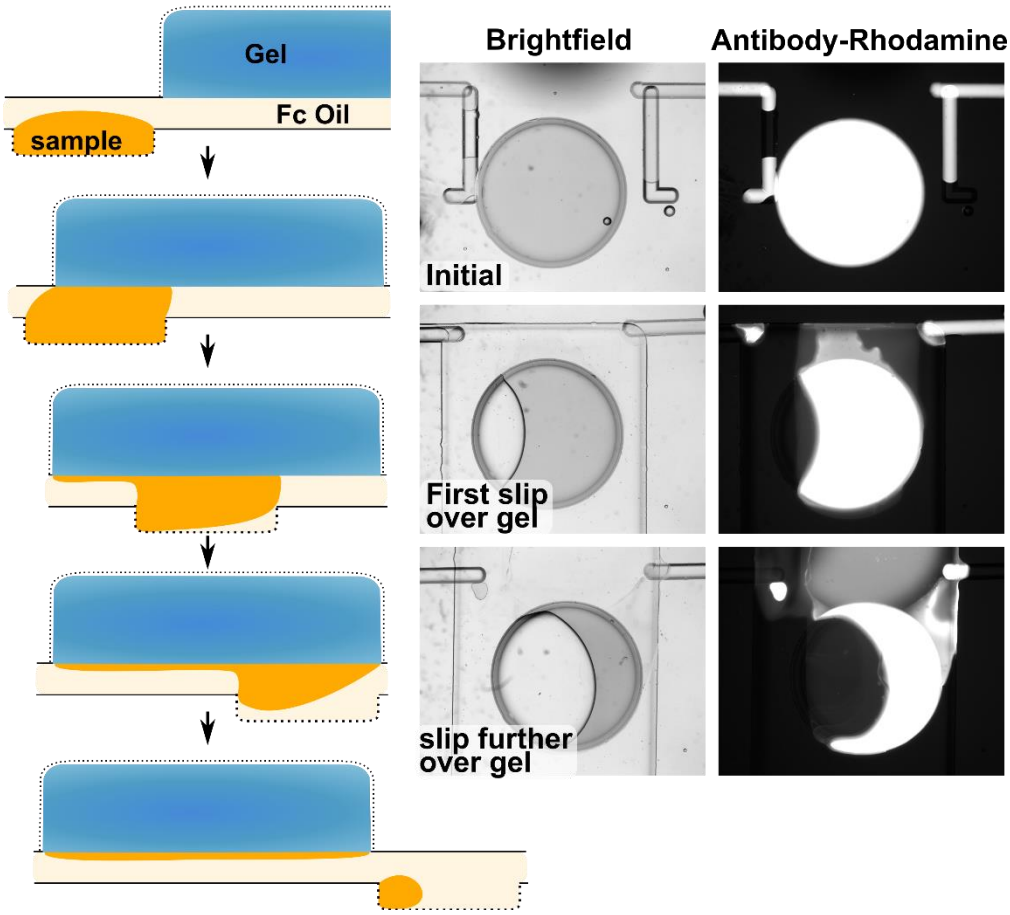

Figure 3-9: Wetting of the sample to the gel. Due to the gap between layers of the chip, the sample can wet to the hydrophilic gel, leaving a thin layer behind as the chip slips, resulting in loss of sample.

To separate excess unbound small MW dye from larger antibodies, we chose a passive sized based exclusion using a densely crosslinked gel, however, there are other separation methods. Unfortunately, some of the most common separation methods are either prohibitively difficult to incorporate, such as membranes for passive diffusion, or

pressure-based chromatography which is non-viable on an open-faced chip. One main challenge to incorporating other methods is the need to keep our sample concentrated for UV/Vis analysis on chip. This was a driving factor for using dense gel to exclude the antibody, and why other methods like size exclusion resins and or affinity beads were less attractive. We did, however, briefly investigate fluorescence polarization as separation free detection method. In fluorescence polarization, the fluorescent sample is excited with plane polarized light. If the samples were static in solution (non-rotating) they would emit light in the same polarized plane, however samples do freely rotate in solution, thus emitting a mixture of polarized and non-polarized light. The amount of polarized to non-polarized is determined by the rate of rotation and the fluorescent lifetime of the dye. Because larger objects will rotate slower (e.g. antibody), they can be differentiated from small free fluorophore, and the amount of bound ligand (e.g. dye) can be calculated. While fluorescent polarization values should be independent of concentration, we observed that higher label ratios resulted in different polarization values, likely due to FRET, thus confounding our results. We also observed that the instrumentation was not sensitive enough to accurately differentiate labeled antibody from molar excess of dye above 5X. At the moment, we believe that the best alternative method for on chip separation is likely gel electrophoresis, as it has been previously shown on Slip Chips.

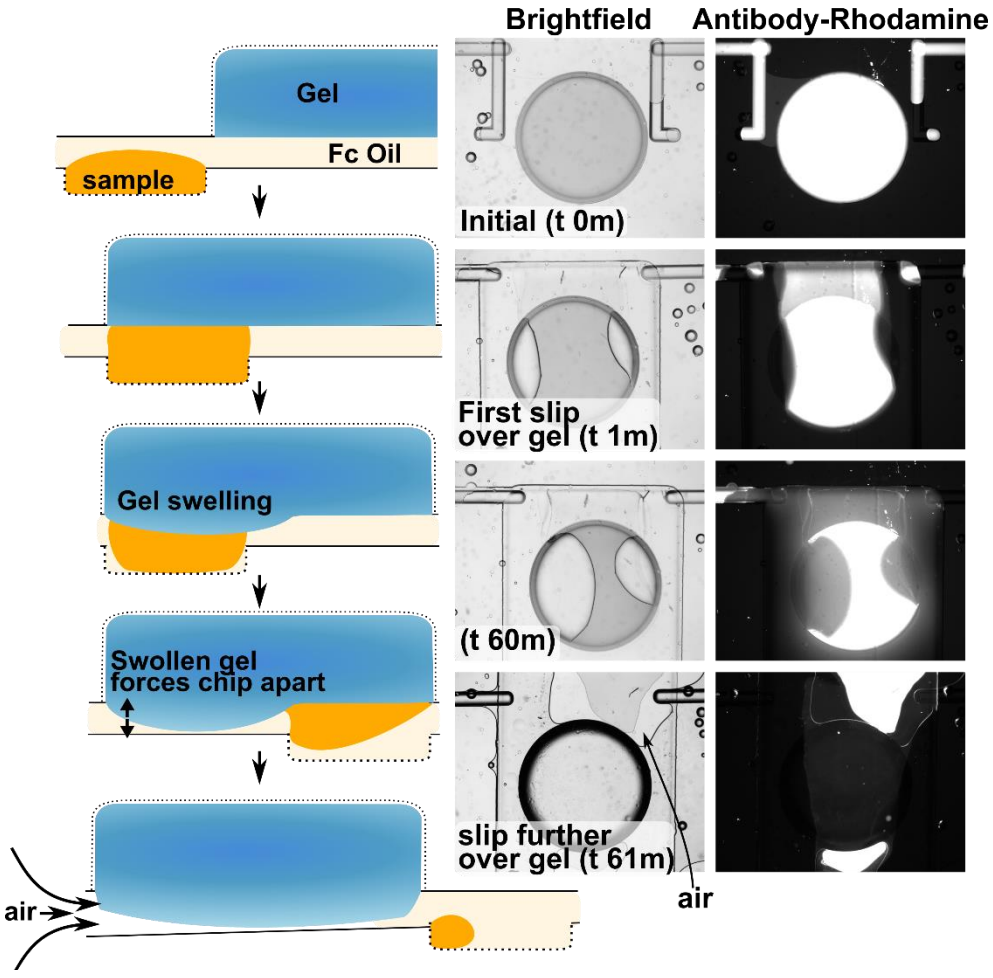

Figure 3-10: Swelling of the gel. Hydrogels will shrink or swell with the loss/addition of aqueous solution. During operation of the chip, the gel may absorb aqueous sample volume, swell, and then force the layers of the chip apart resulting in air intake and leaks.

3.4.4 *Proposed work: Gel on chip*

To solve issues related to gel swelling, we propose testing a series of monolithic rigid gel matrices to identify one that provides > 90% retention of protein and > 95% removal of free dye. We will test UV-cross linkable gels (acrylamide and methacrylate based) as well as silica sol-gels.[142–144] The density and rigidity of each material will be tuned by altering its concentration and extent of cross-linking.[145,146] While polyacrylamide and polymethacrylate are used as soft hydrogels their structural rigidity can be increased

by increasing the proportion of crosslinking monomer. Similarly, which are well established for size-based separations, offer a porous matrix with glass-like rigidity. Sol gels can be prepared in microfluidic devices using the standard tetramethyl orthosilicate (TMOS) chemistry, and can be bonded to glass (or silanizable surface) to immobilize them in the device.[147–151] Alternatively to passive diffusion, we may investigate the use of rigid separation matrixes incorporated with gel electrophoresis to remove charged fluorophores. An electrophoretic design can be easily incorporated into the current design of the chip, taking advantage of existing channels, with minimal changes. The rigid gel matrix would connect the sample wells, but still be dense enough to exclude the antibody sample, only allowing the charged fluorophore to migrate to the outlet/electrode.

To help with sample wetting, we will investigate the addition of hydrophobic monomers to tune the hydrophobicity of the gel and gel surface. While acrylamide does not significantly absorb proteins, more hydrophobic or charged matrices may suffer from protein adsorption and sample wetting.[146] To prevent sample absorption, we will test mixing the gel with polyethylene glycol-methacrylate (PEG-MA) to passivate the surface.[152] To test excess dye removal via passive diffusion into gel, we will use fluorescent antibodies and free small MW fluorophore to observe diffusion into the gel fluorescent microscopy. With the current design, we have calculated that the chip will have > 95% removal of free dye (< 5% of detected absorbance is due to un-conjugated dye) after 4-5 slip/wash steps (Figure 3-11), thus ensuring an accurate determination of label ratio.

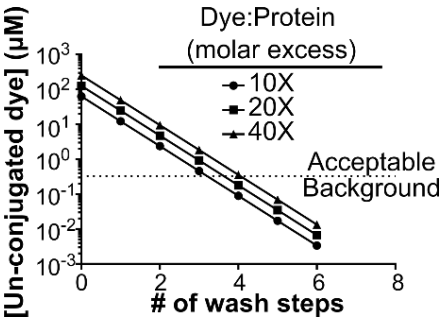

Figure 3-11: Computational datashowing the concentration of free (un-conjugated) dye remaining in the sample after successive wash steps. The acceptable concentration of residual dye (dashed line) was set to 5% of the conjugated dye at a low label ratio of 1:1 dye:protein. For the volumes of the prototype glass chip and a typical use case, 1 mg/mL IgG conjugated to rhodamine, four wash steps will resolve a 1:1 label ratio when using < 40X molar excess of dye. The data assumes that the dye will be equilibrated between the sample and gel wells during each wash step.

3.4.5 *Proposed work: 3D printed adapter for plate reader*

To enable detection of labeling ratios directly on the chip, we will develop a 3D printed adaptor to place the device into a plate reader. The adaptor will clamp the Slip Chip together and align the sample reservoirs to specific x,y coordinates in the instrument, to enable reading like a 1536-well plate. To test alignment, the sample reservoirs will be filled with fluorescent-labeled antibody, and the chip will be placed in the adaptor and read at 280 nm (protein) and λ_{max} (dye). Alignment will be considered successful if the % CV of the absorbance after 5 repetitions is < 5 %, and the mean is within 10 % of expected value. In the event that standard borosilicate glass is not optically clear below 350 nm, so we will transition to quartz glass, which is optically clear above 200 nm and can be wet etched in a similar manner.[153] Additionally, if reproducible placement in the correct x,y position is challenging, we will program a “custom” plate layout that reads every 1 mm (the limit of motor stepping resolution of the Clariostar), or if needed will space the sample wells accordingly to match existing wells for a 384-well plate.

3.4.6 *Proposed work: Scale up and validation*

Finally, we will verify scale-up of labeling ratios found on-chip using conventional Eppendorf tubes. Isotype control antibodies will be labelled on-chip and off-chip with fluorophore-succinimidyl ester. Two isotypes each of rat, human, and mouse antibodies will be tested in duplicate, to cover the most common experimental reagents. Scale-up tests will be conducted at 3 scales: 30, 100, and 1000 μg/sample. The resulting labeling ratio will be measured by UV-Vis (plate reader and Nanodrop spectrophotometer. We have already shown that on-chip and off-chip dilutions are equivalent (Figure 3-5), and we have calculated the necessary number of diffusive mixing steps to match the efficacy of macroscale separation (Figure 3-11). The primary barriers to scaling up single-phase chemical reactions are the time and energy needed for heat and mass transfer, and changes in surface adsorption. Heat transfer is not expected to play a role in this isothermal, room temperature labeling reaction. Mass transfer (mixing) during the reaction step occurs by diffusion on the chip and by continuous convective mixing on a shaker in the microtube; in both cases, mixing is expected to reach completion faster than the timescale of the reaction and therefore will not alter the reaction outcome. Because surface adsorption on-chip is minimized by the fluorinated surfactant, and will be minimized by blocking in the microcentrifuge tubes and negligible at large scales, we do not expect significant deviation between the on-chip and off-chip reactions according to two-way ANOVA analysis. For individual antibodies, deviation of < 10% labeling ratio will be considered acceptable. If the device yields a significantly higher or lower labeling ratio, we will add additional surfactants to address loss of protein or labeling reagent to surface adsorption.[154,155]

3.5 Conclusions and future directions

In conclusion, we have described the design and fabrication of a Slip Chip microfluidic device for small scale optimization of antibody labeling reactions prior to scale up for benchtop antibody labeling which is low cost, easy to use, and uses minimal sample and reagents. We have begun to validate the individual modules of the chip and have proposed several experiments to validate the other modules to ensure that the chip accurately dilutes, reacts, and removes excess dye from antibody sample, and which can be detected by UV/Vis on a plate reader. We additionally have described in detail the challenges with incorporating a gel onto a Slip Chip for our novel separation method, as well as proposed several solutions. This device will allow users to optimize antibody labeling reactions which is an important step for antibody validation, to ensure that over-labeling does not inhibit antibody function. In the future, we plan to transition fabrication to a fully 3D printed chip to enable higher-throughput fabrication a less labor-intensive fabrication is necessary. Transitioning to a high-resolution stereolithography printer, will enable more rapid and affordable prototyping and increased 3D design complexity compared to higher throughput methods such as hot embossing. This will also allow for greater dissemination of our design to labs which do not have the expertise or facilities necessary to wet etch a microfluidic chip. We envision that research laboratories will rapidly integrate this technology into their workflow, thus improving the quality of conjugates that are used nationwide and facilitating the use of optimized reagents for validation.

Chapter 4: Immunofluorescence staining of live lymph node tissue slices

Adapted from: Groff BD, Kinman AWL, Pompano RR., J. Im. Methods 2019, 464, 119-125

4.1 Abstract

Explants of lymphoid tissue provide a rare opportunity to assess the organization of the immune system in a living, dynamic environment. Traditionally, ex vivo immunostaining is conducted in fixed tissue sections, while live tissues are analyzed using genetically engineered fluorescent reporters or adoptively transferred, pre-labelled cell populations. Here, we validated a protocol for immunostaining and imaging in live, thick slices of lymph node tissue, thus providing a spatial "map" of the lymph node while maintaining the viability and functionality of the slices. Using anti-B220/CD45R (B cell) as a prototype antibody, the procedure for immunostaining was tested for sufficient signal to noise with respect to staining time, temperature, and wash time, and the specificity was verified in comparison to isotype controls. Immunostaining signal in live tissue slices was detectable to least 120 μm deep for both whole antibodies and $F(ab')_2$ fragments using the staining procedure. This procedure revealed the expected changes in B cell organization in lymph nodes from immunized mice. Cell surface staining with most antibodies did not induce cytokine secretion, and cytokine secretion in response to T cell stimulation was unaffected by immunostaining. Staining with known a mitogenic antibody (anti-CD3) simultaneously labelled the cells and activated the tissue, confirming that reagents for live immunostaining must be selected judiciously. As a proof of concept, this method was used

to reveal the dynamic distribution of CD69, a T cell activation marker, in lymph node slices before and after ex vivo stimulation.

4.2 Introduction

The normal function and response to stimuli of any tissue affected in part by the spatial arrangement of each component of the tissue. The local clustering of cells, presence of signaling molecule diffusion gradients, nutrient diffusion gradients, interstitial flow, blood flow, extracellular matrix composition, etc., are all factors that can play an important role in cell response. The study of these spatial components in relation to function can help us to better understand the underlying biochemical and biophysical mechanisms occurring in healthy, developing, or unhealthy tissue. For example, this type of information may allow for the identification of critical targets or pathways involved in disease progression, and can better inform the development and testing of novel therapeutics.

Traditional methods to study cell interactions are limited to in-vivo and in-vitro methodologies. In-vivo methods allow for the study whole tissues, but are limited due to practical experimental considerations. For example, visual imaging techniques are limited by light scattering, only being able to penetrate a few mm at most depending on the technique; thus, requiring imaged tissue to be surface deep or surgery to expose the desired region.[156–158] Other techniques may require invasive probes; use of stains such as radio labels or contrast agents, which may be difficult to deliver to desired region of study; require expensive transgenic animals; or require other complex set-ups all while managing a live animal.[156] Alternatively, for in-vitro methods, in-situ conditions are difficult to replicate, and can often only 1 or 2 in-situ conditions can be replicated at a time. Traditional

benchtop in-vitro methods are often limited to single cell or bulk techniques such as flow cytometry for surface markers, immunoassays for secreted proteins, PCR for gene expression, and other similar methods which are un-able to provide spatial information. Additionally, the method of tissue dissociation into a suspended cell culture often requires mechanical crushing and filtering of tissue through a membrane, which can result in the loss of matrix bound cell types, such as dendritic cells from lymph tissue.[159] Microfluidics has been able to address some of these issues, and over the past 20 years microfluidic cell cultures have increased in complexity with some devices being called organs-on-a-chip. However, while microfluidics does allow for precise control over factors like interstitial flow, mechanical stress, and patterning of a few cell types, it often is still unable to faithfully replicate the wholistic function of tissues. Because of challenges such as these, on increasingly common approach to studying spatial function is the dissection and removal of live tissue for culture and experimentation.

Live tissue explants have been used for decades as a unique experimental system that retains the complexity of intact tissue while making it experimentally accessible.[160] The use of tissue explants derives from the technique immunohistochemistry (IHC). However, traditional IHC is often performed on thin fixed tissue sections. This process of fixation preserves the organization of the tissue and increases mechanical stability by crosslinking proteins and stopping cell function. However this also results in cell death and eliminates temporal dynamics of tissue function.[161,162,163,164] Although more challenging, analysis of live tissue allows for the observation of transient events, such as cell interactions, cell surface protein regulation, cell migration, and release and formation of

signaling molecule gradients.[165–167] Live tissue explants also allow for stimulus-response assays where the dose and timing of stimulation can be more precisely controlled without the variations in fluid drainage and pharmacokinetics found in-vivo.[168,169]

Live tissue explants are not without their own set of challenges. Special consideration of tissue reactivity should be taken when using tissue explants, as ex-vivo tissue culture environment is markedly different from in-vivo and can have various effects. Excising or slicing tissue may result in temporary inflammation or reorganization of cells. For example, in brain slices the neurons are axotomized upon slicing the tissue. In neonatal brain tissue this leads to neuronal cell death due to reduction in supply of neuropathic factors, whereas adult tissue may experience a reorganization and expansion of axons to denervated regions to mitigate cell death from axotomy.[170] Additionally, tissue function can change or deteriorate over time and needs to be taken into consideration before performing acute or long term culture experiments.[171] Depending on the tissue, cell count within a sample can decrease over time as the natural egress of cells out of the tissue isn't balanced by incoming cells,[172] unless samples are deliberately co-cultured to counteract these effects.[173] Furthermore ex-vivo tissue does not experience the same interstitial flow, mechanical stress, or chemical gradients as it would in-vivo, leading to altered morphology and function. One such issue is the lack of interstitial or blood flow delivery of nutrients, such as oxygen, which must instead diffuse into the tissue. For most tissue studies, this necessitates the slicing of tissue into smaller sections < 500um, as any larger and the nutrients would be depleted faster than they could diffuse in.

In addition to merely maintaining viability, work with live tissue demands recognition that the tissue may react to the reagents or procedures used for analysis, thus potentially altering the quantity or distribution of the analyte of interest. Several commonly used bioanalytical reagents can activate or otherwise engage cells. For example, multivalent binding reagents such as antibodies and dendrimers may dimerize or cross-link proteins on cell surfaces, which often activates intracellular signaling cascades and may result in internalization of the target.[174,175] In addition, antibody Fc regions can bind to Fc receptors (FcR) of immune cells such as macrophages, B cells, NK cells, follicular dendritic cells, and other effectors cells, which may activate the cells to initiate an immune response.[176,177] One means to mitigate these issues is to use monovalent binding reagents such as single Fab or scFv antibody fragments, though these reagents are of more limited availability than intact antibodies.[178]

There are also other undesired effects can occur when experimenting with live tissue. Some chemical and optical probes are cytotoxic, either through DNA intercalation,[179–181] binding and interfering with proteins and enzymes, or disrupt cell activity through various other mechanisms.[182–184] Some chemicals, like the fluorescent MitoTracker Orange modulate the electric potential across the plasma or mitochondrial membrane, interfering with cell signaling and electron transport chain and ATP production.[185] In addition to effects caused by the addition of chemical probes, tissue can react to the environment in which it is placed during experimentation. For example, the amount of Ca^{2+}, K^{+}, Na^{+} ions present in the buffer being used can have a major effect on cell and tissue function.[186] External factors like temperature, oxygenation, and media

glucose can also play a role in how the tissue responds, even beyond viability.[187] In general, the extent to which viability and the most relevant functions of the tissue are affected by the experimental procedure itself should be validated for each new assay or new tissue.[188]

Lymphatic tissue is one such tissue that would be beneficial to study in an ex-vivo format, as lymph nodes are the "hub" of an immune response. There have been previous studies of ex vivo slices of murine and human lymphoid tissue, however analysis is limited to dissociation for flow cytometry, staining of fixed slices, or uses pre-stained cells overlaid or injected into live tissue.[189–194] A novel method is needed to detect the organization of living lymphoid tissue samples without disrupting the function of the cells. Immunofluorescent labelling has been reported recently for live lung slices and prostate explants[16,17] and would be particularly useful to identify the organization of lymphoid tissues, where many cell types are well-described by surface proteins and fluorescently labelled antibodies are readily available. Immunostaining of live tissue is especially useful to study tissue organization in samples that are not readily labelled genetically, such as human or non-human primate tissue, as well as in readily available mouse models, bypassing the need to breed or acquire specialty transgenic strains that express specific fluorescent reporters. Here we report an optimized protocol to label cell surface markers and tissue structures in slices of live lymph node tissue using antibody-based reagents, while leaving the tissue viable and ready for further study.

4.3 Materials and Methods

4.3.1 Animal work

Female C57BL/6 mice were purchased from Jackson Laboratory or Taconic (USA) and housed in the University of Virginia vivarium with food and water ad libitum. All animal work was approved by the Institutional Animal Care and Use Committee at the University of Virginia under protocol #4042, and was conducted in compliance with guidelines the Office of Laboratory Animal Welfare at the National Institutes of Health (United States). Where noted, mice were vaccinated with chicken egg ovalbumin in complete Freund's adjuvant prior to collection of lymph nodes (see Supporting Methods).

4.3.2 Slice preparation

On the day of the experiment, the animal was anesthetized with isoflurane and euthanized by cervical dislocation. The inguinal, brachial, and axillary lymph nodes were gently removed, carefully stripped of fat and connective tissue, and immediately placed into ice-cold DPBS without calcium or magnesium (Lonza, Walkersville MD, #17-512F) with 2% heat-inactivated FBS (Gibco, Fisher Scientific, Waltham, MA). Where noted, the popliteal node was collected as well. Nodes were embedded in 6% low melting point agarose (Lonza), prepared in 1x phosphate buffered saline (PBS), and allowed to chill on ice. Nodes were oriented flat side down to obtain the widest possible cross-section when sliced. A 10 mm tissue punch was used to obtain a column of agarose for each node. The LN tissue was sliced at a thickness of 300 μm in ice-cold PBS using a vibratome (Leica VT1000S, Bannockburn, IL) set to speed: 0.17 mm/s; freq: 30 Hz. Immediately after slicing, sections were transferred into a 12-well plate containing 2 mL complete media. Complete media consisted of RPMI (Lonza RPMI 1640 without L-glutamine, #12-167F)

supplemented with 10% FBS, 1% L-glutamine, and 1% Pen/Strep, 50 µM beta-mercaptoethanol, 1 mM pyruvate, 1% non-essential amino acids, and 20 mM HEPES (Fisher Scientific). Immediately after slicing, the plate was transferred to a humidified sterile incubator at 37 °C with 5% CO_2 for 1-2 hours for recovery. For sterile slicing, the procedure differed in the following ways: The agarose was sterilized by autoclaving prior to embedding tissue, 1% Pen-Strep was added to PBS buffer during slicing, the vibratome was placed in a biosafety cabinet to prevent contamination, and the vibratome frequency was reduced to 10 Hz.

4.3.3 *Immunostaining and imaging of live lymph node slices*

A 6-well plate was prepared by lining the wells with paraffin film that was sterilized in advance with 70% ethanol and dried. The paraffin film provided a hydrophobic surface to prevent the antibody solution from wicking across the plate under the tissue. Slices were transferred into the plate using a paintbrush and allowed to sit flat on the surface. To conserve antibodies, an A2 stainless steel flat washer (10 mm outer diameter, 5.3 mm inner; Grainger, USA) was placed on top of the slice, creating a 1-mm-deep well over each tissue sample. Slices were Fc-blocked by applying a 20-µL droplet of 25-µg/mL purified anti-mouse CD16/32 antibody (BioLegend, San Diego, CA) in 1x PBS with 2% heat-inactivated FBS (Gibco, Fisher Scientific) to the washer and incubating for 30 minutes in a humidified sterile incubator at 37 ºC with 5% CO_2. To stain, the blocking solution was left in place, an additional 10 µL of antibody cocktail was added (total volume: 30 µL), and the slice was incubated 1 hour or as noted. Antibodies are listed in Table S1, and preparation of fluorescently labelled antibodies and fragments is described in Supporting Methods. Antibodies were used at a concentration of 20 µg/mL (0.2 µg per tissue slice);

preliminary tests showed little difference from 10 – 30 µg/mL. To remove unbound antibodies, the washer was removed, and the wells were filled with 10 mL of PBS and incubated 30 minutes at 37 °C or as noted, refreshing the PBS every 10-15 minutes. Slices were finally transferred into a 24-well plate in 0.5 mL PBS for immediate imaging on a Zeiss AxioZoom macroscope (Carl Zeiss Microscopy, Germany) with a Zeiss Axiocam 506 mono camera. Filters used were Zeiss Filter Set 38 HE (Ex: 470/40, Em: 525/50), 43 HE (Ex: 550/25, Em: 605/70); 64 HE (Ex: 587/25, Em: 647/70); and 50 (Ex: 640/30, Em: 690/50). Care was taken to image the slices from the side on which the antibodies had been applied, as they may not penetrate through the entire depth of the tissue.

4.3.4 *Depth of antibody signal in tissue slices*

Lymph node slices were double-stained with anti-B220 (CD45R) antibody and a fragment thereof (whole IgG–Alexa Fluor 647 and $F(ab')_2$–Alexa Fluor 555), using the staining protocol as described in section 2.3. Tissues were imaged on a Nikon A1Rsi upright confocal microscope (Nikon Instruments Inc., Melville NY) using GaAsP detectors and 40X/0.45NA Plan Apo NIR WD objective, in increments of 10 µm z-steps. Because B220+ cells are not uniformly distributed throughout the tissue, regions were selected for imaging based on having bright B220 staining near the surface of the tissue. For analysis by 2 photon microscopy, slices were stained with FITC-CD4 Fab' (generated in-house). After staining slices were fixed in formalin for 30 minutes and imaged. Two-photon microscopy and second harmonic imaging was performed in the W.M. Keck Center for Cellular Imaging (University of Virginia) on an Axiovert200 MOT inverted microscope with an LSM510 scan head (Zeiss, Germany). Image was collected with 60x/1.20 WD objective.

4.3.5 *Viability of stained lymph node slices*

To assess the viability of immunostained LN slices, LN slices were stained with anti-B220 as per method described above. After staining, a 24-well plate was filled with 2 μM Calcein AM (Fisher Scientific) in PBS, using 0.5 mL/well. Slices were immediately transferred into the wells and incubated for 20 minutes at room temperature, protected from light. Following incubation, wells were washed 3 times with PBS. Calcein intensity was averaged over the slice. Negative controls were prepared by treating a subset of slices with 70% ethanol for 10 minutes, and positive controls were prepared by keeping another subset of slices (unstained: no anti-B220) in a humidified sterile incubator at 37 ºC with 5% CO_2; these were Calcein-stained simultaneously with the experimental slices. Calcein intensity was imaged on a Zeiss AxioZoom macroscope.

4.3.6 *Cytokine secretion assays*

Lymph node slices were obtained from 4 naïve female C57BL/6 mice as described in section 2.2. Slices obtained were randomly assigned to each of 6 conditions: B220 + Lyve-1 staining or unstained for each PHA-L stimulated, CD3 stimulated, and unstimulated. Slices were stained as described in section 2.3 with anti-B220 FITC and anti-Lyve1 eFluor 660. Unstained control condition slices were left in media at 37 °C during this time. After staining, slices were placed in 500 μL of complete media and cultured for 20 hours at 37 °C with or without 25 μg/mL PHA-L (Fisher Scientific) or 1.25 μg/mL anti-CD3Ɛ (BioLegend). After 20 hours, supernatant was collected and analyzed by sandwich ELISA for IFNγ.

To compare activation of slices versus cell suspensions, peripheral lymph nodes (axial, brachial, inguinal) were randomly assigned to be sliced or crushed for lymphocyte culture. Spleen was also removed. For the sliced condition, nodes were sliced 300 µm thick and each slice was placed into 500 µL complete media. For lymphocyte culture and splenocyte culture conditions, nodes and spleen were separately crushed through a 70 µm filter. Cell suspensions were cultured in 500 µL aliquots at cell densities matched to tissue slice samples, where 1X culture was 1.7 $x10^6$ cells/mL, and 2X culture was 3.4 $x10^6$ cells/mL. Slices and lymphocyte cell culture were incubated for 20 hours at 37 °C, 5% CO_2, with anti-mouse/human CD3Ɛ (Biolegend, clone: 145-2C11, Purified grade) at 1, 0.5, or 0 µg/mL, with R848 (Resiquimod, InvivoGen, San Diego, CA) at 10 1, 0.1, or 0, or PHA-L (Millipore Sigma) at 25, 10, or 1 µg/mL.

4.3.7 *Cytokine ELISA*

A high-binding plate (Corning Costar 96 well ½ area, #3690; Fisher Scientific) was coated with 1 µg/mL anti-IFNγ XMG1.2 or 1 µg/mL anti-IL-2 JES6-1A12 (BioLegend) in PBS overnight at 4°C. Wells were blocked for 2 hours with 1% BSA and 0.05% Tween-20 (Fisher Scientific) in PBS (block solution). Serial dilutions of IFNγ and IL-2 cytokines (Peprotech, Rocky Hill, NJ) and sample supernatant dilutions were prepared in a 1:1 v/v mixture of block solution and complete media. These samples were added to the plate and incubated for 2 hours, then washed. Streptavidin-conjugated anti-IFNγ R46A2 or anti-IL-2 JES6-5H4 (BioLegend) were added to the plate at 0.5 µg/mL and 1 µg/mL, respectively, in block solution. All washing steps were performed with 0.05% Tween-20 in PBS. Plates were developed using TMB substrate (Fisher Scientific) and absorbance values were read at 450 nm on a plate reader (CLARIOstar; BMG LabTech, Cary, NC). To determine

concentration of sample solutions, calibration curves were fit in GraphPad Prism 6 with a sigmoidal 4 parameter curve (Eq. (1)), where X is log of concentration, Y is absorbance, min and max are the plateaus of the sigmoidal curve on the Y axis, and HillSlope describes the steepness of the slope.

$$Y = min + \frac{max - min}{1 + 10^{(Log(IC50 - X) * HillSlope)}} \quad (4\text{-}1)$$

4.3.8 *Visualization of CD69 upregulation*

Lymph node slices were obtained using sterile technique from 4 naïve female C57BL/6 mice as described in section 2.2. The slices from each mouse were randomly assigned to each of 4 conditions: 1.) PreStain + Stimulation, 2.) PreStain + No Stimulation, 3.) No PreStain + Stimulation, or 4.) No PreStain + No Stimulation. Slices in the PreStain groups were stained as described in section 2.3 with anti-B220 FITC, anti-Lyve1 eFluor 570, and anti-CD69 Alexa Fluor 647 (Table S1). Unstained control slices were left in media at 37 °C during this time (no prestain). After prestaining, all slices were imaged on Zeiss AxioZoom macroscope. The slices were then placed in 500 µL of complete media in a 24-well plate and cultured for 16 hours at 37 °C, with or without 1.25 µg/mL anti-CD3Ɛ. After incubation, slices were imaged again to quantify loss of signal from the prestain, stained once more using the same reagents and procedure, and imaged again.

4.3.9 *Immunization*

Rhodamine-conjugated chicken egg ovalbumin (Rhod-OVA) was prepared by reacting 1 mg/mL OVA (Ovalbumin, InvivoGen, San Diego, CA) with 10x molar excess NHS-Rhodamine (Fisher Scientific). The reaction was performed for 1 hour at 25 °C. Excess unreacted fluorophore was removed via centrifuge filtration using a 50 kDa

molecular weight cut off (MWCO) filter (Fisher Scientific), spinning at 14,000 G for 3-5 minutes, repeatedly adding PBS until excess dye was removed. A solution of 1.2 mg/mL Rhod-OVA in PBS was mixed 1:1 v/v with Complete Freund's Adjuvant (CFA; Invivogen) and vortexed for 30 min to generate an emulsion. Mice were injected subcutaneously with 25 µL per site, in the left and right shoulders, flanks, and right rear hock (125 µL total per mouse), to ensure drainage to each of the skin-draining LNs and the right popliteal LN. Control animals were vaccinated with PBS only. LNs were harvested 4 and 7 days after vaccination, sliced, and immunostained with anti-B220 FITC and anti-Lyve-1 eFluor 660 (lymphatics).

4.3.10 *Conjugation of antibodies*

Antibodies that were not available with the required fluorophore were conjugated in house using fluorophores with N-hydroxy succinimidyl ester (NHS) to amine conjugation chemistry. NHS fluorophores (Fisher Scientific) were mixed with 50 µg of 1 mg/mL or 0.5 mg/mL antibody at molar excess of 15X or 30X respectively. The reaction was performed for 1 hour at 25 °C. Excess unreacted fluorophore was then removed via centrifuge filtration using a 50-kDa molecular weight cutoff filter (EMD Millipore Amicon Ultra 0.5 mL, Fisher Scientific), spinning at 14,000 G for 3-5 minutes, repeatedly adding PBS until excess dye was removed. Labeling ratio was measured by UV-Vis on a ND1000 nanodrop spectrophotometer (Fisher Scientific) at 280 nm and λ_{max} of fluorophore. Fragments were conjugated in a similar manner.

4.3.11 *Antibody fragmentation*

Anti-CD45R/B220 F(ab')$_2$ antibody fragments were prepared by digestion with pepsin enzyme (Immobilized Pepsin Agarose Resin, Fisher Scientific). Pepsin resin in 20 mM sodium acetate buffer, pH 4.0, was mixed at 10% w/w with antibody at 1 mg/mL and incubated for 5 hours at 37 °C while shaking. Reaction was stopped by removing pepsin resin using a 10-µm pore centrifugal filter (Pierce spin column, Fisher Scientific). Antibody fragments were buffer exchanged into PBS using a 50 kDa MWCO filter. Analysis of fragments was performed via non-reducing SDS PAGE (NuPage 4-12% Bis-Tris, Fisher Scientific) with Commassie stain (Commassie R250, Fisher Scientific).

4.3.12 *Image analysis*

Images were analyzed in ImageJ v1.48. To measure fluorescent intensity, a region of interest was drawn and the average signal was measured. For image display, brightness and contrast were adjusted uniformly across all compared slices unless otherwise specified.

4.4 Results and Discussion

4.4.1 *Development of live immunostaining procedure*

A naïve LN has a distinct cellular organization: B cells are concentrated in follicles around the periphery of the node, T cells are primarily in deep paracortex (center of the organ), and DCs are scattered throughout (Figure 4-1).[195,196] These cells are organized within lobules surrounded by Lyve-1-positive lymphatic sinuses. In a LN undergoing an immune response, B cell follicles expand and/or multiply to maximize interaction with T cells and B-T cell region interfaces may be disrupted.[196,197] Therefore, staining for B cells and lymphatics is often used to provide a first-order map of the gross structure of fixed sections of lymph node.

Here we tested procedures for fluorescent immunostaining of thick, live slices of lymph node. Briefly, immunofluorescence staining was performed by incubating the tissue first with CD16/32 (Fc receptor block) and then adding a cocktail of fluorophore-conjugated antibodies to label cells or structures of interest. Directly conjugated primary antibodies were used to avoid the additional processing time that would be needed to apply a secondary antibody. Only small-molecule fluorophores were used (e.g. Alexa Fluors), rather than the protein-based fluorophores commonly used for flow cytometry, to minimize the barrier to diffusion. After staining, the slices were washed with PBS to remove unbound reagents.

The staining procedure was performed using FITC-labelled anti-B220 as a prototype antibody, seeking to sufficiently maximize the ratio of fluorescent signals from anti-B220 and its Rat IgG2a isotype control (Iso Ctrl) in dual-stained slices. The signal ratio was tested as a function of incubation time, temperature, and wash time (Figure 4-1). We observed that the B220/Iso Ctrl ratio increased significantly with incubation temperature from 4 – 37 °C (Figure 4-1a) and time from 1 – 60 minutes (Figure 4-1b). For wash time, we observed that nonspecific binding of the isotype control was reduced to insignificant levels after a 30 - 60-minute wash in PBS at 37 °C (Figure 4-1c, d-g), thus increasing B220/Iso Ctrl signal. The best observed conditions were a 60-minute stain time at 37 °C followed by a 60-minute wash, but for practical purposes we find that 30-minute staining and washing is often sufficient. We now use this procedure routinely for other antibodies as well, including anti-Lyve-1 for lymphatics and CD69 (see section 4.3.3).

Despite the inclusion of Fc-blocking antibody in the cocktail, the IgG antibodies bound non-specifically to Fc receptors, leading to some undesirable off-target staining particularly in the sinus and medulla of the tissue (Figure 4-1g).[198] We found that for this clone of anti-B220, the degree of off-target staining from the intact antibody was acceptably low, but for some other antibody isotypes it exceeded the on-target staining (data not shown), necessitating the use of antibody fragments instead.

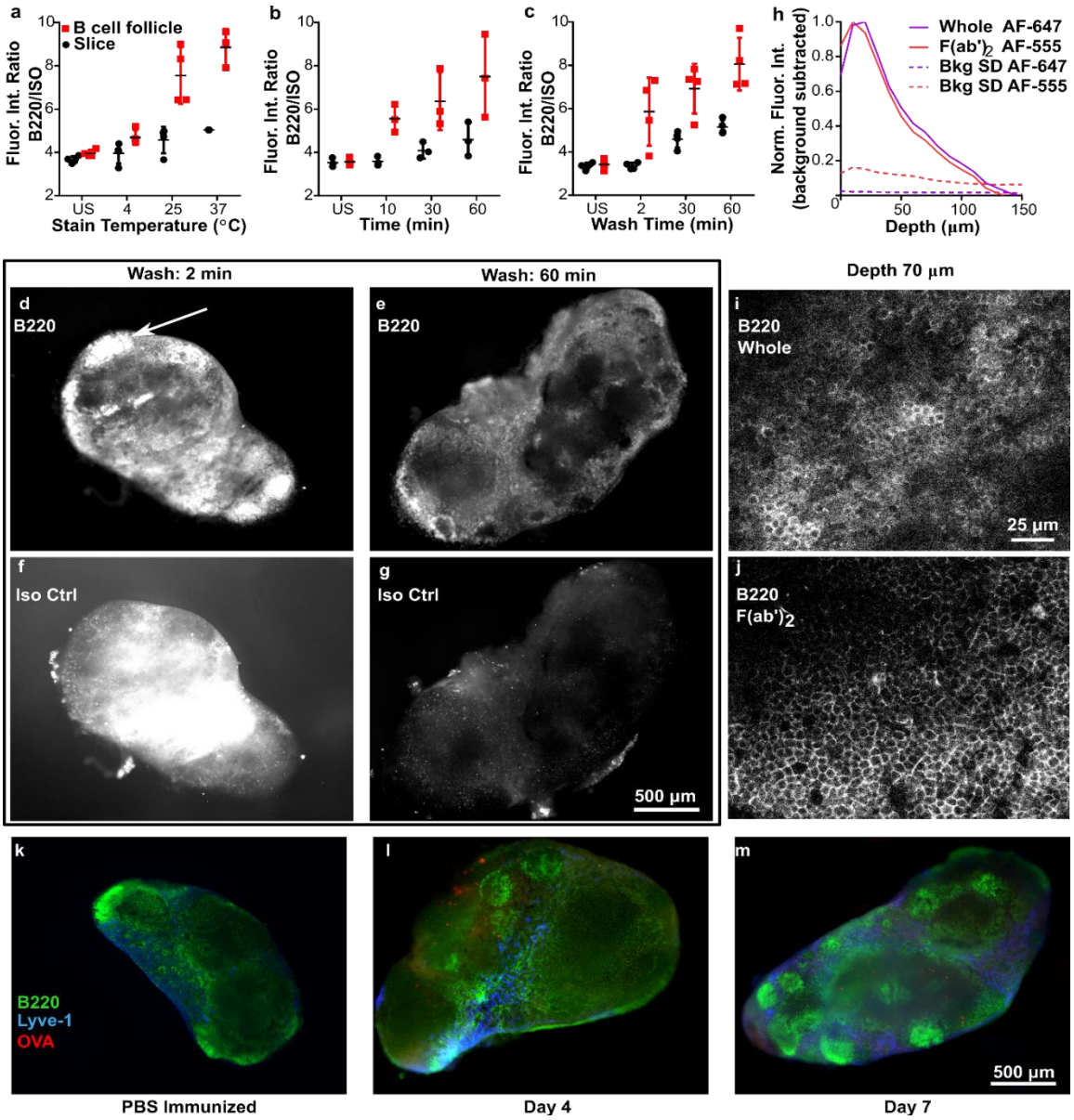

Figure 4-1: Immunostaining procedure yields bright and specific staining at least 70 µm deep and reveals structures in lymph node. (**a-c)** Testing for sufficient stain time, temperature, and wash time. The fluorescent intensity ratio (FITC-anti-B220/ Alexa Fluor 594-IsoCtrl) was averaged over the entire slice or over a selected B cell follicular area. Conditions: 1-hr stain, 30-min wash; b: 37 °C, 30-min wash; c: 37 °C, 1-hr stain. (**d-g)** Representative images of slices stained with anti-B220 and its isotype control, after washing for 2 or 60 minutes. White arrow indicates B cell follicle. **(h)** Fluorescent signal of anti-B220 IgG and F(ab')$_2$ as measured by confocal microscopy. Dotted lines indicate one standard deviation (SD) of autofluorescence background as a function of depth, and solid colored lines indicate the average background-subtracted intensity (N=20). **(i-j)** Confocal images of antibody and fragment staining at a depth of 70 µm, both labeled with Alexa Fluor 647. **(k-m)** Immunostaining of slices at different timepoints can reveal changes in substructure. After vaccination with rhodamine-OVA in CFA or with saline control, slices were stained with FITC-anti-B220 and eFluor 660-anti-Lyve-1.

As cells at the cut faces of the slice are expected to be damaged, it is useful for labelling reagents to penetrate at least several cell layers deep into the tissue. Using confocal microscopy, we observed that anti-B220 whole IgG and F(ab')$_2$ fragments labelled with Alexa Fluor 647 and Alexa Fluor 555, respectively, were both detectable above the autofluorescence signal to ~ 120 μm deep after a 60-minute stain time (Figure 4-1h and Figure 4-2). This is consistent with the expected diffusion coefficients for antibodies in intact tissues.[199,200] Similar results were obtained when the whole IgG and F(ab')$_2$ fragment were labelled with DyLight 488 and Alexa Fluor 647, respectively (data not shown), suggesting that the observed depth of penetration was not influenced significantly by choice of fluorophore. However, we were unable to quantify the exact penetration of antibodies or fragments into the tissue with this method, due to limitations of light scattering in the tissue, and images collected deeper than 70-80 μm showed significant

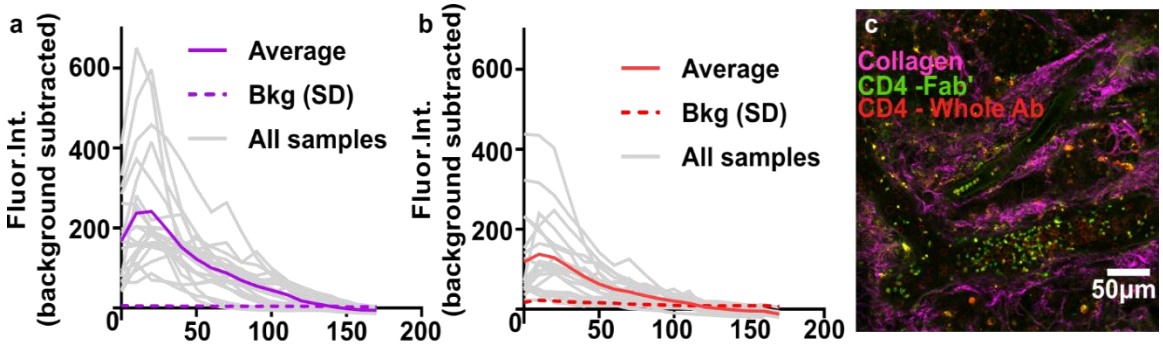

Figure 4-2: Antibody and fragment signal in live lymph node slicesas a function of depth. Slices were stained with **(a)** Alexa Fluor 647-labelled whole IgG and **(b)** Alexa Fluor 555-labeled F(ab')$_2$ fragment for B220. Dotted lines indicate one standard deviation (SD) of autofluorescence background as a function of depth, and solid colored lines indicate the average background-subtracted intensity (averaged across all 20 positions). For the plots shown in Figure 1h, the average and background-SD lines were normalized to the maximum intensity of the average line for each staining reagent. **(c)** Image of lymph node slice collected by two-photon microscopy, showing CD4 positive T cells FITC-CD4 Fab' and Rhodamine-CD4 whole antibody, within the collagen matrix (second harmonic imaging).

drop-off in intensity, quality, and clarity. When labelled with matching fluorophores, $F(ab')_2$ fragments tended to have marginally better image quality than whole IgG at the same depth (Figure 4-1 i-j, and Figure 4-2c), perhaps due to decreased binding by Fc receptors.

As a proof of principle, the live immunostaining protocol was used to visualize immune-driven structural changes after in vivo vaccination. Mice were immunized with Rhodamine-conjugated OVA emulsified with CFA, or with PBS as a negative control. Draining LNs were harvested 4 and 7 days after vaccination, sliced, and live immunostained with anti-B220 and anti-Lyve-1 (lymphatics) (Figure 4-3). Consistent with prior studies,[197] we observed that the LN structure was visibly altered in the vaccinated mice, with an increased variability in B cell follicle size and position throughout the LN (representative images shown in Figure 1 k-m). At 4 and 7 days post vaccination there was increased number of B cell follicles (Figure 4-3a), disruption of the T-B cell boundary, and formation of germinal centers containing B220-negative plasmablasts (Figure 4-3b).[197] For example, in the PBS-immunized mouse, the T cell zones were relatively open and the B cell follicles were restricted to the periphery of the LN. In contrast, in the vaccinated mouse, the B cell follicles were of variable size and spread sporadically throughout the LN. Rhodamine-OVA was visible in a punctate distribution confined to the T cell zones (the central areas unstained by B220 or Lyve-1), consistent with its uptake by antigen-presenting cells (Figure 4-3e inset).

One feature of tissue slices from is that the composition of the slice varies substantially with the position or depth in the lymph node from which the slice was collected. Therefore, structures can be highly variable between slices, and a large number of slices must be examined to determine general trends or, in the future, conduct meaningful quantification of changes. Spatial heterogeneity would be expected in other structured organs as well, including tumors and brain tissue. This variability highlights the benefit of labelling live slices ex vivo to identify phenotypic regions prior to experiments intended to stimulate specific regions with drugs or immunotherapies.[16,191,194]

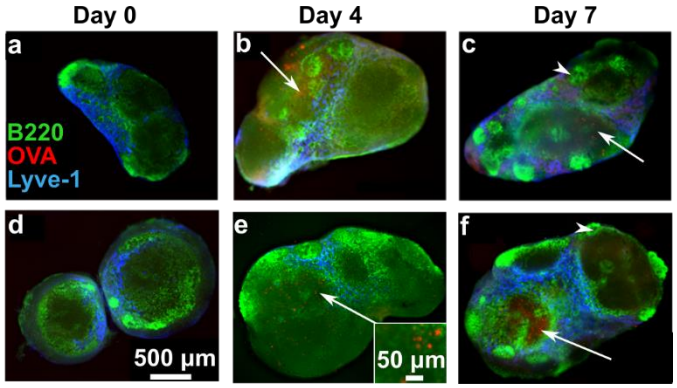

Figure 4-3: Live immunostaining reveals altered structures after in vivo vaccination. Mice were vaccinated with rhodamine-OVA in CFA. LNs were harvested 4 or 7 days following the vaccination, sliced, and stained live with FITC-anti-B220 and eFluor 660-anti-Lyve-1. Axillary LNs from **(a)** PBS immunized, **(b)** day 4, and **(c)** day 7 mice. Brachial LNs from **(d)** PBS-immunized, **(e)** day 4, and **(f)** day 7 mice show increased LN size after vaccination. T-B boundary disruption and change in B cell follicular structure are observed at days 4 and 7. White arrowheads indicate possible germinal centers, and white arrows indicate regions of punctate Rhodamine-OVA (expanded in inset of (e)). Brightness and contrast uniformly adjusted for each fluorophore.

4.4.2 *Slices remained viable and functional after live immunostaining*

As we intended to use live immunostaining on tissue prior to short-term culture (Figure 4-4a), we tested the extent to which immunostaining altered the viability of the tissue or affected its ability to respond to stimuli. Slice viability was measured after immunostaining by using Calcein AM to assess cell membrane integrity.[191] Compared to slices that were never immunostained, viability of immunostained slices was uncompromised (Figure 4-4b), both immediately after staining and 6 hours after staining.

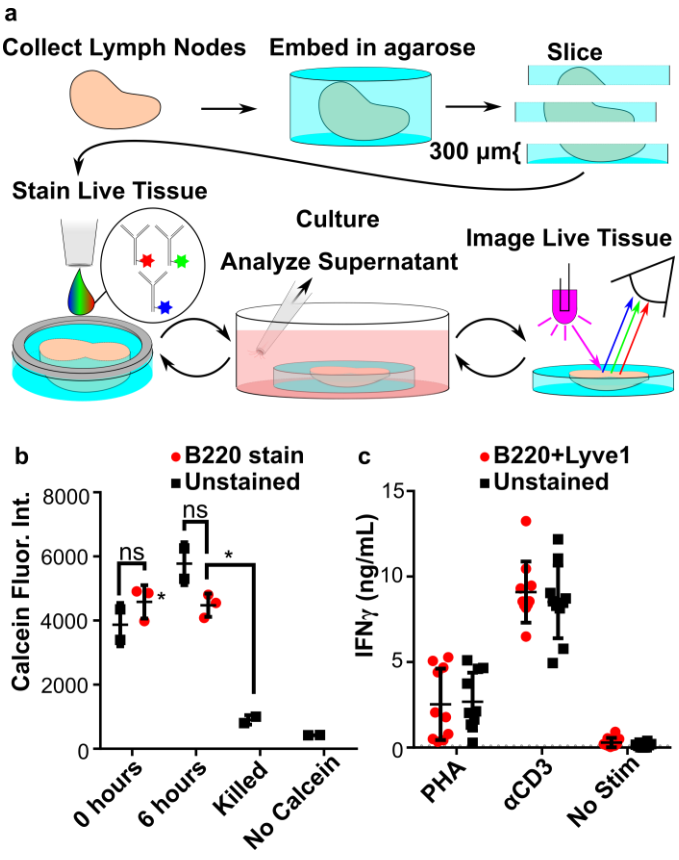

Figure 4-4: Live lymph tissue slices can be stained and culturedwithout impacting viability and function. **(a)** Overview of procedure for live immunostaining. During the culture period, stimuli can be added to slices. **(b)** Slices showed no difference in viability after immunostaining. Calcein fluorescent intensity was at 0 and 6 hours after immunostaining with anti-B220. **(c)** Immunostaining neither inhibited nor promoted an immune response in slices. Slices dual-stained for B220 and Lyve-1 were incubated for 20 hours with or without activation by PHA or anti-CD3Ɛ. IFN-γ was quantified in the supernatant by ELISA.

Tissue function was assessed by measuring the secretion of IFN-γ after stimulation with phytohemagglutinin-L (PHA), a polyclonal T cell activator (Figure 4-4b). Slices that were dual-stained with anti-B220 and anti-Lyve-1 secreted similar quantities of IFN-γ as

unstained slices after stimulation, indicating that immunostaining did not affect T cell responses. Furthermore, in the absence of stimulation, these antibodies did not induce IFN-γ secretion. TNF-α secretion was below the limit of detection (123 pg/mL) for all conditions.

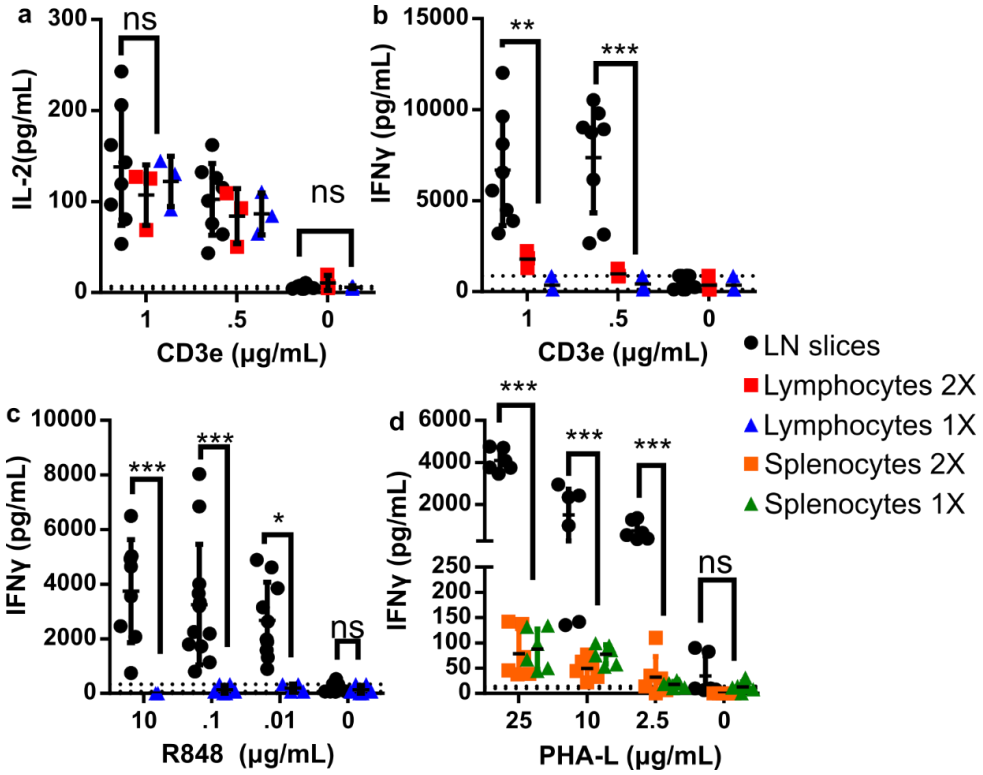

Figure 4-5: Live lymph node slices maintain in-situ conditionsand have more pronounced response to stimuli than cell culture at similar cell density. **(a)** IL-2 secretion after 20-hr stimulation with CD3e. IFNγ secretion after 20-hr stimulation with **(b)** CD3Ɛ, **(c)** R848, and **(d)** PHA-L. N = 6-12 slices and 3-5 cell cultures Mean ± Standard Deviation. 2-way ANOVA with multiple comparisons. *p=0.0102, **p=0.0029, ***p=.00001, ****p<0.0001, n.s. denotes p>0.05.

In contrast to the results with anti-B220 and anti-Lyve-1, immunostaining with anti-mouse CD3Ɛ antibody (clone: 145-2C11) activated T cells significantly more than PHA stimulation ($p < 0.0001$, two-way ANOVA with Sidak's multiple comparisons). This was true for both labeled and unlabeled anti-CD3Ɛ. Antibody-mediated crosslinking of cell

surface CD3 is a standard strategy for T cell activation in cell cultures,[4,5,6] and this result indicates that T cells in intact tissue can be activated in the same manner. Thus, when immunostaining for cell-surface antigens in live lymph node slices prior to subsequent experiments, care must be taken to avoid antigens such as CD3, whose cross-linking leads to cellular activation.

Notably, such type of stimulations are more pronounced in live tissue than in cell culture. Figure 4-5 a,b show that CD3Ɛ, which directly stimulates T cells, caused a dose dependent increase T cell production of IFNγ in live LN slices as compared to lymphocyte cells cultured at a similar concentration. Each LN slice was determined to contain approximately $0.85x10^6$ cells and was cultured in 500µL, just enough media volume to cover each slice. Even when the cell culture density is doubled in respect to slices, the response is still markedly less. We believe that the increased response is likely due to the fact that the microenvironment of the tissue remains intact and thus the increased proximity of cells (cell-cell interactions) and the formation of local cytokine gradients are not as diluted/spread out as they would be in culture. Other stimuli, such as direct T cell stimulation with the lectin PHA-L (Figure 4-5d) and indirect T cell stimulation via antigen presenting cells (APC) with R848 (Figure 4-5c), also show a similar dose dependent IFNγ response that is increased over lymphocyte and splenocyte cultures. Although it may also be that APC dependent responses are decreased in culture due to loss during the crushing/filtering process. Responses like this illustrate the benefit and challenges to using ex-vivo live tissue, namely that ex-vivo maintains the in-situ microenvironment and that live immunostaining must be validated for each specific application, depending on the cells

or behavior of interest (e.g. to test the impact on function of B cells and lymphatic endothelial cells). Furthermore, while these experiments provided a relative assessment of viability and T cell function with respect to the immunostaining procedure, further work is needed to quantify the impact of slicing and extended culture on the viability and function of thick tissue slices. Both physical damage from the blade and depletion of oxygen or nutrient supply may play a role in slice physiology.

4.4.3 Live immunostaining revealed responses to ex vivo stimulation

Live immunostaining of thick tissue slices offers the unique advantage that the tissue can be imaged and then cultured ex vivo, stimulated, and analyzed repeatedly over time to detect changes in organization or function. Repeated analysis of the same tissue is not possible when using flow cytometry or conventional imaging of fixed tissue sections. As a proof of principle, live immunostaining was used to visualize immune-driven changes in the upregulation of CD69 (Figure 3). CD69 is a surface marker that is expressed in activated T Cells and is highly upregulated within several hours of T Cell receptor/CD3 ligation. In addition to testing CD69 upregulation by CD3 ligation, we also tested whether pre-staining the tissue had an impact on the observed response.

To observe baseline surface marker expression prior to stimulation, slices from naive LNs were stained with a cocktail of FITC anit-B220, eFluor570 anti-Lyve-1, and Alexa Fluor 647 anti-CD69, or left unstained, and imaged. After overnight culture with or without anti-CD3Ɛ, all slices were imaged again, then stained and imaged a third time. Prior to re-staining, overnight culture decreased the fluorescent intensity of all three markers by half (Figure 4-6), suggesting that the reagents slowly unbound and diffused out

of the tissue over time. Thus, re-staining the same tissue slices after 1 – 2 days can reveal the organization of the tissue at that time, with only minimal interference from the previous staining step.

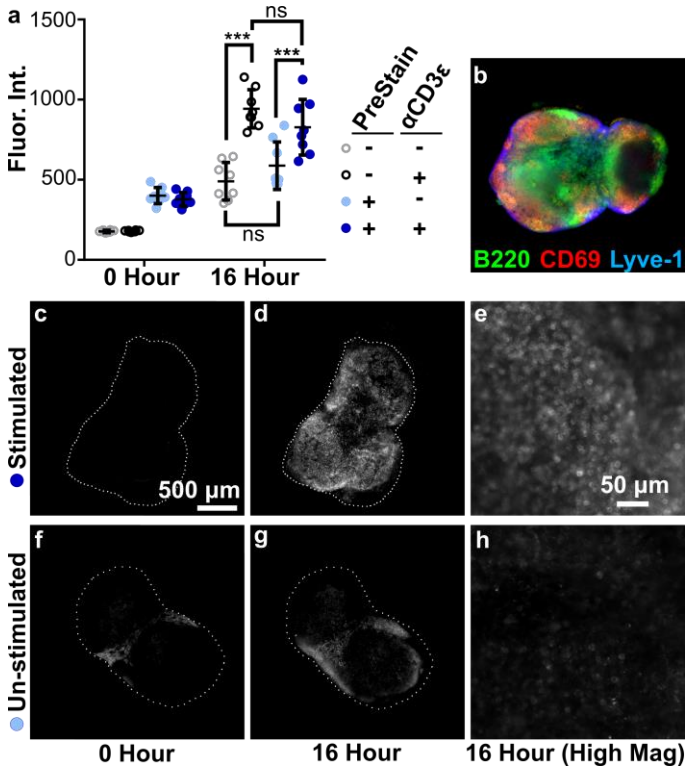

Figure 4-6: Live immunostaining of LN slices before and after CD3 stimulation revealed increase of CD69 surface markers. Live LN's were sliced and stained before stimulation (PreStain) to observe baseline in CD69 presentation. Slices were cultured and stimulated with anti-CD3Ɛ and then stained again. **(a)** Mean fluorescent intensity of CD69 signal, imaged before (0 Hour) and after stimulation (16 Hour). **(b)** A slice after anti-CD3Ɛ stimulation, showing B220, Lyve-1, and CD69. (**c-h**) anti-CD69 images: PreStained + αCD3Ɛ **(c)** before and **(d)** after culture, and **(e)** high magnification after culture in the same slice; PreStained - αCD3Ɛ **(f)** before and **(g)** after culture, and **(h)** high magnification after culture in the same slice. Dashed white lines show the outline of the tissue slice.

After culture, anti-CD3Ɛ stimulated slices showed a drastic increase in CD69 and statistical analysis showed a significant difference between stimulated and unstimulated slices. Interestingly, un-stimulated slices also showed a slight increase in CD69 expression.

In addition, pre-staining the tissue made no difference in overall fluorescent intensity, indicating that the immunostaining method did not, for this readout, significantly affect the behavior of the tissue. Furthermore, the fluorescent intensity of B220 and Lyve-1 did not significantly change before or after stimulation (Figure 4-7), confirming that the increase seen in CD69 signal was the result of a change in state of the tissue rather than an artifact of the procedure.

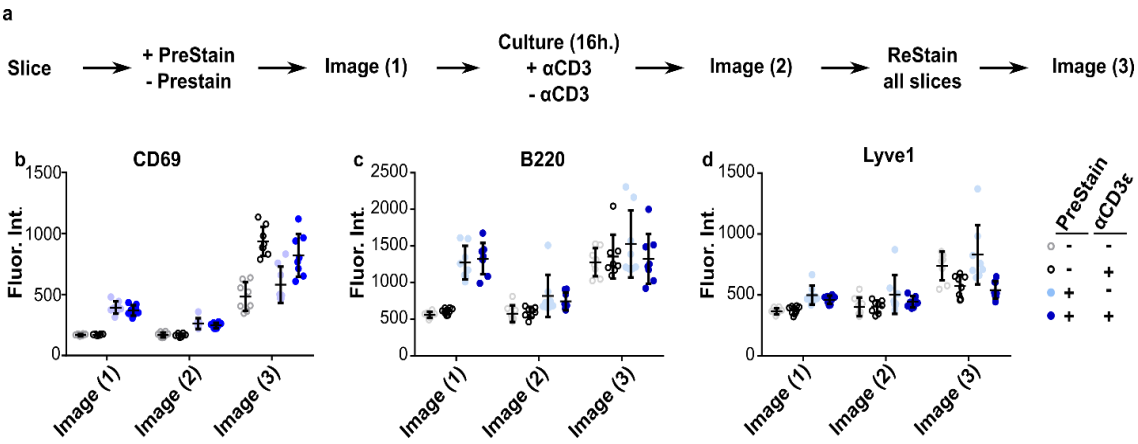

Figure 4-7: Immunostain fades over timeand B220 and Lyve 1 do not change significantly after stimulation with αCD3Ɛ. Slices were stained with a cocktail mix of anti-CD69 Alexa Fluor 647, anti-Lyve1 eFluor 570, and anti-CD45R/B220 FITC. **(a)** Experimental timeline for the PreStaining, stimulation (16 hour culture), and ReStaining of the same lymph node slice to determine change in surface marker presentation over time. Note that Image (1) and Image (3) are referred to as 0 Hour and 16 Hour, respectively, in the main text. Fluorescent intensity for **(b)** anti-CD69 Alexa Fluor 647 (repeated from main text for clarity), **(c)** anti-CD45R/B220 FITC, and **(d)** anti-Lyve1 eFluor 570 is shown for each imaging step listed in the timeline.

2.5 Conclusions

In conclusion, we describe a validated protocol for immunostaining live 300-µm-thick LN slices with fluorescent antibodies or antibody fragments. The live immunostaining protocol provides an organizational map of the LN slices while maintaining viability, allowing continued tissue culture, and preserving cytokine responses. The method was

suitable to detect immune-driven changes not only in slices obtained from mice at different timepoints after vaccination (*in-vivo* structural changes) but also in the same slice at different timepoints during culture and stimulation (*ex-vivo* functional change). Because this method is similar to traditional immunocytochemistry and does not depend on genetic reporters, in principle it can be used to investigate other soft live tissue samples, including human tonsil tissue and murine thymus.[189,190] It has been used previously to provide guidance for local stimulation of specific regions of LN tissue,[191,194] and may prove useful to pre-screen tissue samples for regions of interest prior to experimentation.

Chapter 5: Development of conjugated antibody fragments “dual affinity reagent” for on-cell detection of cytokines in live lymph node tissue

5.1 Abstract

Within the immune system, the lymph nodes are often considered the central hub of the immune response, where cells and cytokine signal pathways are stimulated across highly organized regions of the node. Upon activation, a number of cytokine signaling molecules are also released by both cells to help propagate the immune response. We have previously shown that we can study and observe morphological changes in live lymph node tissue slice substructures in response to a global stimuli or vaccination. However, this is only a portion of an immune response, as the secreted cytokine signals, which play an invaluable role in immune function, are yet unable to be spatially observed within live tissue. We hypothesize that different diseases may produce unique cytokine signatures (spatial and temporal) within the lymph nodes and would allow us in the future to obtain new unique insights into disease progression and may identify key pathways, events, or sub-structures to target for new therapies. Here we present a novel method to perform a cytokine immunoassay within live tissue using a conjugated bispecific antibody “dual affinity reagent.” We discuss the production of the dual affinity reagent and propose several validation experiments for its use in observing spatially discrete cytokine release from lymph tissue in response to immune stimuli.

5.2 Introduction

The immune system is a complex network of cells and signaling proteins called cytokines, which function to protect our body from harmful self and non-self-entities, such as viruses, bacteria, and cancer. During an immune response, cytokine signaling pathways are critical to help coordinate immune cells to function properly and specific types of cytokine signaling have been linked to chronic inflammatory diseases such as multiple sclerosis, cancer, and rheumatoid arthritis[202,203]. Within the immune system, the lymph nodes are often considered the central hub of the immune response, where cells and cytokine signal pathways are stimulated across highly organized regions of the node. As discussed in Chapter 4, lymph nodes have several key sub-structures whose spatial organization can affect immune responses. One such region that is critical for an adaptive immune response is the paracortex, a region that is rich with T cells, wherein the T cells are activated by antigen presenting cells (APC's).[204] To activate, those T cells physically interact with the APC's through surface proteins, T cell receptors (TCR) on T cells, and major histocompatibility complexes (MHC) on APC's. Upon activation, a number of cytokine signaling molecules are also released by both cells to help propagate the immune response.[201]

We have previously shown that we can study and observe morphological changes in live lymph node tissue slice substructures in response to a global stimuli or vaccination. However, this is only revealing half of the story of an immune response, as the secreted cytokine signals, which play an invaluable role in immune function, are yet unable to be spatially observed within live tissue. We hypothesize that different diseases may produce unique cytokine signatures (spatial and temporal) within the lymph nodes and would be

beneficial to study; similarly to how we discussed in Chapter 4 that studying live tissue spatial morphology changes in response to certain diseases may allow provide new unique insights into disease progression and may identify key pathways, events, or sub-structures to target for new therapies.

The purpose of this project is to develop a novel method for the detection of cytokine released by T cells in live lymph node tissue. Doing so will provide a better understanding of the T cell specific signaling pathways and their spatial orientation within

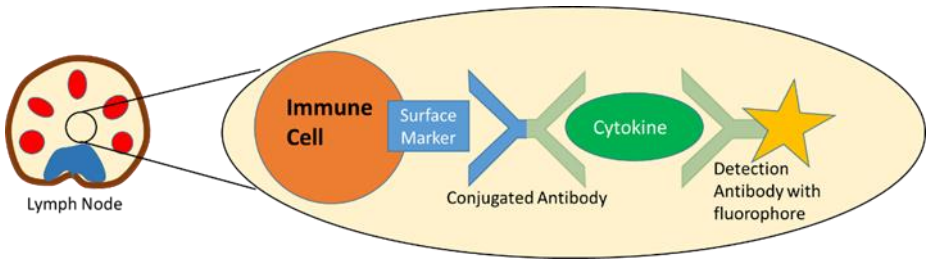

Figure 5-1: A schematic of cytokine detection on an immune cellsurface using a conjugated antibody. The conjugated antibody will bind to a specific immune cell of interest and capture a specific cytokine of interest as it is secreted by the immune cell. A detection antibody labeled with a fluorophore is added to fluorescently detect and quantify the captured cytokine.

the lymph node, thereby providing valuable insight into the complex and unique signaling pathways activated during different disease-driven immune responses. The method for cytokine analysis, as seen in figure 1, involves conjugating an immune cell specific antibody with a cytokine specific antibody in order to detect cytokine secretion from the surface of the immune cell. This method has advantages over the current traditional analyses for cytokine detection from immune cells, namely that our method will allow for analysis within live tissue while maintaining the spatial organization of the local microenvironment. Commonly techniques like enzyme linked immunosorbent assay

(ELISA) and enzyme linked immunospot (ELISpot) assays are used to measure cytokine profiles produced by immune cells. Techniques such as these are limited to in- vitro, as the assays often take place in well plates and require processing of sample before the assay. In many cases, lengthy processing steps are necessary if a single type of immune cell's cytokine profile is to be measured. And while these types of assays have been integrated onto microfluidic devices in order to eliminate the need for lengthy processing steps, they often still require the isolation of a single cell type[205], thereby losing critical information that can be gathered by observing the immune cells response in its natural microenvironment. One alternative to these in-vitro methodologies may be the use of cytokine reporter mice, wherein transgenic mice have a fluorescent protein or other reporter encoded into the cytokine sequence. However, the process of modifying, breeding, and maintaning transgenic mice for a single cytokine reporter is a highly costly and labor intensive affair.[206] A low cost, approachable method for in-situ cytokine detection, such as one that employes conjugated atibodies, would be benificial to have.

The use of conjugated antibodies for cytokine detection has been shown previously by Desombere et al[207] and Manz et al[208] in cell cultures and analysis by flow cytometry. However, this technique has not been performed in live tissue, the reason for which may be that antibodies have inherent immunogenic properties. The function of an antibody is to mark a bound substrate for degradation by effector cells, such as macrophages, B cells, and dendritic cells. Effector cells recognize is the tail region of antibodies, also known as the Fc region, which both initiates an immune response, but also reduces specificity of antibodies as an immunostaining agent. For this reason, in order to use antibodies to detect

cytokines in live tissue, we have removed the immunogenic Fc region of the antibodies to create $F(ab')_2$ antibody fragments. Relying upon established techniques, Fc removal can be enzymatically performed by digestion with pepsin. However, as discussed in Chapter 2, Fc removal efficiency by pepsin digestion is dependent on the host, isotype, and clone of the antibody and needs optimized before use.

For the specific analysis of IFNγ from CD4 T cells, the proposed conjugate must be modified further to avoid an unwanted response by CD4 t cells. The binding of IgM and IgG to CD4 T cells is believed to cause dimerization of CD4 surface marker of the T cell, thereby initiating a T cell response resulting in the inactivation and downregulation of the CD4 surface marker[97,209,210]. Dimerization of the surface marker normally occurs during binding of MHC II complex, when antigens are presented to the T cells, however early dimerization before the MHC II complex is bound can inhibit cell function. For this reason, we plan to reduce the hinge region disulfide bonds of the $F(ab')_2$ fragments to create Fab' antibody fragments, which consist of only one binding site. By binding only, a single CD4 surface marker per conjugated antibody, we hypothesize that we can limit the dimerization of CD4, and prevent loss of cell function.

This chapter describes the process of creating the dual affinity antibody reagents, including the generation of antibody fragments, the troubleshooting of conjugating fragments together via click chemistry, the ongoing validation experiments, and the proposed experiments to highlight their applications and use in live lymph tissue slices.

5.3 Methods:

5.3.1 Antibody Fragmentation and Reduction

The antibody clones used were HRPN, R4-6A2, XMG1.2, GK1.5 (Bio X Cell, West Lebanon, NH), and RA3-6B2 (BioLegend, San Diego, CA). Antibodies were buffer exchanged to the desired pH by using a PEO-treated 50-kDa MWCO centrifuge filter. For fragmentation, antibodies were buffer exchanged into 100 mM formic acid buffer (pH 2.8 – 3.5) or 20 mM sodium acetate buffer (pH 4.0 – 5.0). These buffers were made in house with formic acid or sodium acetate in DI water and adjusting the pH with HCl or NaOH. All reagents were from Fisher Scientific unless otherwise noted.

Antibodies were fragmented using immobilized pepsin on 6 % agarose resin (pepsin resin, Fisher Scientific). This pepsin product was reported to have 1-1.5 mg/mL enzyme in a mix containing glycerol storage buffer. The same batch of pepsin was used for all samples (LOT: SB246536, activity 10,012 Units/mL). To prepare the pepsin resin for use, it was removed from storage buffer, pipetted into a 0.5 mL Peirce spin column (Fisher Scientific), centrifuged for 30 s at 100 G, and resuspended in the desired pH buffer (i.e. formic acid buffer or acetate buffer). Next, the immobilized pepsin and the buffer-exchanged antibody solution were mixed together so that the final concentration of antibody was 1 mg/mL. The sample was placed in an incubator at 37 °C on a shaker, shaking gently for the duration of the reaction. After the reaction, fragmented antibody sample was separated from immobilized pepsin using a 0.5-mL Peirce spin column, which allows the antibody solution to pass through while retaining the resin-bound enzyme above the column. The immobilized pepsin resin was rinsed several times with phosphate

buffered saline (PBS, no calcium or magnesium). The sample (eluent from the first and subsequent rinses) was collected, then buffer exchanged into PBS and concentrated using a PEO-coated 50-kDa MWCO centrifuge filter. $F(ab')_2$. Antibody samples were stored at 4°C in PBS until analysis. GK1.5 $F(ab')_2$ was reduced to single Fab' with 25 mM beta mercaptoethylamine (2MEA, Fisher Scientific) with 5 mM ethylenediaminetetraacetic acid (EDTA, Fisher Scientific) in PBS for 60 min at 37°C. Sample was buffer exchanged with 5mM EDTA in PBS. 10µL of 100mM N ethylmaleimide (Fisher Scientific) in 95% ethanol was added to sample to cap sulfhydryls, and incubated overnight at 4°C. The sample was buffer exchanged with PBS.

5.3.2 *Conjugation with Succinimidyl esters*

Antibodies, antibody fragments, and BSA were conjugated to succinimidyl ester linkers using 5 – 20% molar excess linker in PBS for 1 hour at room temp. Samples were buffer exchanged with PBS to remove excess linker. To determine linker ratio of click chemistry linkers, an aliquot of sample was removed and reacted with 30X molar excess linker – fluorophore overnight at 4°C. Samples were buffer exchanged with PBS and label ratio was analyzed by nanodrop UV/VIS at 280nm and λmax for fluorophore. For click chemistry conjugation, samples were mixed in molar ratios of 1:1 unless otherwise specified, overnight at 4°C.

5.3.3 *SDS PAGE*

Antibody fragmentation samples were analyzed using 4-12 % Bis Tris NuPAGE SDS PAGE (Fisher Scientific) with MOPS buffer (Fisher Scientific). To preserve the structure of antibodies and $F(ab')_2$ during analysis, the samples were not reduced (no beta-

mercapto ethanol) and were not heat-treated, unlike standard treatment prior to SDS PAGE. In addition to the fragmentation samples and controls, a standard curve (1 mg/mL – 0.1 mg/mL) of corresponding whole antibody was also run on the gel. A Precision Plus molecular weight ladder (BioRad, Hercules, CA) was included in lane 1. Samples were prepared according to vendor specifications using Lithium dodecyl sulfate (LDS) sample buffer 4X (Fisher Scientific) and DI water. Sample loading was calculated to never exceed 1.5 µg/lane. SDS PAGE was run at 175 V constant for 52 min, which was long enough for the solvent front to reach the end of the gel. Gels were stained with Commassie R-250 (Fisher Scientific) as per vendor instructions. Images of gel were collected on a ChemiDoc XRS+ (BioRad), and images were analyzed using Image Lab v5.2.1 (BioRad).

5.3.4 *ELISA*

A high-binding plate (Corning Costar 96 well ½ area, #3690; Fisher Scientific) was coated with 2 µg/mL soluble murine CD4 (Sino Biological, Wayne, PA) in PBS overnight at 4°C. Wells were blocked for 2 hours with 1% BSA and 0.05% Tween-20 (Fisher Scientific) in PBS (block solution). 2µg/mL "dual affinity reagent" in block buffer was added and incubated for 2 hours, then washed. Serial dilutions of IFNγ cytokine (Peprotech, Rocky Hill, NJ) were prepared in block solution. These samples were added to the plate and incubated for 2 hours, then washed. Streptavidin-conjugated anti-IFNγ R46A2 (BioLegend) were added to the plate at 0.5 µg/mL in block solution for 2 hours, then washed. Avidin HRP 1:500X (Biolegend) was added at 1X in block buffer for 30 minutes, then washed. All washing steps were performed with 0.05% Tween-20 in PBS. Plates were developed using TMB substrate (Fisher Scientific) and absorbance values were read at 450 nm on a plate reader (CLARIOstar; BMG LabTech, Cary, NC). To determine

concentration of sample solutions, calibration curves were fit in GraphPad Prism 6 with a sigmoidal 4 parameter curve (Eq. (1)), where X is log of concentration, Y is absorbance, min and max are the plateaus of the sigmoidal curve on the Y axis, and HillSlope describes the steepness of the slope.

$$Y = min + \frac{max - min}{1 + 10^{(Log(IC50 - X) * HillSlope)}} \quad (1)$$

5.3.5 *Animal work*

Female C57BL/6 mice were purchased from Jackson Laboratory or Taconic (USA) and housed in the University of Virginia vivarium with food and water ad libitum. All animal work was approved by the Institutional Animal Care and Use Committee at the University of Virginia under protocol #4042, and was conducted in compliance with guidelines the Office of Laboratory Animal Welfare at the National Institutes of Health (United States). Where noted, mice were vaccinated with chicken egg ovalbumin in complete Freund's adjuvant prior to collection of lymph nodes (see Supporting Methods).

5.3.6 *Flow cytometry*

On the day of the experiment, the animal was anesthetized with isoflurane and euthanized by cervical dislocation. The spleen was removed, and immediately placed into ice-cold DPBS without calcium or magnesium (Lonza, Walkersville MD, #17-512F) with 2% heat-inactivated FBS (Gibco, Fisher Scientific, Waltham, MA). Spleens were crushed through a 70μm mesh filter into 10 mL complete media. Complete media consisted of RPMI (Lonza RPMI 1640 without L-glutamine, #12-167F) supplemented with 10% FBS, 1% L-glutamine, and 1% Pen/Strep, 50 μM beta-mercaptoethanol, 1 mM pyruvate, 1% non-essential amino acids, and 20 mM HEPES (Fisher Scientific). All centrifugal steps

were for 5 minues at 400G. Samples were centrifuged, supernatant removed, and lysed with 2mL ACK lysing buffer for 1 minute. 2 mL of 2% serum in PBS (flow buffer) was immediately added. Samples were centrifuged, supernatant removed, and suspended in 10mL complete media. Cells were counted on inverted microscope with hemocytometer and trypan blue (Fisher Scientific) (1:10 sample:trypan blue v/v). Stains were: "dual affinity reagent" – Alexa Fluor 647, anti-CD4 FITC, CD3- PE, and 7AAD (Biolegend) used at 3ug/mL (for 150kDa antibody). Samples were 1M ($1x10^6$) cells at 2M cells/mL, blocked with 25 µg/mL CD16/32 in flow buffer for 5 minutes. Samples were centrifuged, supernatant removed, and stained with 100uL stains in flow buffer for 30 minutes at 4°C. Samples were washed with 500 µL flow buffer, centrifuged, supernatant removed, and resuspended in 500 µL flow buffer. Sample were stored on ice until analysis. Before analysis 10 µL of 7AAD solution was added. For killed control, samples were placed in 500µL 70% ethanol for 10 minutes. Samples were run on Guava flow cytometer (EasyCyte 6-2L, Millipore Sigma, Burlington MA), and analyzed with FCS express.

5.4 Results

5.4.1 Rational for reagent design

In order to prevent unwanted immunogenicity and off-target binding via receptor dimerization and Fc binding, the antibodies first had to be fragmented and reduced to $F(ab')_2$ and Fab' fragments respectively. **Chapter 2** discusses the fragmentation of antibodies in more detail, but briefly, antibody fragmentation via enzymatic digestion often needs to be optimized. In some cases, optimization may look different depending on the application, as some parameters can have trade-offs, such as higher yield digestion using a more acidic buffer may lead to reduced affinity, and vice versa. In some scenarios, the desired product may be mixed with under or over fragmented products, requiring the sample to be purified, or if purification is not available, the fragmentation can be optimized to minimize unwanted byproducts. Notably this is the case for many of the digestions we have performed, as separations of fragments can be difficult to perform, or require access to specialized equipment.

Separation by size exclusion can be done via centrifugal or chromatographic columns, but samples are often extensively diluted during fractionation, requiring time consuming concentration of each fraction before detection. Alternatively, affinity purification can be performed, however for some antibodies, such as the ones used for "dual affinity reagent" standard methods of protein G or A are unusable as protein A doesn't bind to our antibody host type (Rat IgG) and protein G binds to both Fab and Fc. The $F(ab')_2$ fragments can be positively or negatively selected by their binding target (ex. Cytokine), or by a secondary anti-Fc antibody. However, purifying with target proteins such as cytokines can be prohibitively expensive to acquire enough to coat a column and

purify even a small-moderate amount of antibody (ex. 50 µg). We briefly tested purification with anti-Fc antibodies, but as discussed in **Chapter 1**, validation of antibody reagents is important, and commercial antibodies can vary from batch to batch, or during a change in production process. We were able to successfully purify antibody fragments by removing Fc containing unfragmented/partial fragmented antibodies from $F(ab')_2$, however within a few months and purchasing of new antibody batches, the anti-Fc antibodies began to show cross reactivity and bound both Fc and $F(ab')_2$. Over the next few months other antibodies from different vendors were tested, but Fc removal purification still resulted in poor yield of $F(ab')_2$. With this in mind, we chose to optimize our fragmentation procedures to produce as little unfragmented/under-fragmented antibody as possible.

The 3 antibody case studies presented in **Chapter 2** are the antibodies intended for use in formation of the "dual affinity reagent" for on-cell cytokine detection. To briefly summarize the results, 2 anti-IFNγ antibodies and 1 anti-CD4 antibodies were digested to $F(ab')_2$ fragments with the enzyme pepsin. The GK1.5 clone anti-CD4 antibody fragmented with high yield and maintained affinity, whereas both the anti-IFNγ antibodies had to compromise yield to improve purity (clone R46A2) or affinity (clone XMG1.2). After successful fragmentation anti-CD4 $F(ab')_2$ was split into single Fab' fragments (Figure 1 lane 5) by reducing hinge region cysteine disulfide bonds with 2-mercaptoethylamine (2MEA).

5.4.2 *Generation and troubleshooting of Dual affinity reagent*

Once fragments of antibodies were successfully produced, the next challenge was to conjugate them together to form the dual affinity reagent. To link the antibodies together, we initially desired to take advantage of the cysteine sulfhydryl's of the hinge region of the Fab' fragment. Unlike more common targets such as lysine residues being conjugated with succinimidyl esters (as discussed in **Chapter3**), cysteine sulfhydryls are often much less abundant in proteins, and are often inaccessible as they form cysteine disulfide bonds. However, the lack in abundancy of cysteines is desirable when wanting to conjugate the protein to a small number of or single linker. With single Fab' fragments, the 2 hinge region disulfide bonds are exposed, making them an ideal target to site specific conjugation with a linker. Figure 5-2a (lanes 6, 7, 8) shows the initial attempts to conjugate an anti-IFNγ $F(ab')_2$ to an anti-CD4 Fab' using SMCC crosslinker, a linker comprised of a succinimidyl ester for amine conjugation on $F(ab')_2$ and malemide conjugation to cysteines on Fab'. The SMCC reagent would first be added to $F(ab')_2$, allowed to conjugate, and excess linker filtered out before addition of Fab'. A range of molar excess of SMCC to $F(ab')_2$ was tested. Results indicated minimal conjugation of antibodies, with the majority of reactant remaining unconjugated. Even at 20X excess of SMCC, unreacted Fab' concentration remained largely the same. We then tested independently the number of available Fab' cysteines by conjugation with an excess amount of fluorescent maleimide tag. Surprisingly we found that, for this specific anti-CD4 Fab', on average there was approximately 0.5 cysteines/antibody. Indicating that even after disulfide reduction the disulfides were inaccessible, either due to sterics, reformation of disulfide bonds with another Fab' or reduced heavy/ light chain, or more likely formation of a new disulfide between the two

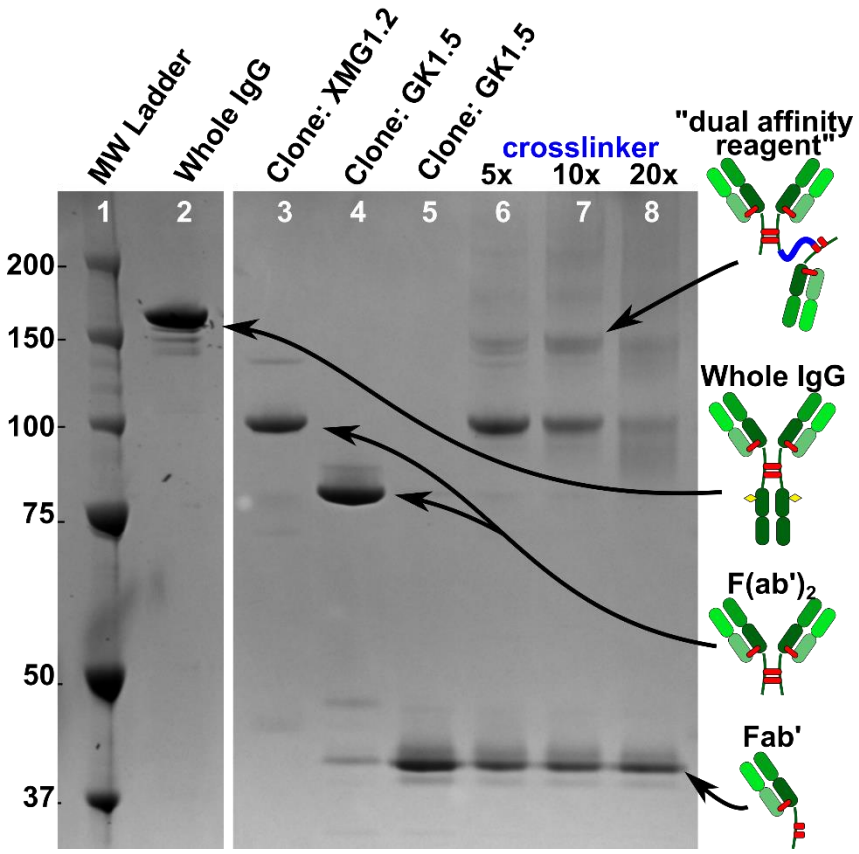

Figure 5-2: Antibody fragments are conjugated togetherto form "dual affinity reagent". SDS PAGE image of whole antibody (lane 2), anti-IFNγ clone: XMG1.2 F(ab')$_2$ (lane 3), anti-CD4 clone: GK1.5 F(ab')$_2$ (lane 4) and reduced Fab' (lane 5), and conjugation of GK1.5 Fab' to XMG1.2 F(ab')$_2$ with increasing amounts of SMCC crosslinker (blue) at 5X (lane 6), 10X (lane 7), and 20X (lane 8) molar excesses.

remaining hinge region cysteines. Additionally, confounding the conjugation of antibodies, maleimides can undergo hydrolysis, thus loosing reactivity. This hydrolysis of the SMCC linker may occur during the time it takes for the conjugation of succinimidyl ester to F(ab')$_2$. For these reasons we decided to move away from a single reagent linker, towards two linkers which could be independently conjugated to the fragments, and then reacted together.

To perform this, we chose to use click chemistry, as click chemistry is highly orthogonal, no unwanted cross-reactivity, and reactions are thermodynamically favorable often occurring in a single step, as if the two reagents simply "clicked" together. We first chose to use a well-known and common click chemistry reaction using azides and alkynes. To test conjugation using succinimidyl ester azide and DBCO alkyne we first tested it on conjugating bovine serum albumin (BSA; 66 kDa) to whole antibody (150 kDa). The number of linkers (linker ratio) attached to Ab and BSA were determined via UV/VIS by reacting with excess click label attached to a fluorophore. Average linker ratios were optimized to be close to be close to 1, to prevent multimer formation. Figure 2 lane 2 shows the results of a 1:1 molar Ab: BSA conjugation, where we observed little to no conjugation. Increasing BSA by 10-fold (Figure 5-3, lane 3) showed an increase in conjugated product (200 kDa); however, it produced < 10% of expected conjugate. We hypothesize that the conjugation reaction may be less efficient than predicted due to two

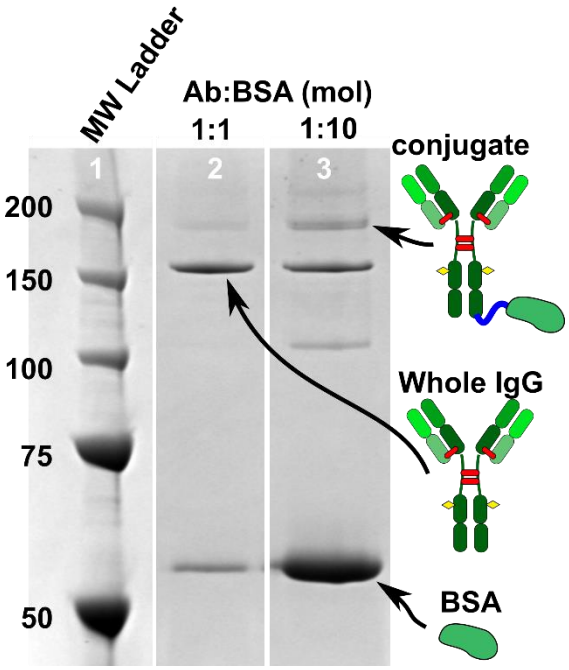

Figure 5-3: Conjugation optimization using azide and DBCOalkyne click chemistry. SDS PAGE image of whole antibody conjugated to bovine serum albumin (BSA) with increasing molar amounts of BSA; 1:1 Ab: BSA (lane 2) and 1:10 Ab: BSA (lane 3). Linker ratio of 0.86 for succinimidyl ester – azide - antibody, and 1.36 for succinimidyl ester – DBCO – BSA.

factors: 1) low average linker ratio and 2) slow reaction time for alkyne – azide click chemistry. Linker ratios for succinimidyl ester linkers are likely to follow a normal distribution due to so many protein lysine residues being available to bind to. While this may vary somewhat from protein to protein, there is expected to be populations of proteins with 0, 1, 2, or even 3 linkers attached. Thus, for protein conjugation of Ab-BSA we expect there to be some non-binding as well as multimer production. While there is indeed a faint band of multimer present in figure 3, the amount of unconjugated BSA and Ab would indicate either a much lower linker ratio than determined, or a slow rate of reaction.

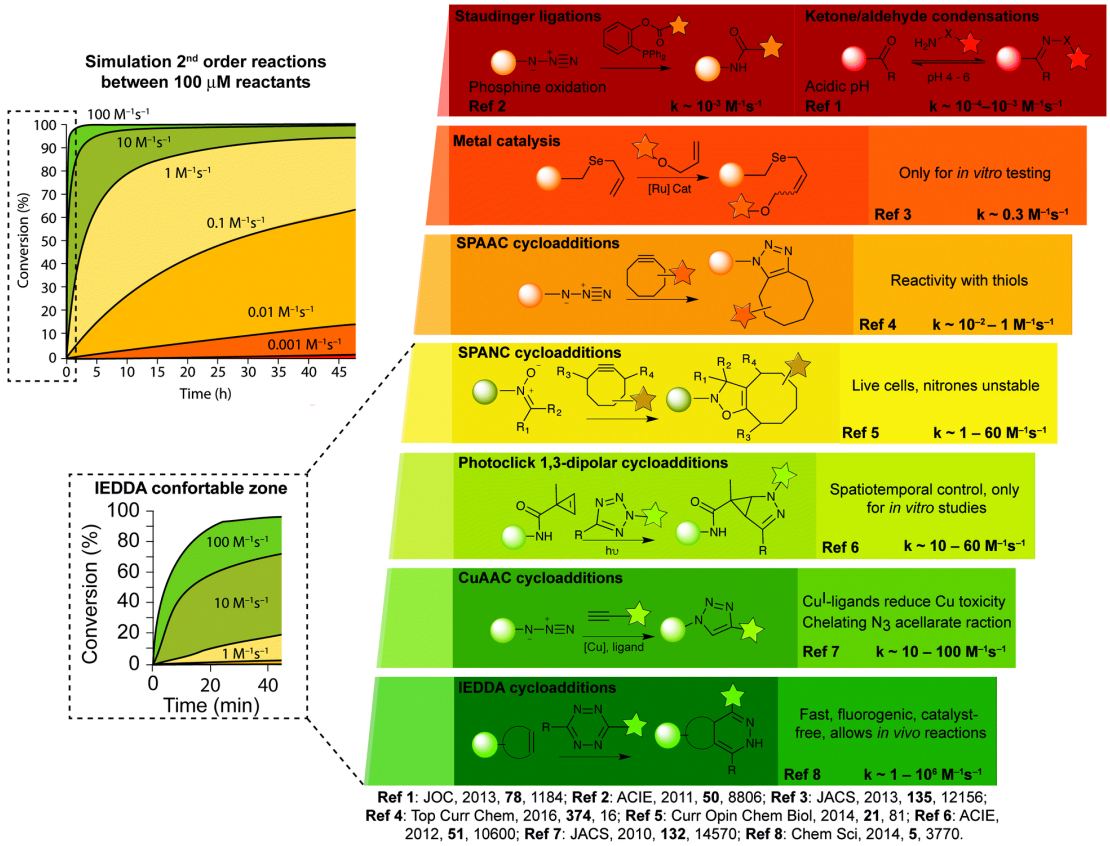

Figure 5-4: Common click chemistries and reaction rates. Reproduced from Oliveira, B.L., Guo, Z., and Bernardes, J.L. Inverse electron demand Diels-Alder reactions in chemical biology. (2017) Chem. Soc. Rev., 46, 4895-4950 with permission from The Royal Society of Chemistry.

Upon further review, we investigated the expected reaction rates for several click chemistry reactions. Figure 5-4 shows an overview of typical reaction rates. The slower reaction rates for azide-alkyne compare well with our observed conjugation experiments, and explain why most published procedures suggest that an excess of 10-50x linker should be used to drive the reaction towards completion within a timely manner. Because antibodies are expensive, and the fragmentation process to produce $F(ab')_2$ and Fab' can be sometimes be inefficient, any reaction procedure involving a large excess of antibody is undesirable. Because of this, we switched to using transcyclooctene (TCO) and tetrazine click chemistry. At the concentrations we are using the antibodies (1mg/mL) in a 1:1 conjugation reaction, TCO – tetrazine should result in 90% conjugation in a few minutes to an hour, as opposed to days/weeks for DBCO alkyne – azide.

Using succinimidyl ester TCO and tetrazine, we were able to successfully conjugate anti-CD4 Fab' to anti-IFNγ $F(ab')_2$ (Figure 5-5a, b). However, production of the conjugate "dual affinity reagent" is difficult to reproduce, likely due to variations in labeling ratio. We observed that an increased linker ratio around 2-3 help improve yield of "dual affinity reagent"; and while there was some unconjugated antibody and multimer formation, we determined that this was likely to minimally impact our experiments. We believed that any unconjugated reagent would not be able to produce a signal without both antibodies, and that multimer reagent immunostaining would not be able to penetrate/diffuse into live tissue due to increased size. We performed a modified sandwich ELISA (Figure 5-6a, b) to validate that the conjugated "dual affinity reagent" maintained functionality to bind both CD4 and IFNγ. Results from the ELISA indicate that the "dual affinity reagent" worked as

expected, and was able to capture IFNγ in a dose dependent manner and provide a quantitative measurement.

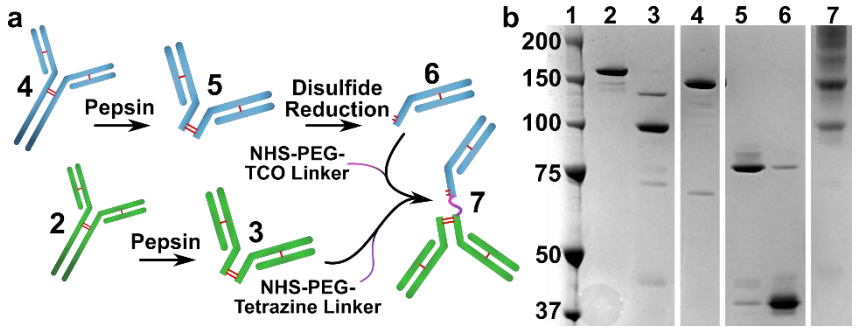

Figure 5-5: TCO and Tetrazine click chemistry conjugated "dual affinity reagent"retains affinity for both CD4 and IFNγ. **a)** Schematic for synthesis of "dual affinity reagent", numbers correspond to **b)** SDS PAGE image of reagent synthesis.

A flow cytometry experiment using splenocyte cell culture was performed to test the specificity of the "dual affinity reagent" for CD4 T cells. The "dual affinity reagent" was labeled with a fluorophore and added to the splenocyte. We observed that while the dual affinity reagent did stain CD4 T cells, it also stained 7% of splenocytes that were not T cells (Figure 5-6d, e), indicating that there is minimal cross reactivity with another cell type. We must note here, that this is current on-going research, and the specific cells to which the "dual affinity reagent" binds, is being investigated. However, we hypothesize that the off-target binding observed may be due to a small amount of Fc containing fragment still present in the sample.

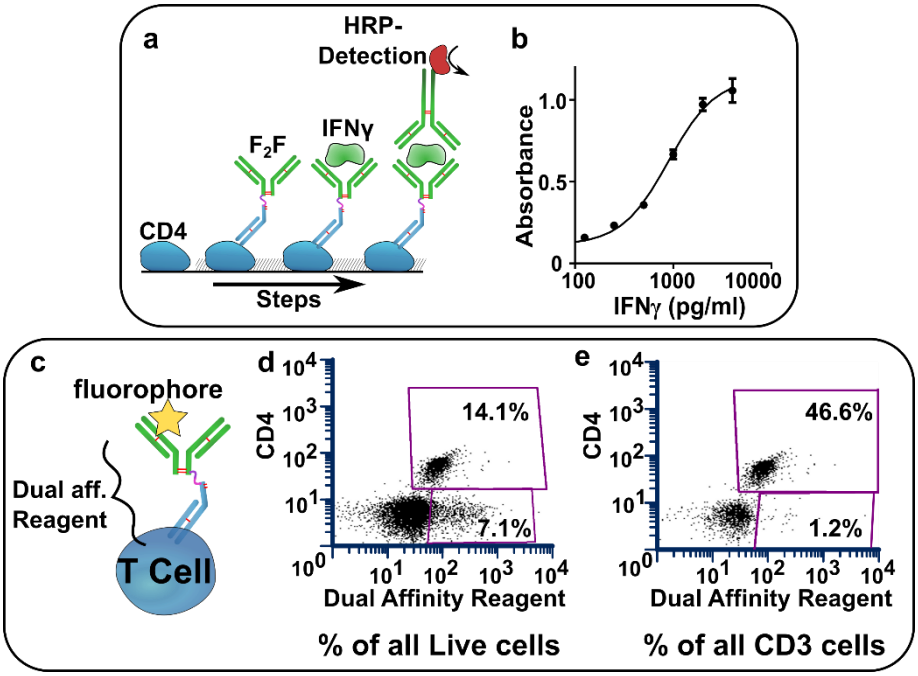

Figure 5-6: Preliminary data for "dual affinity reagent". **a)** schematic for **b)** ELISA analysis of "dual affinity reagent". **c)** schematic for flow analysis of reagent. **d)** population of all live cells and **e)** CD3 cells that the "dual affinity reagent" stained.

5.4.3 *Alternatives to antibody based "dual affinity reagents"*

We briefly investigated the use of short peptide mimics to replace antibodies in the "dual affinity reagent" for on cell detection of IFNγ from CD4 T cells. As discussed in Chapter 1, peptide mimics and DNA aptamers are capable of binding protein targets in a similar manner to antibody binding. Due to their decreased size in comparison to antibodies, aptamers and peptide mimics are capable of diffusing further into tissue, and don't suffer many of the same issues such as antibodies, like Fc receptor binding on effector cells. In collaboration with the Kelly lab, University of Virginia, we tested 4 different 12 a.a. long peptide sequences as an alternative to anti-CD4 antibody. However unfortunately we determined through plate immunoassays and flow cytometric analysis, that the peptides

had a wide range of affinities and a high amount of cross-reactivity, as they tended to non-specifically stain nearly all cells within a splenocyte cell culture.

5.4.4 *Proposed work: Specificity of reagent*

As this is on-going research, we have planned a number of experiments to validate the use of a "dual affinity reagent" for on cell detection of IFNγ from CD4 T cells. First and foremost, we will validate that the "dual affinity reagent" is specific for both CD4 surface marker and IFNγ cytokine. We have already shown that the "dual affinity reagent" is specific for both targets within a simple plate-based immunoassay. Moving forward we will also test specificity with in-vitro cell culture by flow cytometry, and in ex-vivo lymph node slices by IHC. In both in-vitro and ex-vivo, we will use a fluorophore labeled "dual affinity reagent" and fluorescent anti-CD4 $F(ab')_2$ to observe co-staining of CD4 T cells and identify if any of-target binding is occurring. This procedure is more accessible in-vitro with flow cytometry, where in the case of off target binding, we can add additional fluorescent antibodies to stain other common cell types to identify the binding partner. In ex-vivo slices, co-staining of CD4 T cells will be confirmed by confocal fluorescent microscopy, and we will observe the general brightness and pattern of staining to determine if the "dual affinity reagent" is sufficiently diffusing into the tissue similar to a typical antibody stain, or if it is aggregating in unexpected regions. Depth of "dual affinity reagent" penetration in to tissue will be compared to $F(ab')_2$ and whole antibody by either confocal or 2 photon microscopy. During these experiments we will also optimize the live tissue staining procedure of the "dual affinity reagent", similar to Chapter 4, wherein the amount of antibody, staining time, and washing time will be optimized to provide the highest fluorescent signal to noise ratio.

After conformation of CD4 specificity, we will test specificity for IFNγ in both in-vitro cell culture and ex-vivo lymph slices. We will first spike IFNγ into our samples rather than stimulating cell production, in order to approach saturation of "dual affinity reagent" to best ensure binding and thus signal. The samples will then be washed to remove any unbound IFNγ. IFNγ binding will be confirmed by adding a different fluorescent anti-IFNγ $F(ab')_2$. Similar to a sandwich ELISA, the second anti-IFNγ antibody (detection antibody) will be a different clone that binds a different epitope on the opposite side of the IFNγ to ensure minimal blocking/ steric hinderance for both antibodies binding. The procedure and conditions for staining live tissue with the detection antibody will be optimized, similar to that of staining with "dual affinity reagent", to provide the highest signal to noise.

5.4.5 *Proposed work: Quantification and spatial resolution*

We next plan to perform a set of experiments designed to determine how quantitative/qualitative IFNγ capture and detection is, as well as how spatially resolved is the data. For the first part, we will make a calibration curve of slices spiked with different amounts of IFNγ to roughly determine what the limit of detection is, at what concentration of IFNγ is the "dual affinity reagent" saturated, and what is the confidence interval is for the fluorescent signal at any given IFNγ concentration (i.e. how quantitative is the method). To account for differences in local CD4 T cell concentration, fluorescent IFNγ signal will be normalized to the signal from co-staining with a second anti-CD4 antibody.

Once we have characterized and optimized the procedures for live tissue immunostaining with the "dual affinity reagent", we will then investigate how spatially resolved the measurements are. Spatial resolution for the "dual affinity reagent" is

markedly different from that of a normal antibody immunostain. We are not only interested in the spatial location of cells, but the local concentration of cytokine that is being actively secreted from those cells over time. In the ideal scenario, the "dual affinity reagent" will capture IFNγ cytokine immediately after its released, and it would only capture the cytokine released from the cell onto which the "dual affinity reagent" is bound. However, it is more than likely that as the cells slowly secrete cytokines, and as those cytokines diffuse, that the "dual affinity reagent" will capture some cytokines from neighboring cells. The amount of neighbor cytokine bound by the "dual affinity reagent" is likely to increase with increasing incubation (stimulation) time. We need to characterize how far away from parent cells cytokines may be captured and how long it may take to saturate all the "dual affinity reagent" in tissue, indicating a complete loss of spatial resolution.

To determine spatial resolution, we will take several approaches. First, we will determine what is the minimal amount of time that samples need to be incubated with a stimulus to produce a signal above LOD threshold, as well as how long it takes until the "dual affinity reagent" is saturated. These timed experiments will indicate an approximate time range to initially study. We will test several T cell stimuli, such as phytohemataglutanin (PHA-L), anti-CD3, and R848 to find an average range. In the case that the time ranges are very unsimilar, we will use the reagent with the shortest time range, so as to limit the time that the cytokine has to diffuse, thus helping to preserve spatial resolution. Using these time ranges we will then develop an agent based computer model, such as net-logo, to model how far away from the parent cell a cytokine is bound based on experimental data of incubation time, IFNγ diffusion coefficient, and amount of "dual

affinity reagent" bound to each cell. We will also experimentally validate the computer model by performing a local stimulation of T cells and monitoring cytokine capture on nearby (non-stimulated cells). This will be performed using a microfluidic device which our lab has previously published,[211] which can deliver stimulus to multiple discrete regions of the tissue.

3.4.6 *Proposed work: Cytokine "maps" from stimulated tissue*

Lastly, to illustrate an application of our on-cell detection method, we will perform a vaccination experiment to observe local cytokine concentration and distribution and compare to a globally stimulated slice (i.e. a slice bathed in stimuli), as well as an un-stimulated control. To perform this, we would inject mice with OT II T cells, which are reactive to ovalbumin (OVA) protein. The OT II cells will migrate to the lymph node after a 3-4 days, then we will collect and slice the nodes. The OT II T cells will be mixed in with the population of normal T cells. Upon incubation with OVA, antigen presenting cells (APC), such as B cells and macrophages, will take up and process the OVA to then present for recognition by OT II T cells via the major histocompatibility complex (MHC II). OT II T cells will interact with the APC's in discrete regions of the lymph node, such as the boundary between the T cell rich paracortex and the B cell germinal centers. We hypothesize that the resulting IFNγ cytokine response and capture by the "dual affinity reagent" should have distinct "spatial signature" over time as compared to slices in which all T cells are activated simultaneously by bathing slices in a stimulus such as anti-CD3 or PHA which directly stimulate T cells. We do expect these sets of experiments may require extensive optimization; however, we believe that at least some, if not most, of the same

conditions optimized previously for staining time, reagent concentrations, incubation time, washing time will translate to these experiments with minimal fine tuning.

5.5 Conclusions and future directions

In conclusion, we have described the synthesis of a "dual affinity reagent" consisting of a $F(ab')_2$ and Fab' antibody fragment for the purpose of performing an on-cell capture and detection of IFNγ release from CD4 T cells. We have begun to validate the "dual affinity reagent" and have proposed several experiments to show that the reagent maintains functional ability and specificity to bind both CD4 and IFNγ, as well as optimizations for staining procedures to obtain the highest S/N. We have also proposed experiments to characterize how quantitative or qualitative the captured IFNγ signal is, as well as an immunization experiment to show how T cell activation by antigen presenting cell produces a different cytokine spatial "signature" over time as compared to a global direct T cell stimulation. We have also begun investigating the use of small peptide mimics for the "dual affinity reagent", which due to their smaller size and improved penetration into the tissue, may eventually replace the use of antibodies. In the future, we plan to make this detection system for a variety of immune cells and cytokine targets, allowing for the modular mixing and matching of a range cytokine for many types of immune cells. This would allow for the tracking of multiple cytokines and cells, limited only by the number of fluorophores at one time available for fluorescent imaging. We believe that this method of on-cell cytokine detection will be an invaluable tool to study the progression of other immune related diseases such as rheumatoid arthritis or multiple sclerosis. We hypothesize that the spatial and temporal information gathered about cytokine release during the

progression of a disease, may provide insights into the diseases, and reveal key events, timepoints, or spatial regions to target for novel therapies.

Chapter 6: Conclusions and future directions

6.1 Conclusions

This dissertation describes the modifications, validation, and immunohistochemical applications of antibodies. This work was driven by the need for cost effective, approachable, and user-friendly methods to modify and validate antibodies. While recombinant antibodies hold a lot of potential for creating novel therapies or reagents, they are often inaccessible for most research. Recombinant antibodies allow for precise modification such as making fragments or combining two separate sequences to produce humanized Fc antibodies or bispecific antibodies capable of binding two different targets. However, production of recombinant antibodies is a time consuming and expensive process, requiring expertise and specialized equipment that the average research lab does not have. Furthermore, because of the expense, there is a lack of commercially available recombinant antibodies. Thus, cost effective and approachable methods for antibody fragmentation and conjugation are needed.

In Chapter 2, we described a simple and systematic strategy to reach desired levels of yield, efficiency, and function for the production of $F(ab')_2$ fragments from small quantities of IgG, including analysis of affinity after enzymatic digestion. Because antibody enzymatic fragmentation is often difficult to predict, and can vary by isotype and clone, this work provides a quick and cost-effective guide for researchers to produce in-house generated antibody fragments without the need for recombinant expression or haphazard trial and error approaches. As part of this guide, we demonstrated three antibody

fragmentation case studies, for which the antibody fragments are then used for a novel assay in Chapter 5. For fragmentation optimization, we determined that the pH had the largest impact on fragmentation, likely due to affecting the activity of the enzyme pepsin and the interaction of the antibody sample due to unfolding, with the active site of the enzyme. We also showed how enzyme to sample ratio and reaction time can affect fragmentation, and how in certain scenarios there can be trade-offs, such as between fragmentation efficiency and affinity of the generated fragment. Trade-offs such as this illustrate why generation of fragments, and antibody modification in general, also needs to be coupled with reagent validation such as affinity and cross-reactivity analysis.

In Chapter 3, we describe a novel microfluidic Slip Chip device for small scale optimization of antibody labeling prior to scale-up (moderate/large scale production). Antibody labeling via reactive groups such as succinimidyl esters with lysine residues is a common method for attaching fluorescent tags. However, the labelling reaction can often be difficult to predict. If label ratios are too low, then the fluorescent signal may be too low, and if label ratios are too high, it can affect antibody affinity. Due to antibody expense, traditional benchtop optimization can be costly, thus we have developed a microfluidic device that provides quick small-scale optimization of labeling in a cost effective and user-friendly format. This device has been designed to use 5-10 µg total of antibody and test multiple Ab: fluorophore ratios. We have also described on-going work for the incorporation of a gel matrix into a Slip Chip for a novel passive diffusion-based separation of antibody sample and excess un-reacted fluorophore. This chip has also been designed to fit within a 3D printed plate reader adapter, for quick and easy UV/Vis detection. In the

future we will transition fabrication to a fully 3D printed chip to enable a less labor-intensive and higher-throughput fabrication. This will enable more rapid and affordable prototyping, increased 3D design complexity, and will allow for greater dissemination of our design.

The work presented in Chapter 4 demonstrates the use of both fragmented and labeled antibodies for use in staining live lymphatic tissue slices. Live tissue explants are an incredibly useful tool for observing changing morphologies over time and in response to diseases or other stimuli, which would otherwise be difficult to perform in-vivo. Immunohistochemical staining of tissues with antibody reagents is one primary method to detect spatial and morphological changes in tissue, but requires validation for each new tissue type. Here we describe the optimization and validation of several antibody stains for lymphatic immune tissue. The live immunostaining protocol provides an organizational map of the LN slices while maintaining viability, allowing continued tissue culture, and preserving cytokine responses. The method was suitable to detect immune-driven changes not only in slices obtained from mice at different timepoints after vaccination (*in-vivo* structural changes) but also in the same slice at different timepoints during culture and stimulation (*ex-vivo* functional change). Because this method is similar to traditional immunocytochemistry and does not depend on genetic reporters, it can be used, in principle, to investigate other soft live tissue samples, including human tonsil tissue and murine thymus. Similarly, in Chapter 5, we present a novel method to observe the release of cytokine signals from immune cells in live lymph tissue using a conjugated bispecific antibody “dual affinity reagent.” We discuss the production of the dual affinity reagent

and propose several validation experiments for its use in observing spatially discrete cytokine release from lymph tissue in response to immune stimuli.

We believe that studying live tissue spatial morphology changes and cytokine release in response to certain diseases may allow us in the future to obtain new unique insights into disease progression and may identify key pathways, events, or sub-structures to target for new therapies.

6.2 Future work

While some of our presented research is still ongoing, we have also begun to plan for the future for both our Slip Chip device and the on-cell detection of cytokines from live lymph tissue. The Slip Chip device is currently being fabricated in glass, as glass provides a rigid and smooth surface perfect for slipping. Additionally, the surface of glass can be easily modified with silanes to add new chemistries, such as the hydrophobic fluorosilane or the polymerizable methacrylate silane. However, the wet-etching process for glass is time and labor intensive, as well as hazardous (due to the use of hydrofluoric acid). To enable broader dissemination, a less labor-intensive fabrication strategy is necessary. While traditional high throughput fabrication like injection molding and hot embossing are best for mass production, high up-front costs for master molds are prohibitive to ongoing development of the design.[212,213] 3D printing allows for simultaneous rapid prototyping and

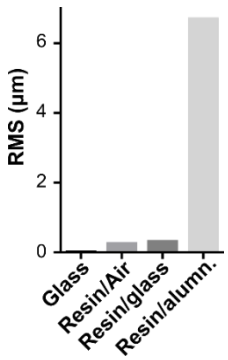

Figure 6-1: Preliminary surface roughness results indicate that surface roughness (root mean square: RMS) of glass compared to 3D resins printed a glass coverslip and aluminum printing plate. Measurements taken on Zygo optical profilometer.

medium-throughput production,[214–217] particularly stereolithography (SLA) printing, which uses LED light to polymerize a liquid precursor solution, or resin, in the desired pattern.[217] This technology has successfully generated a variety of microfluidic devices for analytical chemistry, including droplet-based systems.[215,218]

We have begun experiments to identify a resin that provides suitable resolution of features (void volume), optical transparency for UV-Vis detection, rigidity and smooth surface, and hydrophobic surface chemistry. For example, we will investigate commercially available resins such as PLASclear from Asiga, BV-007 from MiiCraft, that are transparent, rigid, and compatible with SLA printing.[219,220] If needed, we will also test a fully transparent, water-impermeable resin poly(ethylene glycol)-based resin.[221] We will prioritize optical transparency and surface roughness of the resin, as they are essential for readability on a UV-Vis and slipping without leakage on a Slip Chip. Given that most photo initiators absorb at 280 nm, we may find that no resins are sufficiently transparent. In that case, we will print the chip with openings in each plate for a small quartz slide to be bonded into place. Glass will be located over the sample wells to create a "viewing window" for UV/Vis detection.

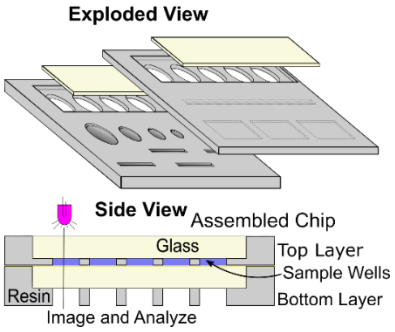

Figure 6-2: Modified 3D printed chip. A quartz glass slide (tan) insert can be placed into a 3D printed design for optically transparent sample wells, and bonded into place to prevent leaking.

We also plan to refine the device design for 3D printing. Small build size is often a tradeoff for high resolution. For example, our SLA printer can print objects up to 57 x 32 x 120 mm, but our prototype glass-etched device is 63.5 x 63.5 mm in 0.7-mm thick glass. To overcome this size mismatch, we will reduce the x,y dimensions by printing reagent wells at higher aspect ratios than is possible with glass etching (Figure 6-3a). 3D printing also allows for more complex designs, as enclosed channels can be printed within the body of the chip, above the wells of interest, thus simplifying the design exposed surface features.[217] We also propose 3D print guided routes for slipping the layers of the Slip Chip to avoid fine manual manipulation by the user. In the current planar design, the user can slip in any xy direction, but misalignment results in unwanted mixing of reagents. We will design a guide consisting of a pin that fits into a track/channel on the opposing layer (Figure 6-3c). We will test a simple straight pin, which would only guide the user, and a T-shaped pin that both guides and "locks" the top layer into the bottom layer. If successful, a T-shaped pin may replace the need for clips to hold the chip together.

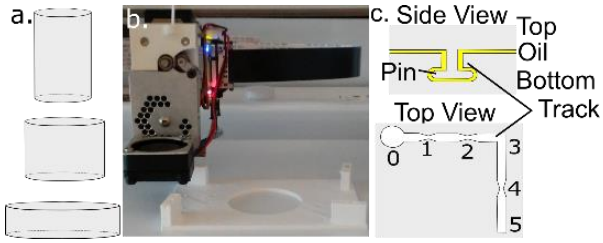

Figure 6-3: Features enabled by 3D printing the Slip Chip. a) High aspect ratio wells (top, center) are possible with printing. Only low aspect ratio wells (bottom) are possible with glass etching. b) Fused filament deposition printing. c) A proposed pin guide through a track. The pin is inserted at Position 0 and moved to stop positions 1-5.

This work will generate a platform for rapid, multiplexed, small-scale optimization of protein derivatization using a minimal volume of protein, which is compatible with standard UV-VIS detection on a plate reader and requires no more than a pipet and the user's hands to operate. We envision that this

technology will be widely used for basic and translation research, enabling higher quality conjugations prior to reagent validation.

For IHC staining of live immune tissue, we believe that in the future this work could be translated to other immune tissue such as human tonsil or murine thymus tissue with minimal change to procedures, allowing for a relatively quick validation of IHC stains for those tissues. As we've previously discussed, we believe that the study of spatial and morphological changes in tissue can provide a deeper understanding into disease progression and function, which may allow for the development and study of the efficacy of novel immunotherapies. For example, rheumatoid arthritis (RA) is an immune-related chronic inflammatory disease caused by the inflammation of synovium and results in destruction of the cartilage and erosion of the bone.[222] There are a number of immunotherapies for RA that aim to reduce the pro-inflammatory cytokines that cause synovitis. One new treatment that does show promise is the blocking of IL-6 cytokine. Currently, there exists only one FDA approved IL-6 inhibitory treatment: an anti-IL-6R antibody (tocilizumab) that binds to IL-6 receptor on B and T cells and acts to block IL-6 cytokine binding.[223,224] Treatment with tocilizumab antibody has shown results comparable to that of TNFα inhibitors. However, there is still concern about both side and long term effects such as abnormal liver function and potential for increased resurgence of diseases like tuberculosis, which indicates a need for the devolvement of new IL-6R immunotherapies. [225,226] Our methodologies to study intact live tissue over time may help facilitate this type of research by allowing for rapid screening of existing and new therapies prior to animal and human testing.

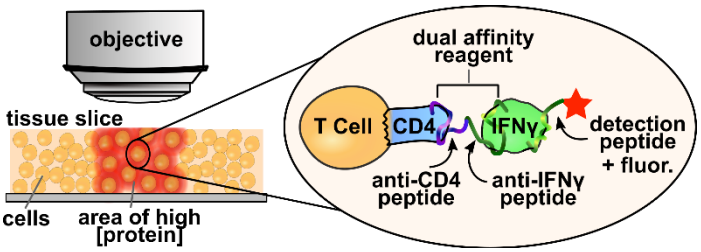

Figure 6-4: Peptide Immunoassaysembedded throughout the slice yield fluorescence (*red*) in locations where the protein is secreted. The peptide dual-affinity reagent would bind to a cell (T cell) and capture the target protein (IFN-γ), after which a second protein-binding peptide with a fluorophore would be added for detection.

We also plan to expand our development of the "dual affinity reagent" antibody to provide detection of multiple cytokines and cells, limited only by the number of fluorophores at one time available for fluorescent imaging. In essence, this would allow for the modular mixing and matching of a range cytokine for many types of immune cells. We have also begun working on the next phase of on-cell detection, which utilizes small peptides in leu of antibodies. Peptides are 20-50-fold smaller than antibody fragments, thus offering deeper penetration into tissue. In addition, peptide synthesis is robust and reproducible at the mg and g scale, making these reagents far more affordable and predictable than antibodies. Unfortunately, very few high-affinity cytokine-binding or lymphocyte-binding peptide sequences have been reported.[227,228] Here we will use high-content peptide screening techniques invented by our collaborator Dr. Kelly (UVA) to efficiently identify sequences for tight binding to murine and human lymphocytes and cytokines.

6.3 Summary

Antibodies are a valuable component in many types of research, however their expense and lack of availability with certain fluorophores or as fragments can limit research. The work presented in this thesis describes rapid, low cost, approachable methods to modify antibodies and validate them for use in novel research. We also show how novel

research, such as live tissue immunostaining, may help us to better understand the underlying biological and chemical mechanisms at play and how it may also provide insight into disease progression and efficacy of novel therapies.

References

1. Wu, A. H. B. A selected history and future of immunoassay development and applications in clinical chemistry. *Clin. Chim. Acta Int. J. Clin. Chem.* **369**, 119–124 (2006).
2. Buss, N. A., Henderson, S. J., McFarlane, M., Shenton, J. M. & de Haan, L. Monoclonal antibody therapeutics: history and future. *Curr. Opin. Pharmacol.* **12**, 615–622 (2012).
3. Liu, J. K. H. The history of monoclonal antibody development – Progress, remaining challenges and future innovations. *Ann. Med. Surg.* **3**, 113–116 (2014).
4. Lu, R.-M. *et al.* Development of therapeutic antibodies for the treatment of diseases. *J. Biomed. Sci.* **27**, 1 (2020).
5. Ecker, D. M., Jones, S. D. & Levine, H. L. The therapeutic monoclonal antibody market. *mAbs* **7**, 9–14 (2014).
6. Research Antibodies Market Size & Share | Industry Report, 2027. https://www.grandviewresearch.com/industry-analysis/research-antibodies-market.
7. Major, S. M. *et al.* AbMiner: A bioinformatic resource on available monoclonal antibodies and corresponding gene identifiers for genomic, proteomic, and immunologic studies. *BMC Bioinformatics* **7**, 192 (2006).
8. Singh, S. *et al.* Monoclonal Antibodies: A Review. *Curr. Clin. Pharmacol.* **13**, 85–99 (2018).
9. Duraiyan, J., Govindarajan, R., Kaliyappan, K. & Palanisamy, M. Applications of immunohistochemistry. *J. Pharm. Bioallied Sci.* **4**, S307–S309 (2012).
10. McKinnon, K. M. Flow Cytometry: An Overview. *Curr. Protoc. Immunol.* **120**, 5.1.1-5.1.11 (2018).
11. Duraiyan, J., Govindarajan, R., Kaliyappan, K. & Palanisamy, M. Applications of immunohistochemistry. *J. Pharm. Bioallied Sci.* **4**, S307–S309 (2012).

12. de Matos, L. L., Trufelli, D. C., de Matos, M. G. L. & da Silva Pinhal, M. A. Immunohistochemistry as an Important Tool in Biomarkers Detection and Clinical Practice. *Biomark. Insights* **5**, 9–20 (2010).
13. Teruya-Feldstein, J. The immunohistochemistry laboratory: looking at molecules and preparing for tomorrow. *Arch. Pathol. Lab. Med.* **134**, 1659–1665 (2010).
14. Groff, B. D., Kinman, A. W. L., Woodroof, J. F. & Pompano, R. R. Immunofluorescence staining of live lymph node tissue slices. *J. Immunol. Methods* **464**, 119–125 (2019).
15. Ross, A. E., Belanger, M. C., Woodroof, J. F. & Pompano, R. R. Spatially resolved microfluidic stimulation of lymphoid tissue ex vivo. *Analyst* **142**, 649–659 (2017).
16. Johnson, B. P. *et al.* Vital ex vivo tissue labeling and pathology-guided micropunching to characterize cellular heterogeneity in the tissue microenvironment. *BioTechniques* **64**, 13–19 (2018).
17. Thornton, E. E., Krummel, M. F. & Looney, M. R. Live imaging of the lung. *Curr. Protoc. Cytom.* **Chapter 12**, Unit12.28 (2012).
18. Chen, X. & Jensen, P. E. The role of B lymphocytes as antigen-presenting cells. *Arch. Immunol. Ther. Exp. (Warsz.)* **56**, 77–83 (2008).
19. Nicholson, L. B. The immune system. *Essays Biochem.* **60**, 275–301 (2016).
20. Warrington, R., Watson, W., Kim, H. L. & Antonetti, F. R. An introduction to immunology and immunopathology. *Allergy Asthma Clin. Immunol.* **7**, S1 (2011).
21. Chaplin, D. D. Overview of the Immune Response. *J. Allergy Clin. Immunol.* **125**, S3-23 (2010).
22. Hanly, W. C., Artwohl, J. E. & Bennett, B. T. Review of Polyclonal Antibody Production Procedures in Mammals and Poultry. *ILAR J.* **37**, 93–118 (1995).
23. Köhler, G. & Milstein, C. Continuous cultures of fused cells secreting antibody of predefined specificity. *Nature* **256**, 495–497 (1975).

24. Nelson, P. N. *et al.* Monoclonal antibodies. *Mol. Pathol. MP* **53**, 111–117 (2000).

25. Frenzel, A., Hust, M. & Schirrmann, T. Expression of Recombinant Antibodies. *Front. Immunol.* **4**, (2013).

26. Smith, K. A. *et al.* Demystified… recombinant antibodies. *J. Clin. Pathol.* **57**, 912–917 (2004).

27. Vidarsson, G., Dekkers, G. & Rispens, T. IgG Subclasses and Allotypes: From Structure to Effector Functions. *Front. Immunol.* **5**, (2014).

28. Arnold, J. N., Wormald, M. R., Sim, R. B., Rudd, P. M. & Dwek, R. A. The impact of glycosylation on the biological function and structure of human immunoglobulins. *Annu. Rev. Immunol.* **25**, 21–50 (2007).

29. Charles A Janeway, J., Travers, P., Walport, M. & Shlomchik, M. J. The distribution and functions of immunoglobulin isotypes. *Immunobiol. Immune Syst. Health Dis. 5th Ed.* (2001).

30. Chiu, M. L., Goulet, D. R., Teplyakov, A. & Gilliland, G. L. Antibody Structure and Function: The Basis for Engineering Therapeutics. *Antibodies* **8**, (2019).

31. Charles A Janeway, J., Travers, P., Walport, M. & Shlomchik, M. J. The interaction of the antibody molecule with specific antigen. *Immunobiol. Immune Syst. Health Dis. 5th Ed.* (2001).

32. Preiner, J. *et al.* IgGs are made for walking on bacterial and viral surfaces. *Nat. Commun.* **5**, 4394 (2014).

33. Porter, R. R. The hydrolysis of rabbit y-globulin and antibodies with crystalline papain. *Biochem. J.* **73**, 119–126 (1959).

34. Schroeder, H. W. & Cavacini, L. Structure and Function of Immunoglobulins. *J. Allergy Clin. Immunol.* **125**, S41–S52 (2010).

35. Hinner, M. J. & Johnsson, K. How to obtain labeled proteins and what to do with them. *Curr. Opin. Biotechnol.* **21**, 766–776 (2010).

36. Stephanopoulos, N. & Francis, M. B. Choosing an effective protein bioconjugation strategy. *Nat. Chem. Biol.* **7**, 876–884 (2011).

37. Spicer, C. D. & Davis, B. G. Selective chemical protein modification. *Nat. Commun.* **5**, 4740 (2014).

38. A little less conjugation, a little more accuracy. *Nat. Chem.* **8**, 91–91 (2016).

39. Szabó, Á. *et al.* The Effect of Fluorophore Conjugation on Antibody Affinity and the Photophysical Properties of Dyes. *Biophys. J.* **114**, 688–700 (2018).

40. McCormack, T., O'Keeffe, G., Craith, B. M. & O'Kennedy, R. Assessment of the Effect of Increased Fluorophore Labelling on the Binding Ability of an Antibody. *Anal. Lett.* **29**, 953–968 (1996).

41. Tsuchikama, K. & An, Z. Antibody-drug conjugates: recent advances in conjugation and linker chemistries. *Protein Cell* **9**, 33–46 (2018).

42. Vira, S., Mekhedov, E., Humphrey, G. & Blank, P. S. Fluorescent labeled antibodies - balancing functionality and degree of labeling. *Anal. Biochem.* **402**, 146–150 (2010).

43. Holmes, K. L. & Lantz, L. M. Chapter 9 Protein labeling with fluorescent probes. in *Methods in Cell Biology* vol. 63 185–204 (Elsevier, 2001).

44. Xenaki, K. T., Oliveira, S. & van Bergen en Henegouwen, P. M. P. Antibody or Antibody Fragments: Implications for Molecular Imaging and Targeted Therapy of Solid Tumors. *Front. Immunol.* **8**, (2017).

45. Nelson, A. L. Antibody fragments: hope and hype. *mAbs* **2**, 77–83 (2010).

46. Liu, W. & Wu, C. A mini-review and perspective on multicyclic peptide mimics of antibodies. *Chin. Chem. Lett.* **29**, 1063–1066 (2018).

47. Lakhin, A. V., Tarantul, V. Z. & Gening, L. V. Aptamers: Problems, Solutions and Prospects. *Acta Naturae* **5**, 34–43 (2013).

48. Groß, A., Hashimoto, C., Sticht, H. & Eichler, J. Synthetic Peptides as Protein Mimics. *Front. Bioeng. Biotechnol.* **3**, (2016).

49. Dissanayake, S. & Hay, F. C. Pepsin digestion of mouse IgG immunoglobulins subfragments of the Fc region. *Immunochemistry* **12**, 373–378 (1975).

50. Coulter, A. & Harris, R. Simplified preparation of rabbit Fab fragments. *J. Immunol. Methods* **59**, 199–203 (1983).

51. Lamoyi, E. & Nisonoff, A. Preparation of F(ab')2 fragments from mouse IgG of various subclasses. *J. Immunol. Methods* **56**, 235–243 (1983).

52. Rousseaux, J., Rousseaux-Prévost, R. & Bazin, H. Optimal conditions for the preparation of Fab and F(ab')2 fragments from monoclonal IgG of different rat IgG subclasses. *J. Immunol. Methods* **64**, 141–146 (1983).

53. Sjögren, J., Olsson, F. & Beck, A. Rapid and improved characterization of therapeutic antibodies and antibody related products using IdeS digestion and subunit analysis. *The Analyst* **141**, 3114–3125 (2016).

54. Switzar, L., Giera, M. & Niessen, W. M. A. Protein digestion: an overview of the available techniques and recent developments. *J. Proteome Res.* **12**, 1067–1077 (2013).

55. Andrew, S. M. & Titus, J. A. Fragmentation of immunoglobulin G. *Curr. Protoc. Cell Biol.* **Chapter 16**, Unit 16.4 (2003).

56. Plaut, A. G. & Tomasi, T. B. Immunoglobulin M: pentameric Fcmu fragments released by trypsin at higher temperatures. *Proc. Natl. Acad. Sci. U. S. A.* **65**, 318–322 (1970).

57. King, D. J. *Applications And Engineering Of Monoclonal Antibodies*. (CRC Press, 1998).

58. Goding, J. W. *Monoclonal Antibodies: Principles and Practice*. (Elsevier, 1996).

59. Vidarsson, G., Dekkers, G. & Rispens, T. IgG Subclasses and Allotypes: From Structure to Effector Functions. *Front. Immunol.* **5**, (2014).

60. Bordeaux, J. *et al.* Antibody validation. *BioTechniques* **48**, 197–209 (2010).

61. Voskuil, J. L. A. The challenges with the validation of research antibodies. *F1000Research* **6**, (2017).

62. Baker, M. Reproducibility crisis: Blame it on the antibodies. *Nat. News* **521**, 274 (2015).

63. Michel, M. C., Wieland, T. & Tsujimoto, G. How reliable are G-protein-coupled receptor antibodies? *Naunyn. Schmiedebergs Arch. Pharmacol.* **379**, 385–388 (2009).

64. Egelhofer, T. A. *et al.* An assessment of histone-modification antibody quality. *Nat. Struct. Mol. Biol.* **18**, 91–93 (2011).

65. Berglund, L. *et al.* A genecentric Human Protein Atlas for expression profiles based on antibodies. *Mol. Cell. Proteomics MCP* **7**, 2019–2027 (2008).

66. Prinz, F., Schlange, T. & Asadullah, K. Believe it or not: how much can we rely on published data on potential drug targets? *Nat. Rev. Drug Discov.* **10**, 712–712 (2011).

67. Weller, M. G. Ten Basic Rules of Antibody Validation. *Anal. Chem. Insights* **13**, (2018).

68. Sfanos, K. S. *et al.* If this is true, what does it imply? How end-user antibody validation facilitates insights into biology and disease. *Asian J. Urol.* **6**, 10–25 (2019).

69. Ramos-Vara, J. A. Technical aspects of immunohistochemistry. *Vet. Pathol.* **42**, 405–426 (2005).

70. O'Kennedy, R. *et al.* Applications of antibodies in microfluidics-based analytical systems: challenges and strategies for success. *J. Micromechanics Microengineering* **28**, 063001 (2018).

71. Regnault, C., Dheeman, D. S. & Hochstetter, A. Microfluidic Devices for Drug Assays. *High-Throughput* **7**, 18 (2018).

72. Seah, Y. F. S., Hu, H. & Merten, C. A. Microfluidic single-cell technology in immunology and antibody screening. *Mol. Aspects Med.* **59**, 47–61 (2018).

73. Friedensohn, S., Khan, T. A. & Reddy, S. T. Advanced Methodologies in High-Throughput Sequencing of Immune Repertoires. *Trends Biotechnol.* **35**, 203–214 (2017).

74. Jayamohan, H. *et al.* Chapter 11 - Advances in Microfluidics and Lab-on-a-Chip Technologies. in *Molecular Diagnostics (Third Edition)* (ed. Patrinos, G. P.) 197–217 (Academic Press, 2017). doi:10.1016/B978-0-12-802971-8.00011-0.

75. Debs, B. E., Utharala, R., Balyasnikova, I. V., Griffiths, A. D. & Merten, C. A. Functional single-cell hybridoma screening using droplet-based microfluidics. *Proc. Natl. Acad. Sci.* **109**, 11570–11575 (2012).

76. Eyer, K. *et al.* Single-cell deep phenotyping of IgG-secreting cells for high-resolution immune monitoring. *Nat. Biotechnol.* **35**, 977–982 (2017).

77. Shembekar, N., Hu, H., Eustace, D. & Merten, C. A. Single-Cell Droplet Microfluidic Screening for Antibodies Specifically Binding to Target Cells. *Cell Rep.* **22**, 2206–2215 (2018).

78. Adler, A. S. *et al.* Rare, high-affinity anti-pathogen antibodies from human repertoires, discovered using microfluidics and molecular genomics. *mAbs* **9**, 1282–1296 (2017).

79. Wu, A. R. *et al.* High throughput automated chromatin immunoprecipitation as a platform for drug screening and antibody validation. *Lab. Chip* **12**, 2190–2198 (2012).

80. Kapil, M. A. & Herr, A. E. Binding Kinetic Rates Measured via Electrophoretic Band Crossing in a Pseudohomogeneous Format. *Anal. Chem.* **86**, 2601–2609 (2014).

81. Quaranta, A., Sroka-Bartnicka, A., Tengstrand, E. & Thorsén, G. N-Glycan profile analysis of transferrin using a microfluidic compact disc and MALDI-MS. *Anal. Bioanal. Chem.* **408**, 4765–4776 (2016).

82. Kopp, M. R. G., Villois, A., Capasso Palmiero, U. & Arosio, P. Microfluidic Diffusion Analysis of the Size Distribution and Microrheological Properties of Antibody Solutions at High Concentrations. *Ind. Eng. Chem. Res.* **57**, 7112–7120 (2018).

83. Convery, N. & Gadegaard, N. 30 years of microfluidics. *Micro Nano Eng.* **2**, 76–91 (2019).

84. Terry, S. C., Jerman, J. H. & Angell, J. B. A gas chromatographic air analyzer fabricated on a silicon wafer. *IEEE Trans. Electron Devices* **26**, 1880–1886 (1979).

85. Manz, A., Graber, N. & Widmer, H. M. Miniaturized total chemical analysis systems: A novel concept for chemical sensing. *Sens. Actuators B Chem.* **1**, 244–248 (1990).

86. McDonald, J. C. *et al.* Fabrication of microfluidic systems in poly(dimethylsiloxane). *ELECTROPHORESIS* **21**, 27–40 (2000).

87. Martinez, A. W., Phillips, S. T., Butte, M. J. & Whitesides, G. M. Patterned Paper as a Platform for Inexpensive, Low-Volume, Portable Bioassays. *Angew. Chem. Int. Ed.* **46**, 1318–1320 (2007).

88. Ouyang, Y. *et al.* Rapid patterning of 'tunable' hydrophobic valves on disposable microchips by laser printer lithography. *Lab. Chip* **13**, 1762–1771 (2013).

89. Symes, M. D. *et al.* Integrated 3D-printed reactionware for chemical synthesis and analysis. *Nat. Chem.* **4**, 349–354 (2012).

90. Spivey, E. C., Xhemalce, B., Shear, J. B. & Finkelstein, I. J. 3D-Printed Microfluidic Microdissector for High-Throughput Studies of Cellular Aging. *Anal. Chem.* **86**, 7406–7412 (2014).

91. Chapter 12 - Antibody fragments as therapeutics. in *Therapeutic Antibody Engineering* (eds. Strohl, W. R. & Strohl, L. M.) 265–595 (Woodhead Publishing, 2012). doi:10.1533/9781908818096.265.

92. Groff, B. D., Kinman, A. W. L., Woodroof, J. F. & Pompano, R. R. Immunofluorescence staining of live lymph node tissue slices. *J. Immunol. Methods* (2018) doi:10.1016/j.jim.2018.10.010.

93. Crivianu-Gaita, V. & Thompson, M. Aptamers, antibody scFv, and antibody Fab' fragments: An overview and comparison of three of the most versatile biosensor biorecognition elements. *Biosens. Bioelectron.* **85**, 32–45 (2016).

94. Nugent, L. J. & Jain, R. K. Extravascular diffusion in normal and neoplastic tissues. *Cancer Res.* **44**, 238–244 (1984).

95. Jamali, I., Field, E. H., Fleming, A. & Cowdery, J. S. Kinetics of anti-CD4-induced T helper cell depletion and inhibition of function. Activation of T cells by the CD3 pathway inhibits anti-CD4-mediated T cell elimination and down-regulation of cell surface CD4. *J. Immunol. Baltim. Md 1950* **148**, 1613–1619 (1992).

96. Moldovan, M.-C., Sabbagh, L., Breton, G., Sékaly, R.-P. & Krummel, M. F. Triggering of T cell activation via CD4 dimers. *J. Immunol. Baltim. Md 1950* **176**, 5438–5445 (2006).

97. Dianzani, U., Shaw, A., Fernandez-Cabezudo, M. & Janeway, C. A. Extensive CD4 cross-linking inhibits T cell activation by anti-receptor antibody but not by antigen. *Int. Immunol.* **4**, 995–1001 (1992).

98. Li, W. *et al.* Antibody Aggregation: Insights from Sequence and Structure. *Antibodies* **5**, (2016).

99. Vlasak, J. & Ionescu, R. Fragmentation of monoclonal antibodies. *mAbs* **3**, 253–263 (2011).

100. Ma, H. & O'Kennedy, R. Recombinant antibody fragment production. *Methods* **116**, 23–33 (2017).

101. Ahn, J., Cao, M.-J., Yu, Y. Q. & Engen, J. R. Accessing the Reproducibility and Specificity of Pepsin and other Aspartic Proteases. *Biochim. Biophys. Acta* **1834**, 1222–1229 (2013).

102. Sanny, C. G., Hartsuck, J. A. & Tang, J. Conversion of pepsinogen to pepsin. Further evidence for intramolecular and pepsin-catalyzed activation. *J. Biol. Chem.* **250**, 2635–2639 (1975).

103. Piper, D. W. & Fenton, B. H. pH stability and activity curves of pepsin with special reference to their clinical importance. *Gut* **6**, 506–508 (1965).

104. Desnuelle, P., Neurath, H. & Ottesen, M. *Structure–Function Relationships of Proteolytic Enzymes: Proceedings of the International Symposium, Copenhagen June 16-18, 1969, No.*

37 in the Series of the International Union of Biochemistry Sponsored Symposia. (Elsevier, 2014).

105. Kamatari, Y. O., Dobson, C. M. & Konno, T. Structural dissection of alkaline-denatured pepsin. *Protein Sci. Publ. Protein Soc.* **12**, 717–724 (2003).
106. Campos, L. A. & Sancho, J. The active site of pepsin is formed in the intermediate conformation dominant at mildly acidic pH. *FEBS Lett.* **538**, 89–95 (2003).
107. Dunn, B. M. Structure and mechanism of the pepsin-like family of aspartic peptidases. *Chem. Rev.* **102**, 4431–4458 (2002).
108. Okoniewska, M., Tanaka, T. & Yada, R. Y. The role of the flap residue, threonine 77, in the activation and catalytic activity of pepsin A. *Protein Eng.* **12**, 55–61 (1999).
109. Ahn, J., Cao, M.-J., Yu, Y. Q. & Engen, J. R. Accessing the Reproducibility and Specificity of Pepsin and other Aspartic Proteases. *Biochim. Biophys. Acta* **1834**, 1222–1229 (2013).
110. Thermo Fisher Scientific. Manual: Pierce F(ab')2 Preparation Kit. MAN0017019.
111. Demignot, S., Garnett, M. C. & Baldwin, R. W. Mouse IgG2b monoclonal antibody fragmentation: Preparation and purification of Fab, Fc and Fab/c fragments. *J. Immunol. Methods* **121**, 209–217 (1989).
112. Parham, P. On the fragmentation of monoclonal IgG1, IgG2a, and IgG2b from BALB/c mice. *J. Immunol. Baltim. Md 1950* **131**, 2895–2902 (1983).
113. Millipore Corporation. Passivation of Amicon Centricon Concentrators for Improved Recovery. (1999).
114. Martineau, P. Affinity Measurements by Competition ELISA. in *Antibody Engineering* (eds. Kontermann, R. & Dübel, S.) 657–665 (Springer Berlin Heidelberg, 2010). doi:10.1007/978-3-642-01144-3_41.

115. Friguet, B., Chaffotte, A. F., Djavadi-Ohaniance, L. & Goldberg, M. E. Measurements of the true affinity constant in solution of antigen-antibody complexes by enzyme-linked immunosorbent assay. *J. Immunol. Methods* **77**, 305–319 (1985).

116. Latypov, R. F., Hogan, S., Lau, H., Gadgil, H. & Liu, D. Elucidation of Acid-induced Unfolding and Aggregation of Human Immunoglobulin IgG1 and IgG2 Fc. *J. Biol. Chem.* **287**, 1381–1396 (2012).

117. Zheng, K., Yarmarkovich, M., Bantog, C., Bayer, R. & Patapoff, T. W. Influence of glycosylation pattern on the molecular properties of monoclonal antibodies. *mAbs* **6**, 649–658 (2014).

118. Mandenius, C.-F. & Brundin, A. Bioprocess optimization using design-of-experiments methodology. *Biotechnol. Prog.* **24**, 1191–1203 (2008).

119. Inouye, K. & Ohnaka, S. Pepsin digestion of a mouse monoclonal antibody of IgG1 class formed F(ab′)2 fragments in which the light chains as well as the heavy chains were truncated. *J. Biochem. Biophys. Methods* **48**, 23–32 (2001).

120. Hong, P., Koza, S. & Bouvier, E. S. P. Size-Exclusion Chromatography for the Analysis of Protein Biotherapeutics and their Aggregates. *J. Liq. Chromatogr. Relat. Technol.* **35**, 2923–2950 (2012).

121. Ma, H. & O'Kennedy, R. The Purification of Natural and Recombinant Peptide Antibodies by Affinity Chromatographic Strategies. in *Peptide Antibodies: Methods and Protocols* (ed. Houen, G.) 153–165 (Springer New York, 2015). doi:10.1007/978-1-4939-2999-3_15.

122. Rousseaux, J., Picque, M. T., Bazin, H. & Biserte, G. Rat IgG subclasses: Differences in affinity to protein A-Sepharose. *Mol. Immunol.* **18**, 639–645 (1981).

123. Choe, W., Durgannavar, T. A. & Chung, S. J. Fc-Binding Ligands of Immunoglobulin G: An Overview of High Affinity Proteins and Peptides. *Materials* **9**, (2016).

124. Gruber, H. J. *et al.* Anomalous fluorescence enhancement of Cy3 and cy3.5 versus anomalous fluorescence loss of Cy5 and Cy7 upon covalent linking to IgG and noncovalent binding to avidin. *Bioconjug. Chem.* **11**, 696–704 (2000).

125. Berlier, J. E. *et al.* Quantitative comparison of long-wavelength Alexa Fluor dyes to Cy dyes: fluorescence of the dyes and their bioconjugates. *J. Histochem. Cytochem. Off. J. Histochem. Soc.* **51**, 1699–1712 (2003).

126. Shrestha, D., Bagosi, A., Szöllősi, J. & Jenei, A. Comparative study of the three different fluorophore antibody conjugation strategies. *Anal. Bioanal. Chem.* **404**, 1449–1463 (2012).

127. Haugland, R. P. Coupling of Monoclonal Antibodies with Fluorophores. in *Monoclonal Antibody Protocols* 205–221 (Humana Press, 1995).

128. Hahn, C. D., Riener, C. K. & Gruber, H. J. Labeling of Antibodies with Cy3-, Cy3.5-, Cy5-, and Cy5.5-monofunctional Dyes at Defined Dye/Protein Ratios. *Single Mol.* **2**, 149–149 (2001).

129. Mahler, H.-C. *et al.* Adsorption behavior of a surfactant and a monoclonal antibody to sterilizing-grade filters. *J. Pharm. Sci.* **99**, 2620–2627 (2010).

130. Cline, G. W. & Hanna, S. B. Kinetics and mechanisms of the aminolysis of N-hydroxysuccinimide esters in aqueous buffers. *J. Org. Chem.* **53**, 3583–3586 (1988).

131. Nge, P. N., Pagaduan, J. V., Yu, M. & Woolley, A. T. Microfluidic chips with reversed-phase monoliths for solid phase extraction and on-chip labeling. *J. Chromatogr. A* **1261**, 129–135 (2012).

132. Yu, M., Wang, H.-Y. & Woolley, A. Polymer microchip capillary electrophoresis of proteins either off- or on-chip labeled with chameleon dye for simplified analysis. *Electrophoresis* **30**, 4230–4236 (2009).

133. Yang, R., Pagaduan, J. V., Yu, M. & Woolley, A. T. On chip preconcentration and fluorescence labeling of model proteins by use of monolithic columns: device fabrication, optimization, and automation. *Anal. Bioanal. Chem.* **407**, 737–747 (2015).

134. Wang, C. *et al.* Rapid protein concentration, efficient fluorescence labeling and purification on a micro/nanofluidics chip. *Lab. Chip* **12**, 2664–2671 (2012).

135. Du, W., Li, L., Nichols, K. P. & Ismagilov, R. F. SlipChip. *Lab. Chip* **9**, 2286–2292 (2009).

136. Chang, C.-W., Peng, C.-C., Liao, W.-H. & Tung, Y.-C. Polydimethylsiloxane SlipChip for mammalian cell culture applications. *Analyst* **140**, 7355–7365 (2015).

137. Liang *et al.* Individually addressable arrays of replica microbial cultures enabled by splitting SlipChips. *Integr. Biol.* **6**, 796 (2014).

138. Li, L. & Ismagilov, R. F. Protein crystallization using Microfluidic technologies based on valves, droplets, and SlipChip. (2010) doi:10.1146/annurev.biophys.050708.133630.

139. Li, L., Du, W. & Ismagilov, R. User-Loaded SlipChip for Equipment-Free Multiplexed Nanoliter-Scale Experiments. *J. Am. Chem. Soc.* **132**, 106–111 (2010).

140. Hassan, S., Morgan, H., Zhang, X. & Niu, X. Droplet Interfaced Parallel and Quantitative Microfluidic-Based Separations. *Anal. Chem.* **87**, 3895–3901 (2015).

141. Zhao, Y., Pereira, F., deMello, A. J., Morgan, H. & Niu, X. Droplet-based in situ compartmentalization of chemically separated components after isoelectric focusing in a Slipchip. *Lab. Chip* **14**, 555–561 (2013).

142. Wen, J., Guillo, C., Ferrance, J. P. & Landers, J. P. DNA extraction using a tetramethyl orthosilicate-grafted photopolymerized monolithic solid phase. *Anal. Chem.* **78**, 1673–1681 (2006).

143. He, M. & Herr, A. E. Microfluidic polyacrylamide gel electrophoresis with in situ immunoblotting for native protein analysis. *Anal. Chem.* **81**, 8177–8184 (2009).

144. Yue, K. *et al.* Synthesis, properties, and biomedical applications of gelatin methacryloyl (GelMA) hydrogels. *Biomaterials* **73**, 254–271 (2015).

145. Breadmore, M. C. *et al.* Towards a microchip-based chromatographic platform. Part 1: Evaluation of sol-gel phases for capillary electrochromatography. *Electrophoresis* **23**, 3487–3495 (2002).

146. Li, Y. & Lee, M. L. Biocompatible polymeric monoliths for protein and peptide separations. *J. Sep. Sci.* **32**, 3369–3378 (2009).

147. Siouffi, A. M. Silica gel-based monoliths prepared by the sol-gel method: facts and figures. *J. Chromatogr. A* **1000**, 801–818 (2003).

148. Walcarius, A. & Collinson, M. M. Analytical chemistry with silica sol-gels: traditional routes to new materials for chemical analysis. *Annu. Rev. Anal. Chem. Palo Alto Calif* **2**, 121–143 (2009).

149. Feinle, A., Elsaesser, M. S. & Hüsing, N. Sol–gel synthesis of monolithic materials with hierarchical porosity. *Chem. Soc. Rev.* **45**, 3377–3399 (2016).

150. Wen, J. & Wilkes, G. L. Organic/Inorganic Hybrid Network Materials by the Sol−Gel Approach. *Chem. Mater.* **8**, 1667–1681 (1996).

151. Wu, Q. *et al.* Microchip-based macroporous silica sol-gel monolith for efficient isolation of DNA from clinical samples. *Anal. Chem.* **78**, 5704–5710 (2006).

152. Gu, B., Armenta, J. M. & Lee, M. L. Preparation and evaluation of poly(polyethylene glycol methyl ether acrylate-co-polyethylene glycol diacrylate) monolith for protein analysis. *J. Chromatogr. A* **1079**, 382–391 (2005).

153. Zhu, H., Holl, M., Ray, T., Bhushan, S. & Meldrum, D. R. Characterization of deep wet etching of fused silica glass for single cell and optical sensor deposition. *J. Micromechanics Microengineering* **19**, 065013 (2009).

154. Pompano, R. R., Platt, C. E., Karymov, M. A. & Ismagilov, R. F. Control of Initiation, Rate, and Routing of Spontaneous Capillary-Driven Flow of Liquid Droplets through Microfluidic Channels on SlipChip. *Langmuir* **28**, 1931–1941 (2012).

155. Roach, L. S., Song, H. & Ismagilov, R. F. Controlling nonspecific protein adsorption in a plug-based microfluidic system by controlling interfacial chemistry using fluorous-phase surfactants. *Anal. Chem.* **77**, 785–796 (2005).

156. Crosignani, V. *et al.* Deep tissue fluorescence imaging and in vivo biological applications. *J. Biomed. Opt.* **17**, 116023 (2012).

157. Luker, G. D. & Luker, K. E. Optical Imaging: Current Applications and Future Directions. *J. Nucl. Med.* **49**, 1–4 (2008).

158. Ji, N. The Practical and Fundamental Limits of Optical Imaging in Mammalian Brains. *Neuron* **83**, 1242–1245 (2014).

159. Gerner, M. Y., Kastenmuller, W., Ifrim, I., Kabat, J. & Germain, R. N. Histo-Cytometry: A Method for Highly Multiplex Quantitative Tissue Imaging Analysis Applied to Dendritic Cell Subset Microanatomy in Lymph Nodes. *Immunity* **37**, 364–376 (2012).

160. Bach, P. H. *et al.* The use of tissue slices for pharmacotoxicology studies : The report and recommendations of ecvam workshop 20. *ATLA Altern. Lab. Anim.* **24**, 893–923 (1996).

161. Bachman, J. Chapter Thirteen - Immunohistochemistry on Freely Floating Fixed Tissue Sections. in *Methods in Enzymology* (ed. Lorsch, J.) vol. 533 207–215 (Academic Press, 2013).

162. Balgley, B. M. *et al.* EVALUATION OF ARCHIVAL TIME ON SHOTGUN PROTEOMICS OF FORMALIN-FIXED AND PARAFFIN-EMBEDDED TISSUES. *J. Proteome Res.* **8**, 917–925 (2009).

163. Kokkat, T. J., Patel, M. S., McGarvey, D., LiVolsi, V. A. & Baloch, Z. W. Archived Formalin-Fixed Paraffin-Embedded (FFPE) Blocks: A Valuable Underexploited Resource for Extraction of DNA, RNA, and Protein. *Biopreservation Biobanking* **11**, 101–106 (2013).

164. Bauer, D. R., Otter, M. & Chafin, D. R. A New Paradigm for Tissue Diagnostics: Tools and Techniques to Standardize Tissue Collection, Transport, and Fixation. *Curr. Pathobiol. Rep.* **6**, 135–143 (2018).

165. Chao, D. L., Ma, L. & Shen, K. Transient cell–cell interactions in neural circuit formation. *Nat. Rev. Neurosci.* **10**, 262–271 (2009).

166. Prieto, G. A. & Cotman, C. W. Cytokines and cytokine networks target neurons to modulate long-term potentiation. *Cytokine Growth Factor Rev.* **34**, 27–33 (2017).

167. Murphy, T. W., Zhang, Q., Naler, L. B., Ma, S. & Lu, C. Recent advances in the use of microfluidic technologies for single cell analysis. *The Analyst* **143**, 60–80 (2018).

168. Groff, B. D., Kinman, A. W. L., Woodroof, J. F. & Pompano, R. R. Immunofluorescence staining of live lymph node tissue slices. *J. Immunol. Methods* **464**, 119–125 (2019).

169. Chang, T. C. *et al.* Parallel Microfluidic Chemosensitivity Testing on Individual Slice Cultures. *Lab. Chip* **14**, 4540–4551 (2014).

170. HUMPEL, C. ORGANOTYPIC BRAIN SLICE CULTURES: A REVIEW. *Neuroscience* **305**, 86–98 (2015).

171. Lossi, L., Alasia, S., Salio, C. & Merighi, A. Cell death and proliferation in acute slices and organotypic cultures of mammalian CNS. *Prog. Neurobiol.* **88**, 221–245 (2009).

172. Grivel, J.-C. & Margolis, L. Use of human tissue explants to study human infectious agents. *Nat. Protoc.* **4**, 256–269 (2009).

173. Shim, S., Belanger, M. C., Harris, A. R., Munson, J. M. & Pompano, R. R. Two-way communication between ex vivo tissues on a microfluidic chip: application to tumor-lymph node interaction. *Lab. Chip* **19**, 1013–1026 (2019).

174. Jamali, I., Field, E. H., Fleming, A. & Cowdery, J. S. Kinetics of anti-CD4-induced T helper cell depletion and inhibition of function. Activation of T cells by the CD3 pathway inhibits anti-CD4-mediated T cell elimination and down-regulation of cell surface CD4. *J. Immunol. Baltim. Md 1950* **148**, 1613–1619 (1992).

175. Dianzani, U., Shaw, A., Fernandez-Cabezudo, M. & Janeway, C. A. Extensive CD4 cross-linking inhibits T cell activation by anti-receptor antibody but not by antigen. *Int. Immunol.* **4**, 995–1001 (1992).

176. Sun, P. Chapter 7 - Structural Recognition of Immunoglobulins by Fcγ Receptors. in *Antibody Fc* (eds. Ackerman, M. E. & Nimmerjahn, F.) 131–144 (Academic Press, 2014). doi:10.1016/B978-0-12-394802-1.00007-8.

177. Luo, Y., Pollard, J. W. & Casadevall, A. Fcγ Receptor Cross-linking Stimulates Cell Proliferation of Macrophages via the ERK Pathway. *J. Biol. Chem.* **285**, 4232–4242 (2010).

178. Nelson, A. L. Antibody fragments: hope and hype. *mAbs* **2**, 77–83 (2010).

179. Hurley, L. H. DNA and its associated processes as targets for cancer therapy. *Nat. Rev. Cancer* **2**, 188–200 (2002).

180. Koster, D. A., Palle, K., Bot, E. S. M., Bjornsti, M.-A. & Dekker, N. H. Antitumour drugs impede DNA uncoiling by topoisomerase I. *Nature* **448**, 213–217 (2007).

181. Biebricher, A. S. *et al.* The impact of DNA intercalators on DNA and DNA-processing enzymes elucidated through force-dependent binding kinetics. *Nat. Commun.* **6**, 7304 (2015).

182. Progatzky, F., Dallman, M. J. & Lo Celso, C. From seeing to believing: labelling strategies for in vivo cell-tracking experiments. *Interface Focus* **3**, 20130001 (2013).

183. Parish, C. R. Fluorescent dyes for lymphocyte migration and proliferation studies. *Immunol. Cell Biol.* **77**, 499–508 (1999).

184. Anderson, W. M. & Trgovcich-Zacok, D. Carbocyanine dyes with long alkyl side chains: Broad spectrum inhibitors of mitochondrial electron transport chain activity. *Biochem. Pharmacol.* **49**, 1303–1311 (1995).

185. Nicholls, D. G. & Ward, M. W. Mitochondrial membrane potential and neuronal glutamate excitotoxicity: mortality and millivolts. *Trends Neurosci.* **23**, 166–174 (2000).

186. Will, M. A., Clark, N. A. & Swain, J. E. Biological pH buffers in IVF: help or hindrance to success. *J. Assist. Reprod. Genet.* **28**, 711–724 (2011).

187. Ma, E. H. *et al.* Metabolic Profiling Using Stable Isotope Tracing Reveals Distinct Patterns of Glucose Utilization by Physiologically Activated CD8+ T Cells. *Immunity* **51**, 856-870.e5 (2019).

188. Blagg, J. & Workman, P. Choose and Use Your Chemical Probe Wisely to Explore Cancer Biology. *Cancer Cell* **32**, 9–25 (2017).

189. Giger, B. *et al.* Human tonsillar tissue block cultures differ from autologous tonsillar cell suspension cultures in lymphocyte subset activation and cytokine gene expression. *J. Immunol. Methods* **289**, 179–190 (2004).

190. Ross, JennyO., Melichar, HeatherJ., Halkias, J. & Robey, EllenA. Studying T Cell Development in Thymic Slices. in *T-Cell Development* (eds. Bosselut, R., S. Vacchio, M. & Vacchio, M. S.) 131–140 (Springer New York, 2016). doi:10.1007/978-1-4939-2809-5_11.

191. Ross, A. E., Belanger, M. C., Woodroof, J. F. & Pompano, R. R. Spatially resolved microfluidic stimulation of lymphoid tissue ex vivo. *Analyst* **142**, 649–659 (2017).

192. Hoffmann, P., Skibinski, G. & James, K. Organ culture of human lymphoid tissue. I. Characteristics of the system. *J. Immunol. Methods* **179**, 37–49 (1995).

193. Katakai, T., Habiro, K. & Kinashi, T. Dendritic Cells Regulate High-Speed Interstitial T Cell Migration in the Lymph Node via LFA-1/ICAM-1. *J. Immunol.* **191**, 1188–1199 (2013).

194. Ross, A. E. & Pompano, R. R. Diffusion of cytokines in live lymph node tissue using microfluidic integrated optical imaging. *Anal. Chim. Acta* **1000**, 205–213 (2018).

195. Germain, R. N. *et al.* Making friends in out-of-the-way places: how cells of the immune system get together and how they conduct their business as revealed by intravital imaging. *Immunol. Rev.* **221**, 163–181 (2008).

196. Willard-Mack, C. L. Normal Structure, Function, and Histology of Lymph Nodes. *Toxicol. Pathol.* **34**, 409–424 (2006).

197. Katakai, T., Hara, T., Sugai, M., Gonda, H. & Shimizu, A. Lymph Node Fibroblastic Reticular Cells Construct the Stromal Reticulum via Contact with Lymphocytes. *J. Exp. Med.* **200**, 783–795 (2004).

198. Kilarski, W. W. *et al.* Intravital Immunofluorescence for Visualizing the Microcirculatory and Immune Microenvironments in the Mouse Ear Dermis. *PLOS ONE* **8**, e57135 (2013).

199. Li, J., Czajkowsky, D. M., Li, X. & Shao, Z. Fast immuno-labeling by electrophoretically driven infiltration for intact tissue imaging. *Sci. Rep.* **5**, 10640 (2015).

200. Chung, K. *et al.* Structural and molecular interrogation of intact biological systems. *Nature* **497**, 332–337 (2013).

201. Curtsinger, J. M. & Mescher, M. F. Inflammatory Cytokines as a Third Signal for T Cell Activation. *Curr. Opin. Immunol.* **22**, 333–340 (2010).

202. Rohowsky-Kochan, C., Molinaro, D. & Cook, S. D. Cytokine secretion profile of myelin basic protein-specific T cells in multiple sclerosis. *Mult. Scler.* **6**, 69–77 (2000).

203. Lin, W.-W. & Karin, M. A cytokine-mediated link between innate immunity, inflammation, and cancer. *J. Clin. Invest.* **117**, 1175–1183 (2007).

204. Willard-Mack, C. L. Normal Structure, Function, and Histology of Lymph Nodes. *Toxicol. Pathol.* **34**, 409–424 (2006).

205. 1.4928128.pdf.

206. Croxford, A. L. & Buch, T. Cytokine reporter mice in immunological research: perspectives and lessons learned. *Immunology* **132**, 1–8 (2011).

207. Desombere, I. *et al.* The interferon gamma secretion assay: a reliable tool to study interferon gamma production at the single cell level. *J. Immunol. Methods* **286**, 167–185 (2004).

208. 1921.full.pdf.

209. Moldovan, M.-C. *et al.* CD4 Dimers Constitute the Functional Component Required for T Cell Activation. *J. Immunol.* **169**, 6261–6268 (2002).

210. Wang, Z. *et al.* Polyspecific Self-Reactive Antibodies in Individuals Infected with Human Immunodeficiency Virus Facilitate T Cell Deletion and Inhibit Costimulatory Accessory Cell Function. *J. Infect. Dis.* **180**, 1072–1079 (1999).

211. Ross, A. E., Belanger, M. C., Woodroof, J. F. & Pompano, R. R. Spatially resolved microfluidic stimulation of lymphoid tissue ex vivo. *Analyst* **142**, 649–659 (2017).

212. Gale, B. K. *et al.* A Review of Current Methods in Microfluidic Device Fabrication and Future Commercialization Prospects. *Inventions* **3**, 60 (2018).

213. Silverio, V. & Freitas, S. C. de. Chapter 2 Microfabrication Techniques for Microfluidic Devices. in (2018).

214. Au, A. K., Lee, W. & Folch, A. Mail-order microfluidics: evaluation of stereolithography for the production of microfluidic devices. *Lab. Chip* **14**, 1294–1301 (2014).

215. Gross, B., Lockwood, S. Y. & Spence, D. M. Recent Advances in Analytical Chemistry by 3D Printing. *Anal. Chem.* **89**, 57–70 (2017).

216. MacDonald, E. & Wicker, R. Multiprocess 3D printing for increasing component functionality. *Science* **353**, aaf2093 (2016).

217. Bhattacharjee, N., Urrios, A., Kang, S. & Folch, A. The upcoming 3D-printing revolution in microfluidics. *Lab. Chip* **16**, 1720–1742 (2016).

218. Shang, L., Cheng, Y. & Zhao, Y. Emerging Droplet Microfluidics. *Chem. Rev.* **117**, 7964–8040 (2017).

219. Gong, H., Beauchamp, M., Perry, S., Woolley, A. T. & Nordin, G. P. Optical approach to resin formulation for 3D printed microfluidics. *RSC Adv.* **5**, 106621–106632 (2015).

220. Brunet, A. R., Labelle, F., Wong, P. & Gervais, T. Reconfigurable Microfluidic Magnetic Valve Arrays: Towards a Radiotherapy-Compatible Spheroid Culture Platform for the Combinatorial Screening of Cancer Therapies. *Sensors* **17**, (2017).

221. Urrios, A. *et al.* 3D-PRINTING OF TRANSPARENT BIO-MICROFLUIDIC DEVICES IN PEG-DA. *Lab. Chip* **16**, 2287–2294 (2016).

222. Izquierdo, E. *et al.* Synovial fibroblast hyperplasia in rheumatoid arthritis: clinicopathologic correlations and partial reversal by anti-tumor necrosis factor therapy. *Arthritis Rheum.* **63**, 2575–2583 (2011).

223. Kaly, L. & Rosner, I. Tocilizumab – A novel therapy for non-organ-specific autoimmune diseases. *Best Pract. Res. Clin. Rheumatol.* **26**, 157–165 (2012).

224. Mihara, M. *et al.* Tocilizumab inhibits signal transduction mediated by both mIL-6R and sIL-6R, but not by the receptors of other members of IL-6 cytokine family. *Int. Immunopharmacol.* **5**, 1731–1740 (2005).

225. Md Yusof, M. Y. & Emery, P. Targeting interleukin-6 in rheumatoid arthritis. *Drugs* **73**, 341–356 (2013).

226. Richardson, S. & Isaacs, J. Novel immunotherapies for rheumatoid arthritis. *Clin. Med.* **13**, 391–394 (2013).

227. Ranganath, S. *et al.* Discovery and Characterization of a Potent Interleukin-6 Binding Peptide with Neutralizing Activity In Vivo. *PLOS ONE* **10**, e0141330 (2015).

228. Sclavons, C. *et al.* Phage Display Screening for Tumor Necrosis Factor-α-Binding Peptides: Detection of Inflammation in a Mouse Model of Hepatitis. *International Journal of Peptides* vol. 2013 e348409 https://www.hindawi.com/journals/ijpep/2013/348409/ (2013).